Multiplexing experiments in NMR and multi-nuclear MRI

Kupce, E.; Mote, K.R.; Webb, A.; Madhu, P.K.; Claridge, T.D.W.

Multiplexing experiments in NMR and multi-nuclear MRI

Ēriks Kupče [a,*], Kaustubh R. Mote [b], Andrew Webb [c], Perunthiruthy K. Madhu [b], Tim D.W. Claridge [d]

[a] Bruker UK Ltd., Banner Lane, Coventry CV4 9GH, United Kingdom
[b] TIFR Centre for Interdisciplinary Sciences, Tata Institute of Fundamental Research-Hyderabad, 36/P Gopanpally Village, Ranga Reddy District, Hyderabad 500 046, Telangana, India
[c] Department of Radiology, Leiden University Medical Center, Albinusdreef 2, 2333 ZA Leiden, Netherlands
[d] Department of Chemistry, University of Oxford, Chemistry Research Laboratory, Mansfield Road, Oxford OX1 3TA, UK

Edited by: Gareth Morris and Geoffrey Bodenhausen

ARTICLE INFO

ABSTRACT

Multiplexing NMR experiments by direct detection of multiple free induction decays (FIDs) in a single experiment offers a dramatic increase in the spectral information content and often yields significant improvement in sensitivity per unit time. Experiments with multi-FID detection have been designed with both homonuclear and multinuclear acquisition, and the advent of multiple receivers on commercial spectrometers opens up new possibilities for recording spectra from different nuclear species in parallel. Here we provide an extensive overview of such techniques, designed for applications in liquid- and solid-state NMR as well as in hyperpolarized samples. A brief overview of multinuclear MRI is also provided, to stimulate cross fertilization of ideas between the two areas of research (NMR and MRI). It is shown how such techniques enable the design of experiments that allow structure elucidation of small molecules from a single measurement. Likewise, in biomolecular NMR experiments multi-FID detection allows complete resonance assignment in proteins. Probes with multiple RF microcoils routed to multiple NMR receivers provide an alternative way of increasing the throughput of modern NMR systems, effectively reducing the cost of NMR analysis and increasing the information content at the same time. Solid-state NMR experiments have also benefited immensely from both parallel and sequential multi-FID detection in a variety of multi-dimensional pulse schemes. We are confident that multi-FID detection will become an essential component of future NMR methodologies, effectively increasing the sensitivity and information content of NMR measurements.

© 2021 Elsevier B.V. All rights reserved.

Contents

---

* Corresponding author.
   E-mail address: eriks.kupce@bruker.com (Ē. Kupče).

1. Introduction

Characterization of small molecules by NMR spectroscopy in solution is largely based on well-established two-dimensional correlation techniques such COSY, TOCSY, NOESY, HSQC, HMBC and similar methods, which have been extended to higher dimensionality experiments for biomolecular applications based on the same basic experiment design principles [1–3]. Once the principal techniques for molecular analysis were established, the main focus in NMR spectroscopy turned to developing experimental methods that reduce the data acquisition time, often exploiting the technological advances offered by modern instrumental developments [4,5]. Over the past two decades many such techniques have been introduced for speeding up multi-dimensional NMR – ultrafast NMR [6–9], fast-pulsing techniques [9–14], non-conventional sampling techniques [15–23], parallel NMR [24,25], and hyperdimensional NMR [26–29], to name a few. Each such development becomes particularly important if it complements other fast techniques.

A requirement common to all multi-dimensional NMR experiments is for sufficient longitudinal spin relaxation to occur before repeating the pulse sequences as necessary for signal averaging and for sampling the indirect frequency dimensions. The longitudinal relaxation times (T_1) of small molecules in solution phases can be many seconds, and the associated recovery times typically represent the longest periods within pulse sequences and thus, in part, define their minimal duration. Experiments with direct detection of multiple Free Induction Decays (FIDs), either multinuclear [25] or homonuclear [30,31], are designed to optimally manipulate and sample the various magnetization reservoirs available within a molecule and, hence, to maximize the information content acquired per measurement. In contrast, conventional single-FID methods seek to exploit only a single magnetization reservoir per experiment, generally destroying or discarding all other magnetization. The latter presents an inherently less efficient way to collect multi-dimensional data. Multi-FID detection techniques may store magnetization during an FID acquisition period for later use in the same experiment, or may detect magnetization multiple times, provided that acquisition periods are separated by pulse sequences (modules) designed to exploit different coherence trans-

fer pathways each time. The slow relaxation associated with small molecules in liquids can be used to advantage in such cases, utilizing magnetization that would otherwise be left to simply recover after single-FID detection. In addition to their increased information content, multi-FID experiments often improve spectral sensitivity for a given measurement duration relative to conventional techniques [32,33].

Magnetically abundant nuclei, such as ^{1}H, ^{19}F, ^{31}P and similar, are particularly well suited for experiments involving multinuclear direct detection schemes. In particular, high natural abundance, large chemical shift ranges, excellent signal dispersion and NMR sensitivity that is inferior only to that of protons and tritium make fluorine-19 a very popular NMR nucleus [34-37]. ^{19}F NMR plays an important role in drug discovery methodology and in the pharmaceutical industry. Due to high sensitivity of the fluorine atom to its local electronic environment, ^{19}F NMR is becoming an increasingly popular tool for fragment-based drug design [36]. Simultaneous acquisition of ^{1}H and ^{19}F spectra is particularly beneficial because of the high sensitivities of the two nuclear species leading to substantial increase in signal that is detected in a single measurement [38].

Improving resolution and sensitivity have historically been critically important research objectives in NMR, due to the inherently low sensitivity of NMR spectroscopy. One of the first applications of multi-FID detection was for sensitivity improvement in instances where $T_2^* \ll T_2$ [39,40]. In solids, where T_1 can be very long, the detection of multiple FIDs before the mandatory recycle delay is an attractive approach to boost sensitivity. Detection of multiple FIDs after sequential cross-polarization steps was first demonstrated by Pines and Waugh as early as 1973 [41]. In spite of this, the use of multi-FID detection techniques in solid state NMR has lagged behind that in solution NMR. It is only in the last decade or so that the use of these techniques has seen a resurgence, especially in the context of biomolecular NMR spectroscopy.

Many techniques involving multi-FID detection require use of multiple receivers. The benefits of multiple receivers were first discovered in MRI. Before such instrumentation became commercially available, multi-receiver experiments were often implemented on home-built or modified equipment. The first parallel *multinuclear* detection experiments monitoring phosphate metabolism in rabbit

Multinuclear Detection

Homonuclear Detection
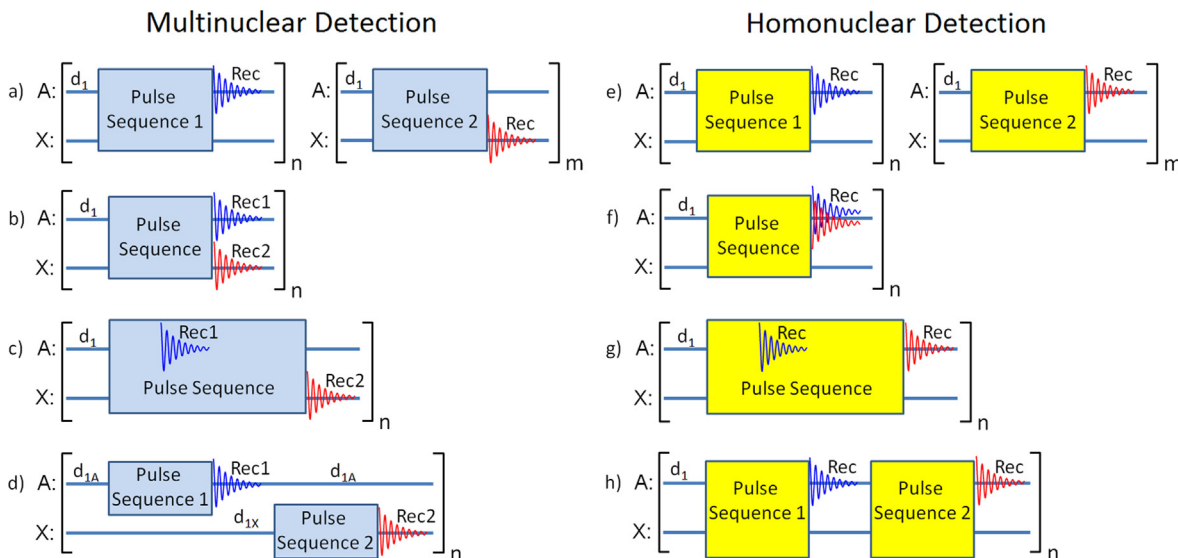
Fig. 1. Basic types of multi-FID detection experiments employing multiple receivers where *n* and *m* are integers representing the number of increments in multi-dimensional NMR. *A* and *X* represent the observed nuclear species. (a, e) The experiments sequentially, (b, f) parallel detection and time-shared experiments, (c, g) sequential detection experiments and (d, h) interleaved experiments. The recovery (relaxation) delay, d_1 can be joint or nucleus- (channel-) specific.
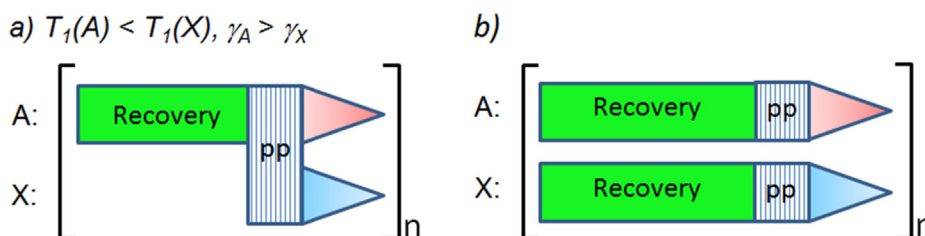
Fig. 2. Parallel data acquisition schemes – a) involving coherence transfer from nuclei *A* to *X* and b) recording independently in spin systems without any couplings between spins *A* and *X*; *pp* denotes pulse program.

skeletal muscle were implemented using two spectrometers connected to separate ^{1}H and ^{31}P surface coils in a single magnet [42]. In MRI the idea initially was to increase signal-to-noise ratio by using multiple, higher sensitivity, smaller coils for signal reception rather than a single, lower sensitivity, larger coil. The sensitivity defined as the B_1 field produced per unit current is inversely proportional to the coil diameter. A key requirement in the design of coil arrays, in which all coils are tuned to the same frequency, is to decouple each coil from all the others in the array [43,44]. Later, several groups showed that by using the spatial information from each coil, the amount of the required gradient-induced spatial encoding could be reduced [45–49], thus reducing the total image acquisition time. This concept is used for almost all clinical proton-based imaging and is referred to as parallel imaging [50]. Multinuclear (^{23}Na, ^{31}P and ^{13}C) coil arrays have also been designed [51], although these are typically used for the original purpose of increasing signal-to-noise ratio (SNR) rather than for parallel imaging. The great success of parallel MRI has stimulated interest in potential applications of multiple receivers in NMR spectroscopy.

Multi-receiver technology has been gradually introduced into NMR, [24,52] becoming a standard feature on state-of-the-art NMR consoles in the last couple of years. However, unlike in MRI, multi-receiver NMR experiments are typically designed with multinuclear detection in mind, mainly because commercially available NMR probes are designed to accommodate only one sample. Home-built probes housing multiple microcoils [53] routed to multiple (^{1}H) receivers have been shown to greatly increase the throughput of NMR spectroscopy [54,55]. The availability of multi-

ple receivers in state-of-the-art NMR systems is expected to further fuel developments in this area.

Here, we present a comprehensive overview of different approaches and techniques used in experiments with multi-FID detection - the technique aptly termed MACSY (Multiple ACquisition SpectroscopY) [56]. In order to avoid confusion with data averaging techniques we shall use the term 'multi-FID detection' rather than 'multi-FID acquisition' that sometimes is used in literature. Furthermore, we shall classify multi-FID detection techniques into two main categories – homonuclear and multinuclear, corresponding to direct detection of a single nuclear species or of two or more nuclear species, respectively. Both types of multi-FID detection schemes may involve multinuclear resonance experiments and employ either a single receiver or multiple receivers. While several researchers have pointed out that some multi-receiver experiments can also be implemented on single receiver systems, although often not without compromises, on state-of-the-art NMR systems where every channel is equipped with its own receiver, the issue is fast becoming irrelevant. Therefore, we shall focus on the possibilities and new experimental design principles offered by multi-receiver technology and by multi-FID detection techniques.

2. Basic types of multi-FID detection experiments

Traditionally, different NMR spectra are recorded in separate experiments, one at a time (see Fig. 1a, e). multi-FID detection
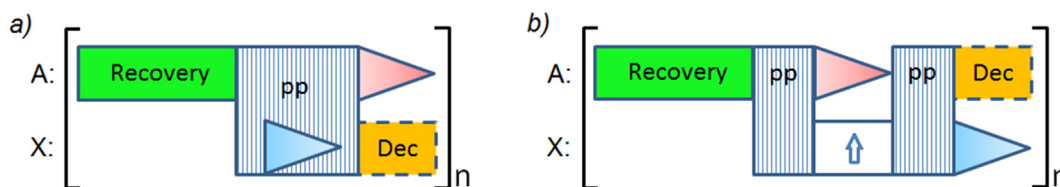
Fig. 3. Pulse schemes with sequential data acquisition. a) The FID of X-nuclei is recorded during a long delay, e.g., during a J-evolution or a mixing period in the pulse scheme, and b) the magnetization of X-nuclei is stored along the Z axis and following the detection of the FID from A-nuclei the experiment is continued, ending with detection of an FID from X-nuclei. The dotted box (Dec) denotes optional decoupling, which reduces the recovery time by the duration of the X-FID (b).
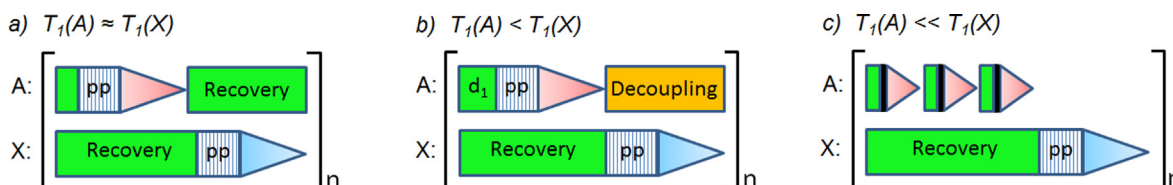
Fig. 4. Schematics of interleaved experiments. a) The FID of A-nuclei is recorded during the recovery period of X-nuclei and vice versa, where the nuclear species have comparable relaxation times and no decoupling is feasible. b) The same as in (a) except that the T_1 relaxation time of A-nuclei is significantly shorter than that of X-nuclei. The recovery period is determined by the more slowly relaxing X-nuclei, enabling decoupling of A-nuclei. c) Relaxation of A-nuclei is very fast as compared to that of X-nuclei, allowing recording of several FID-s of A-nuclei during the recovery period of X-nuclei. Decoupling of A-nuclei is possible, but may not always be needed, e.g., for quadrupolar nuclei due to self-decoupling arising from rapid relaxation.

techniques allow several spectra to be obtained in one measurement, and such experiments can be loosely categorized into three basic types – (a) pulse schemes involving parallel acquisition (Fig. 1b, f), (b) pulse sequences based on sequential data acquisition (Fig. 1c, g) and (c) interleaved experiments (Fig. 1d, h). A further classification into experiments with multinuclear (Fig. 1b-d) and homonuclear (Fig. 1f-h) detection can be made within each of the three categories. While many basic experiments fit nicely into one of these categories, more complex experiments often use mixed types of multi-FID detection. For instance, parallel acquisition can be combined with sequential detection schemes, and multinuclear acquisition can be combined with homonuclear multi-FID detection within the same pulse scheme, as will be discussed in detail later.

2.1. Multinuclear detection schemes

In parallel multi-FID detection schemes, FIDs from two or more different nuclear species are acquired simultaneously (in parallel). Such pulse schemes usually include polarization transfer from high γ nuclei A (e.g., ^1H) to low γ nuclei X (e.g., ^{13}C) designed to improve the sensitivity of the X-detected spectra (Fig. 2a). In situations where A and X nuclei have comparable γ (e.g., ^1H and ^{19}F) it may be possible to reduce the recovery time, d_1, by transferring coherence from nuclei with faster T_1 relaxation and thus improve sensitivity per unit time. Alternatively, in samples where the A and X nuclei are not coupled, or belong to different molecules or isotopomers, the two spectra can be recorded in parallel completely independently (Fig. 2b). Clearly, nuclear species that are observed simultaneously cannot be directly decoupled from each other. Therefore, parallel acquisition is most useful in spin systems where the mutual couplings between the directly observed spins are negligible or can be ignored. A significant advantage of this approach is that all spectra are acquired under exactly the same conditions.

In sequential multi-FID detection experiments, magnetization in one of the coherence transfer pathways that is not used or cannot be used in the current experiment is preserved (typically 'parked' on a slowly relaxing nuclear species X, such as ^{15}N or ^{13}C) and later utilized to acquire a different type of spectrum. Alternatively, such magnetization can be refocused and re-used in a later part of the multi-FID detection experiment(s). Usually, in sequential multi-FID detection experiments it is possible to decou-

ple nuclear species that are observed sequentially. For instance, an X-nucleus FID may be recorded during an A-nucleus spin-lock or isotropic mixing period that also serves as a decoupling sequence (Fig. 3a). Decoupling can typically be used during the detection period of the last FID (Fig. 3a, b).

A clear distinction should be made between acquiring spectra sequentially (Fig. 1a, e), which is the conventional way of recording NMR spectra, and sequential detection of several FIDs in a single experiment that typically involves several coherence pathways generated by a given pulse sequence (Fig. 3).

Finally, interleaved experiments avoid disturbing spins detected in the alternating acquisition periods. Typically, one or more experiments is placed in the recovery period of another experiment, thus reducing the total acquisition time by approximately a factor of two or more (Fig. 4a). Depending on the relaxation properties of the nuclei involved, mutual decoupling of the observed spins may be possible (Fig. 4b) [38]. Several experiments involving rapidly relaxing nuclei may fit into the recovery period of experiments with direct detection of slowly relaxing nuclei (Fig. 4c).

2.2. Homonuclear detection schemes and parallel acquisition in time-shared experiments

Homonuclear multi-FID detection experiments are largely based on the same approaches as multinuclear multi-FID detection experiments and can be implemented on single receiver systems, except for parallel acquisition experiments. The latter require either multiple coil probes routed to multiple receivers, [53,54] or some form of encoding, such as spatial [57] or phase [58] encoding. Parallel acquisition experiments based on phase encoding are better known as time-shared (*TS*) experiments, and are used routinely on standard instrumentation [32]. Typical examples of the *TS* technique are experiments with parallel acquisition of ^{15}N-H and ^{13}C-H correlated spectra that are phase encoded in alternate data blocks and extracted from the data by post-processing [59–62]. Indeed, this technique is nowadays used routinely - suffice it to mention IPAP methods separating spectra containing either in-phase or anti-phase spectral components [63,64], spectral simplification using 'virtual decoupling' [65,66] and many other experiments that greatly benefit from the *TS* technique. This method is well understood and has been extensively reviewed in the litera-
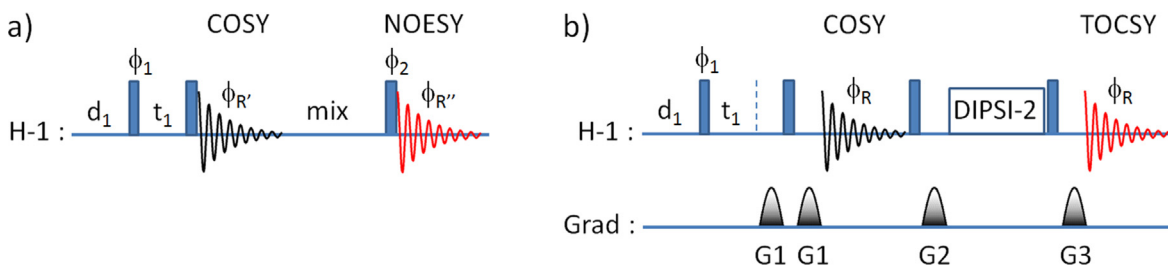
Fig. 5. a) The COCONOSY pulse scheme [30,31] with phase cycling: $\phi_1 = \phi_{R'} = x, -x$; $\phi_2 = x, x, -x, -x$; $\phi_{R''} = x, -x, -x, x$. b) The COSY/TOCSY pulse scheme [82] with phase cycling: $\phi_1 = \phi_R = x, -x$. The gradient ratio G1:G2:G3 is 10:33:20.

ture [32]. Therefore, we shall only mention the *TS* technique where it has been incorporated into other multi-FID detection pulse schemes.

Most *sequential* homonuclear multi-FID detection schemes are based on the principle of preservation of equivalent pathways (PEP) [67,68] to prepare and store various pools of magnetization for subsequent coherence transfers and detection. This approach is very similar to the techniques employed in multinuclear detection schemes. *Interleaved* experiments avoid disturbing magnetization used in subsequent pulse sequences. In homonuclear multi-FID detection schemes this is typically achieved using isotope filters and modified phase cycling schemes. Alternatively, techniques adopted from MRI, such as spatially selective excitation or use of probes with multiple microcoils, are employed.

3. Experiments with multi-FID detection in liquids

3.1. Multi-FID experiments with homonuclear (^1H) detection

As previously indicated, multinuclear and homonuclear multi-FID detected experiments are conceptually very similar. Not surprisingly, many *sequential* multinuclear multi-FID detection experiments can easily be adapted for homonuclear applications. For instance, the COSY/HOESY pulse scheme (Section 3.2.1.6) [38] closely resembles the COSY/NOESY (COCONOSY) pulse sequence introduced in the following section [30,31]. Sequential acquisition pulse schemes are combined with interleaved experiments in the NOAH (<u>N</u>MR by <u>O</u>rdered <u>A</u>cquisition using $^1\underline{H}$-detection) supersequences, [69,70] where the magnetization employed in individual NOAH modules must be prepared and preserved by the preceding NOAH modules. The NOAH approach combining various multi-FID detection techniques considerably increases the flexibility of homonuclear multi-FID detection experiment design compared to the widely used *TS* method. For instance, the feasibility of simultaneous acquisition of ^1H-^{13}C HSQC and ^1H-^{13}C HMBC data in time-shared mode has been explored by several groups [71–74]. However, these *TS* pulse schemes do not permit ^{13}C decoupling in the HSQC spectra, reducing their usefulness. On the other hand, interleaving the ^1H-^{13}C HMBC and ^{13}C decoupled ^1H-^{13}C HSQC experiments in various combinations is straightforward, leading to more versatile pulse schemes. The same applies to experiments [75] involving ^1H homodecoupling [76–78].

3.1.1. Early multi-FID implementations

The COCONOSY (COmbined COrrelated and Nuclear Overhauser enhancement SpectroscopY) experiment was the first multi-FID experiment recorded in liquids with a single receiver [30,31], and was subsequently adapted in solid-state NMR [79]. Two of the most useful and widely used 2D ^1H-^1H correlation techniques, the COSY and NOESY experiments, are combined in a single experiment by exploiting a shared t_1 evolution period that is followed by acquiring the COSY data during the NOESY mixing period (see

Fig. 5a). Therefore, in a single measurement the COSY spectrum identifies proton spins connected via scalar ^1H-^1H couplings, whilst the NOESY spectrum delivers distance information via dipolar (through space) interactions. The combined information from the COCONOSY pulse scheme was used for spectral assignment and structure elucidation of BPTI and other small proteins in the early days of biomolecular NMR spectroscopy [80]. At that time recording COSY and NOESY spectra separately often required a total of up to 70 h of experiment time, and the time savings offered by the COCONOSY experiment were significant. Furthermore, in order to guarantee perfect signal alignment, the two spectra have to be recorded under identical and stable conditions. This can be a problem when dealing with unstable and degrading samples, as is often the case in biomolecular NMR. In the COCONOSY experiment the peak alignment in the F_1 domain is guaranteed because the COSY and NOESY pulse schemes share the same t_1-evolution period. Stated otherwise, their spectral spaces share a joint F_1 frequency axis. Thus, not only does COCONOSY reduce the total experiment time to that of a NOESY experiment, but it also ensures that COSY and NOESY spectra are recorded under identical conditions.

Cavanagh and Rance proposed a combined 2D TOCSY/NOESY experiment that exploits similar design principles [81]. In this experiment the 2D TOCSY spectrum is recorded during the NOESY mixing period. Consequently, the time required to record both TOCSY and relayed-NOESY spectra is the same as that for a conventional 2D NOESY experiment.

3.1.2. Subsequent multi-FID developments

The use of multi-FID detection in homonuclear experiments has been extended to exploit longitudinal and/or transverse magnetization that may remain after an FID in a conventional 2D experiment has been collected. The utilization of residual transverse magnetization is most relevant for small molecules that have slow proton transverse relaxation. This magnetization would usually be left to decay before the start of the subsequent cycle, but since this is already frequency labelled in t_1 it may be utilized directly for further detection. Parella *et al.* have demonstrated the use of this "afterglow" magnetization for obtaining a series of relayed COSY FIDs after the conventional COSY FIDs through the application of sequential *90°-Acquire* stages to give stepwise coherence transfers [82]. In this manner, a single experiment yielded a COSY data set and three relayed-COSY data sets (see Fig. 6). Related schemes utilizing residual transverse magnetization have instead exploited TOCSY type transfers after the first FID detection to yield COSY-TOCSY (Fig. 5b) and HMBC-TOCSY combinations. Due to the evolution of magnetization during the first FID, the results of such experiments must necessarily be presented in magnitude mode.

A variation on this idea is to employ magnetization that has been stored as frequency-encoded longitudinal magnetization during the first FID detection period and follows a different coherence transfer pathway (CTP) that can be sampled independently. In this, the magnetization can be used directly for mixing after the FID. For
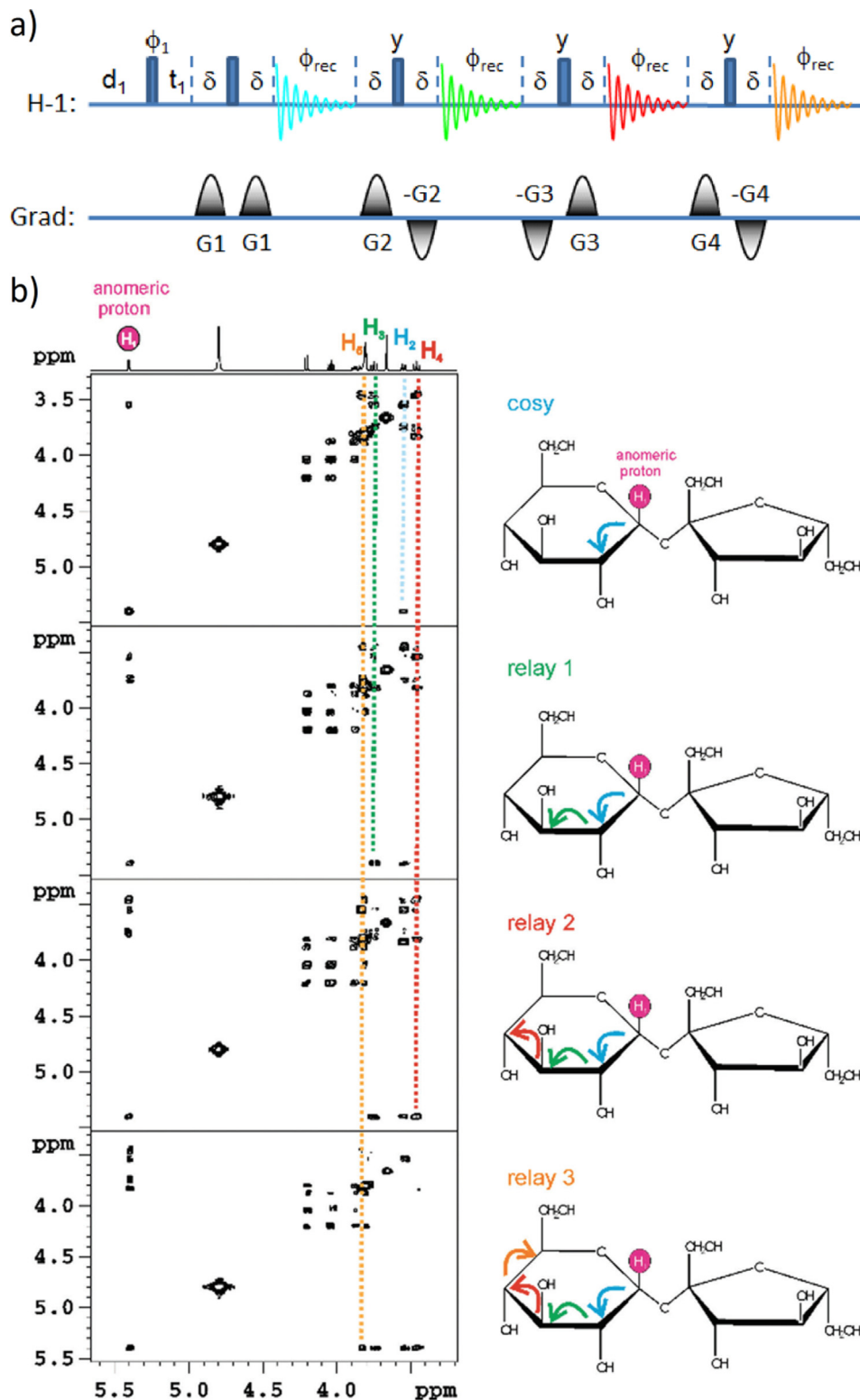
Fig. 6. a) Pulse scheme for the multi-FID COSY/RELAY experiment with phase cycling: $\phi_1 = x, -x$; $\phi_{rec} = x, -x$ and gradient ratio G1:G2:G3:G4 of 50:30:40:17. b) Example spectra of sucrose in D_2O for COSY and relayed-COSY with 1, 2 and 3 relay steps. Reproduced from Ref. [82] with permission.

example, use of isotropic mixing by DIPSI-2 produced the COSY/TOCSY combination (COTO), by analogy with the COCONOSY [30,31] and TOCSY/NOESY [81] discussed above. In a related approach, magnetization that relaxes during the first FID may also be reused, but since this has no memory of prior frequency labelling it requires a subsequent and independent t_1-evolution period,

in a manner similar to the interleaved NOAH methodology presented in Section 3.1.3 (hence referred to as NOAH-2 CT). Various combinations of CTP-based COSY/TOCSY schemes yielding CO/TO/CO and CO/TO/TO variants (with differing TOCSY mixing times) have been proposed [83] and their sensitivity performance analyzed in detail. In general, the use of longer FID acquisition times
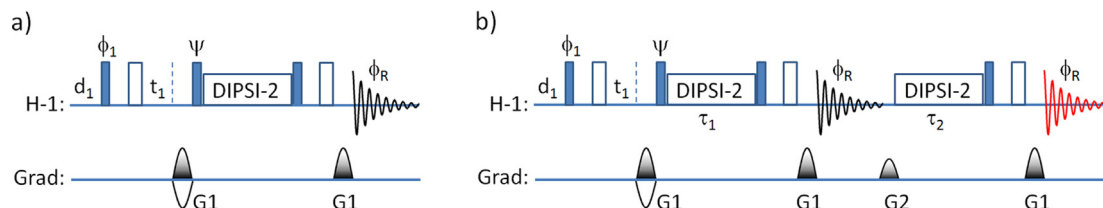
Fig. 7. Pulse schemes for a) conventional sensitivity-enhanced 2D TOCSY designed to detect both components of magnetization, and b) dual-FID TOCSY-TOCSY recorded with two different mixing times τ_1 and τ_2. The first FID is designed to sample transverse I_x magnetization whilst the orthogonal I_z magnetization is preserved and used for subsequent mixing and detection in the second FID [84]. Phase cycling: $\phi_1 = \phi_R = x, -x$; gradient ratio, G1:G2 was 30:23.
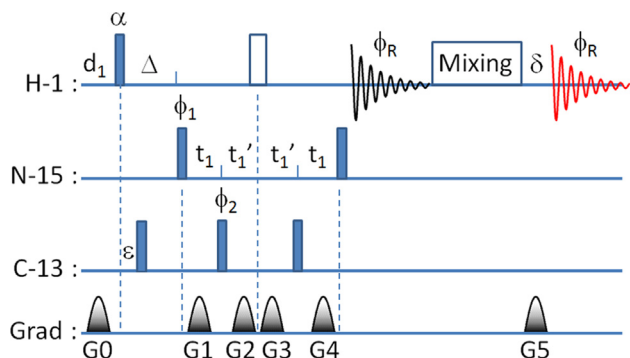
Fig. 8. The MATS (Multiple-Acquisition Time-Shared) HMBC experiment; delays $\Delta = 0.5/$ ^nJ, $\varepsilon = 0.5/^1J(CH)$; gradients (% of 53.5 G/cm): 15, 60, 50, 30, 60, and 40 for 1 ms long G0–G5, respectively. Two data sets were recorded in an interleaved mode with basic two-step phase cycling: $\phi_1 = \phi_R = x, -x$; (data A: $\phi_2 = x, -x$; data B: $\phi_2 = -x, x$) [85].

in such combinations of homonuclear correlation experiments is beneficial as it improves both resolution and sensitivity as long as excessive relaxation and $J(^1H^{-1}H)$ evolution are not detrimental to the subsequent experiment(s).

The manipulation and independent sampling of two different CTPs have also been exploited in TOCSY and in HSQC experiments in which the orthogonal pathways typically combined in traditional Preservation of Equivalent Pathways (PEP) schemes for sensitivity improvement [67,68] are instead kept separate [84]. This provides for sequential acquisition of two TOCSY spectra with different mixing times (see Fig. 7). Orthogonal pathways can similarly be used to acquire two HSQC spectra with different characteristics, e.g., with and without ^{13}C decoupling or without and with homonuclear (pure-shift) decoupling in the same experiment. Alternatively, HSQC and HSQC-TOCSY spectra can be recorded in a single measurement.
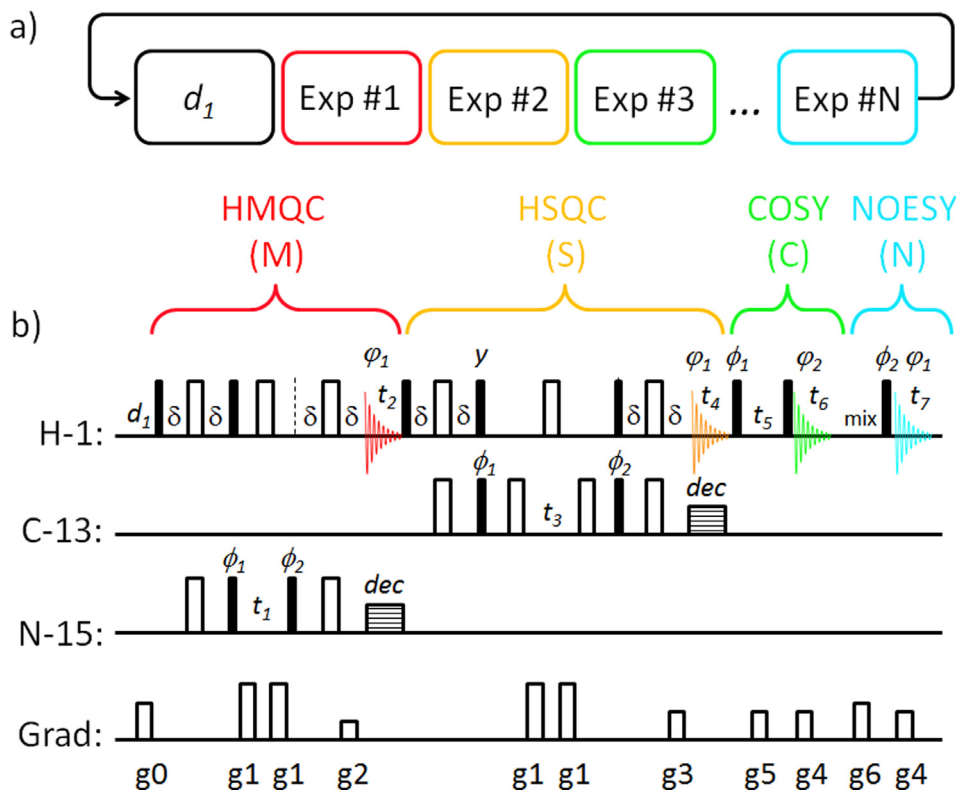
Fig. 9. a) Assembling NOAH modules into supersequences employing only a single recovery delay, d_1. b) The NOAH-4 MSCN supersequence consists of four NOAH modules – ^{15}N HMQC (M), ^{13}C HSQC (S), COSY (C) and NOESY (N). All pulses are applied with phase 'x' unless indicated otherwise and all gradients are of 1 *ms* duration. Phase cycles: $\phi_1 = x, -x$; $\phi_2 = x, -x, -x, x$; receiver phase cycles: $\varphi_1 = x, -x, -x, x$; $\varphi_2 = x, -x$; gradients (G/cm): g0 = 7, g1 = 40, g2 = 8.1, g3 = 20.1, g4 = g5 = 20, g6 = 17; the polarities of gradient pulses g1 and g4, and all receiver phases, are inverted for even increments. J-evolution delays (δ) set to $0.25/^1J(NH)$ and $0.25/^1J(CH)$ in the HMQC and HSQC modules, respectively; *mix* is the NOESY mixing time; the 180° ^{13}C pulses are constant adiabaticity WURST (wideband, uniform rate, smooth truncation) pulses. Figure adapted from Ref. [69] with permission from.

The use of multi-FID detection has also been combined with time-sharing, as exemplified in the recording of C—H and N—H HMBC spectra in a single measurement [85]. The pulse sequence (see Fig. 8) called MATS HMBC (Multiple-Acquisition Time-Shared HMBC) exploits directly the residual transverse magnetization after the first FID, and can be used to simultaneously record up to four spectra – H-C HMBC, H-N HMBC, H-C HMBC-COSY and H-N HMBC-COSY. The COSY-type mixing can also be replaced with isotropic mixing to produce the corresponding TOCSY versions of the experiment. The HMBC and HMBC-COSY experiments share the same t_1 evolution period, ensuring perfect spectral alignment and facilitating peak assignments. The technique has also been extended to HSQC / HSQC-TOCSY experiments [82,84].

3.1.3. NOAH supersequences

NOAH (NMR by Ordered Acquisition using ^{1}H-detection) experiments combine several techniques for multiple FID detection, allowing multiple complementary spectra to be recorded in a single measurement [69,70]. Supersequences are constructed by linking individual, specially adapted basic NMR sequences (modules) according to the domino principle – the tailored output of one module serves as an input to the following module (Fig. 9a). Hence, a supersequence is defined as a concatenated sequence of such modules. Conceptually, NOAH experiments aim to exploit different ^{1}H magnetization reservoirs that exist in molecules for each module, so that these may be sampled in succession without the need for lengthy recovery delays between modules. For example, protons that are bound directly to ^{13}C may be differentiated from those bound to ^{12}C or to ^{15}N, and hence separately manipulated and sampled. It has been proposed that hundreds of NOAH-type supersequences can be constructed from basic NMR sequences, by combining 2D HMQC, HSQC, HMBC, COSY, DQF-COSY, TOCSY, NOESY and ROESY adapted as NOAH modules [69]. To distinguish between these experiments, a nomenclature has been adopted that describes a NOAH-*N* experiment as comprising *N* modules with each identified by a single letter code. For example, a NOAH-3 SCN comprises sequential HSQC (S), COSY (C) and NOESY (N) modules.
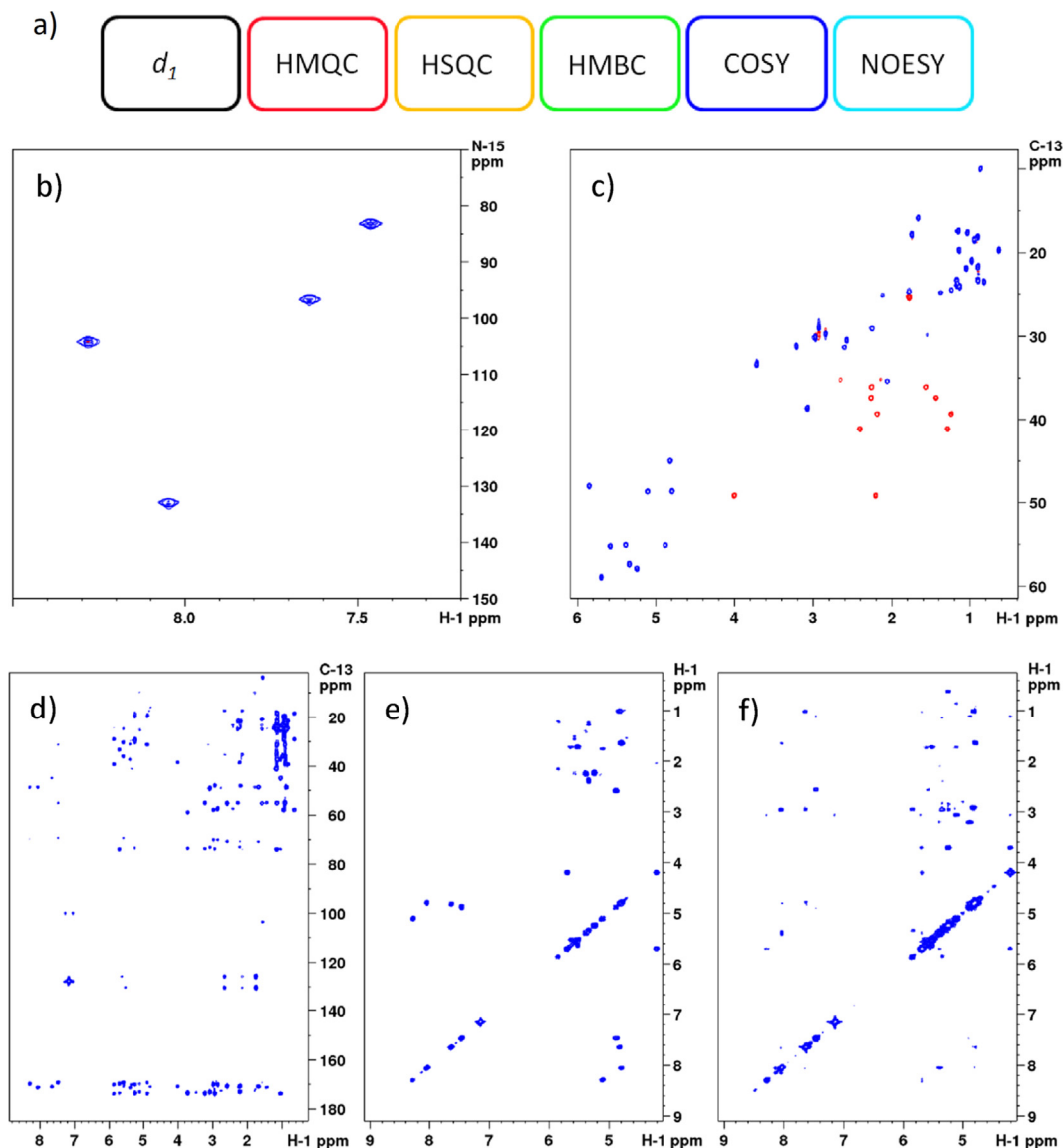
Fig. 10. a) Order of the NOAH modules in the NOAH-5 MSBCN supersequence used to record five 2D spectra in a single measurement – b) ^{15}N HMQC, c) multiplicity edited ^{13}C HSQC, d) ^{13}C HMBC, e) ^{1}H-^{1}H COSY and f) ^{1}H-^{1}H NOESY; the sample is 50 mM cyclosporine in benzene d_6; the spectra were recorded in 44 min with 2 scans per increment and 512 t_1-increments per module, resulting in a 2 k × 2560 raw data matrix; AVANCE III spectrometer equipped with a TCI CryoProbe. Reproduced from Ref. [69] with permission.

Several NMR techniques achieve significant time savings by reducing the magnetization recovery time, d_1, which is typically by far the longest time period in conventional NMR experiments [9–14]. NOAH supersequences require only one recovery delay d_1 to record several 2D spectra, thus offering significant time savings that increase as more modules are combined into a single supersequence. In addition to the significant time efficiency, recording the required spectra in a single measurement benefits from the fact that all spectra are collected under identical conditions and in an identical experimental environment. This can be particularly beneficial when used in automated structure elucidation applications.

As an example, consider one such NOAH-4 supersequence consisting of four modules as shown in Fig. 9b [69]. In this example, the NOAH-4 MSCN experiment starts with the ^{15}N HMQC module (abbreviated by the letter M), derived from the ASAP-HMQC pulse sequence [13]. The HMQC rather than HSQC sequence is chosen for recording the ^{15}N-^{1}H correlation spectra because it manages the bulk magnetization more efficiently, and typically the N-H multiplicity editing provided by HSQC is of little interest in small molecule NMR. However, the differences are quite marginal and in the presence of ^{1}H-^{1}H couplings the HSQC experiment is more efficient [14] so that either of the two modules can be used depending on the spin systems involved. The ^{15}N-^{1}H HMQC module only uses the magnetization of protons directly bound to the ^{15}N nuclei, i.e. 0.36% of the total proton magnetization, and the rest of the bulk magnetization (minus losses due to pulse imperfections) is kept along the Z axis for use in the following NOAH modules. The HMQC module is followed by the ^{13}C-^{1}H HSQC module (abbreviated with the letter S), with optional multiplicity editing. This module is derived from the ASAP-HSQC pulse sequence [14] and exploits the magnetization of protons directly bound to ^{13}C nuclei that constitute 1.1% of the total proton magnetization. The rest of the bulk proton magnetization is kept along the Z axis for most of the duration of the HSQC module, including the FID detection period. Finally, this NOAH-4 supersequence is completed with COSY (C) and NOESY (N) modules derived from the COCONOSY experiment [30,31]. Spectra of cyclosporine recorded using a NOAH-5 (MSBCN) supersequence that also includes the HMBC module (B) are shown in Fig. 10.

Whilst a large number of NOAH supersequences can be constructed from the basic modules, not all combinations are equally efficient and/or practical. For instance, the BC (HMBC/COSY) combination suffers from proton T_2 relaxation losses. Specifically, following the HMBC module the bulk magnetization is left in the transverse (X,Y) plane and is subjected to transverse relaxation (T_2) effects, which can be quite different for individual peaks in the molecule(s) of interest. This produces different levels of cross-peak attenuation in the 2D COSY spectra, and in extreme cases may lead to loss of correlation information.

As an example, consider the SBC supersequence (HSQC-HMBC-COSY) that is similarly susceptible to such losses. The S and B modules can, however, be swapped and arranged optimally by placing the least sensitive, HMBC, module before the HSQC module. To achieve this, a specially designed ZZ-HMBC module that preserves the magnetization of protons directly bound to ^{13}C (retained for use in the following HSQC element) was introduced [70]. The bulk proton magnetization that is dephased by the coherence selection gradients of the HMBC module partially recovers during the HMBC and HSQC acquisition periods, to yield longitudinal magnetization that may be utilized for the final COSY module. Here, the conventional COSY sequence was replaced with the ASAP-COSY module to ensure more uniform COSY peak intensities, reducing the variability that may result from differing proton longitudinal (T_1) recovery rates. Thus, the resulting NOAH-3 BSC supersequence proves to be a better-balanced experiment than the alternative SBC.

A number of variations on the BSX triplet sequence have been presented in which the final module (X) has been substituted with various alternative homonuclear correlation experiments that have found widespread use in small molecule characterization, including DQF-COSY, TOCSY, NOESY, ROESY and the more recent Clean, In-Phase COSY (CLIP-COSY) sequence [86]. In comparison to traditional sequential data collection, all these experiments gave an approximately 2-fold time saving. NOAH methods have also been shown to be compatible with non-uniform sampling (NUS) schemes, to further provide time efficiency when sample concentrations allow, or alternatively to enhance spectral resolution.

Extension of the BSC triplet scheme to include the ^{15}N HMQC module has also been demonstrated, yielding the NOAH-4 BMSC or NOAH-5 BMSCN experiments. For these, it is necessary to select and preserve both the one-bond ^{1}H-^{15}N and ^{1}H-^{13}C magnetization reservoirs prior to the ^{1}H-^{13}C HMBC module, which has been achieved by use of a double-ZZ filter at the start of the sequence [33]. The collection of ^{15}N and ^{13}C HSQC spectra from a NOAH-2 S_N-S_C experiment has been proposed for observation of protein-ligand
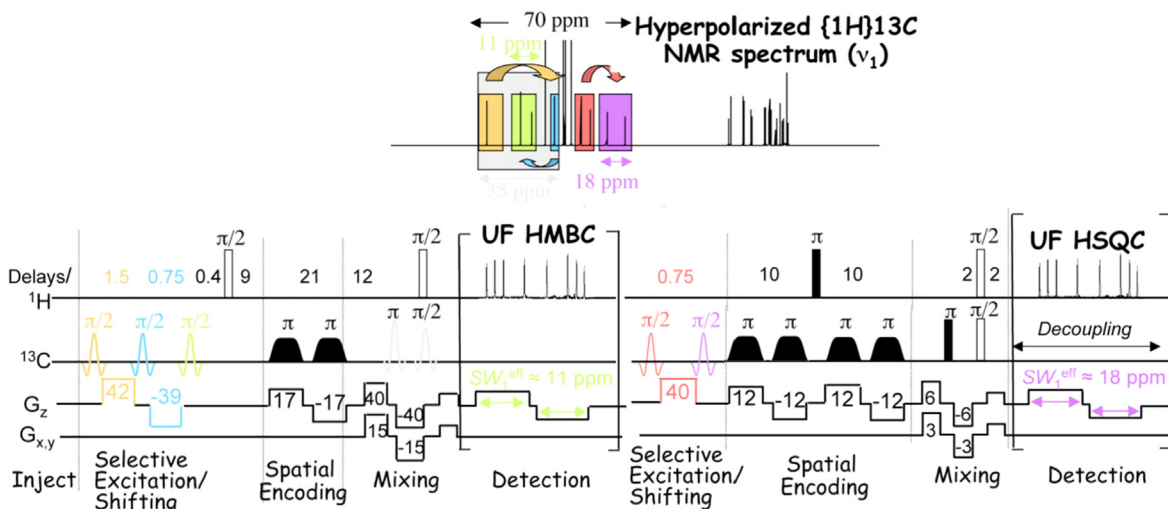
Fig. 11. Interleaved ultra-fast 2D C-H HMBC/HSQC pulse scheme (UF NOAH-2 BS supersequence) ; δ = 0.4 ms, Δ_1 = 9 ms, Δ_2 = 12 ms, τ = 0.4 ms, dwell time, dw = 2 μs. Reproduced from Ref. [88] with permission.

interactions, through the simultaneous monitoring of the ^{15}N HSQC spectra of an isotopically labelled protein and the ^{13}C HSQC spectra of small molecule ligands at natural isotopic abundance [75]. This approach independently samples magnetization from different molecular species and ensures these are collected under identical conditions at the same time, as was illustrated for the 140 amino acid neuronal protein α-*synuclein* with a mixture of monosaccharides. The proposed sequence also incorporated BIRD pure-shift ^{1}H homonuclear broadband decoupling in the ^{13}C module to improve resolution [87], leading to the title PROSMASH-HSQC^2 (PROtein-HSQC and SMAll molecule-HSQC Signals with Homodecoupling).

3.1.4. Interleaved ultrafast multi-FID experiments

Giraudeau *et al.* have proposed an interleaved ultrafast (UF) 2D ^{13}C-^{1}H HSQC/HMBC pulse scheme [88] designed for applications in hyperpolarized samples [89–91]. This allowed the recording of 2D ^{13}C-^{1}H HMBC and HSQC spectra in *ca.* 1 mM mixtures of natural products in a single scan. The pulse scheme shown in Fig. 11 is based on spatially selective excitation to record the HMBC and HSQC spectra sequentially. A new spatial/spectral encoding technique that "shifts" the ^{13}C resonances to arbitrary positions in UF NMR spectra was proposed, to overcome the problems associated with wide spectral ranges that require the use of prohibitively strong acquisition gradients.

The UF 2D ^{13}C-^{1}H HMBC module starts with a series of selective excitation pulses on the non-protonated ^{13}C sites, followed by magnetic field gradient pulses imposing site-specific spatial encoding. Suitably chosen gradients shift the ^{13}C resonances to arbitrary positions in the indirectly detected dimension of the UF 2D spectrum. In this way the final spectral window is reduced, thus minimizing the required strength of the acquisition gradients and enabling characterization of ^{13}C bandwidths in excess of 70 ppm with high resolution in both the direct and indirect domains. The new site-specific spatial encoding scheme is followed by constant-time spatial encoding, additional evolution delays, pulses and coherence-selective gradient pulses designed to extract the sought-for C-H correlations.

Notably, all the remaining ^{13}C sites retain their initial hyperpolarized state save for the ^{13}C sites that were selected in the HMBC module. Consequently, UF 2D HSQC based on similar spectral/spatial encoding schemes is started immediately after the HMBC module, taking advantage of the remaining hyperpolarized ^{13}C nuclei and providing information about directly bonded ^{13}C-^{1}H spin pairs in the same measurement without the need to repolarize the sample.

3.1.5. Spatial encoding techniques for multiple samples

Spatial encoding and spatial selection techniques are finding an increasing number of applications in NMR and have been extensively discussed by Dumez [57]. The SUSHY technique (Spectral Unraveling by Space-selective Hadamard spectroscopY) proposed by Murali *et al.* [92] allows recording NMR spectra from typically 4 samples simultaneously, using regular NMR probes and standard configurations of NMR hardware. Up to four sample tubes are loaded in a modified spinner turbine and a standard 5 mm liquids NMR probe, albeit equipped with triple axis gradients, is used. The individual spectrum from each sample is extracted by adding and subtracting data that are recorded simultaneously from all 4 samples, combining the principles of spatially resolved spectroscopy and Hadamard encoding [19]. This technique has a potential to reduce the total experiment time by up to a factor of four in 4-tube mode. Note, however, that in the 4-sample setup a minimum of four scans per time increment is required for the Hadamard encoding/decoding to work.

The PALSY technique (PArallel Localized SpectroscopY) [93] is based on slice selective excitation in a regular (5 mm) NMR sample tube and allows recording several 2D spectra in a single measurement. The sample is virtually divided into a discrete number of non-overlapping slices that relax independently during consecutive scans of the experiment. 2D COSY, 2D DQF-COSY and 2D TQF-COSY spectra have been recorded simultaneously in 3 min with 128 increments in t_1 dimension.

Up to 19 capillary samples have been placed in a single NMR coil and their spectra separated using spectral localization [94]. Note that at least M gradient increments are required to obtain M clean spectra with these methods, making this intrinsically a slow technique. Furthermore, the sensitivity is low due to the low effective filling factor for each individual sample.

3.1.6. Biomolecular multi-FID experiments

Ramachandran et al. have proposed several experiments with sequential acquisition of ^{1}H detected 3D experiments [95,96]. Two such supersequences – 3D HCCNH / HNCACONH and 3D HNCOCANH / HNCACONH – were designed for protein backbone assignment from a single measurement. The approach is based on similar experiments developed for applications in solids [97–99]. Namely, two experiments that share part of their magnetization transfer pathway are started simultaneously. At some point, the ^{13}C or ^{15}N magnetization belonging to one of the pathways is 'parked' as longitudinal magnetization while the first data set is acquired. Then, the stored ^{13}C/^{15}N magnetization is recovered to complete the coherence pathway of the second experiment and the second data set is acquired. As a result, the total experiment time of the two 3D experiments is cut by a factor of about two.
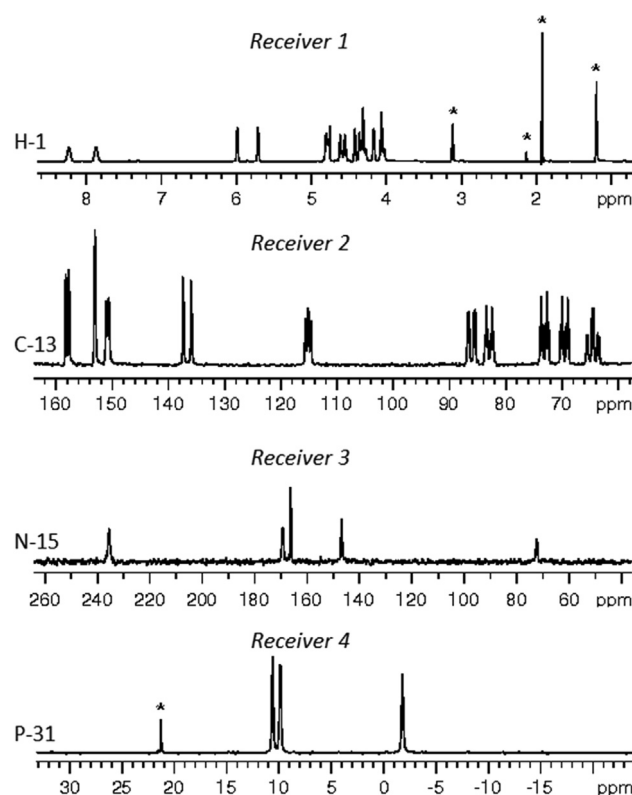
Fig. 12. Four 1D spectra of CN-labelled guanosine triphosphate in DMSO d_6 recorded simultaneously on a Varian 600 MHz NMR system. Impurities in the ^{1}H and ^{31}P spectra are marked with asterisks. Reproduced from Ref. [101] with permission.
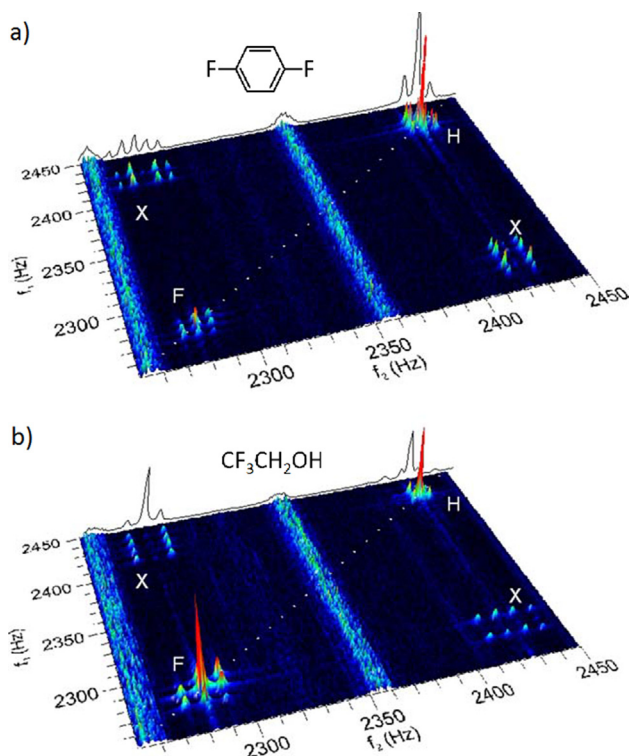
Fig. 13. The 2D ^{1}H/^{19}F COSY NMR spectra of a) difluorobenzene and b) trifluoroethanol recorded at Earth's magnetic field (*ca.* 60 μT) corresponding to 2.28 kHz (^{19}F) and 2.43 kHz (^{1}H) resonance frequencies with *X* representing the cross-peaks between ^{1}H and ^{19}F nuclei. Reproduced from Ref. [102] with permission.

The HNCACONH part of the sequential 3D HCCNH / HNCACONH experiment starts by transferring the ^{1}H^N magnetization along the pathway ^{1}H$^N(t_1) \rightarrow ^{15}$N $\rightarrow ^{13}$Cα $\rightarrow ^{13}$CO $\rightarrow ^{15}$N$(t_2) \rightarrow ^1$H$^N(t_3)$ via the corresponding one-bond couplings. At the same time the HCCNH part of the 3D experiment is started from the side chain protons (^{1}H^{sc}) and follows a similar pathway ^{1}Hsc$(t_1) \rightarrow ^{13}$Csc $\rightarrow ^{13}$Cα $\rightarrow ^{15}$-N$(t_2) \rightarrow ^1$H$^N(t_3)$. The two coherence pathways intersect at the ^{13}C$^\alpha$ site, at which point part of the ^{13}Cα magnetization is parked as longitudinal magnetization whereas the remaining ^{13}Cα magnetization is transferred to ^{15}N and then to ^{1}H^N for detection, completing the HCCNH part of the experiment. Following the 3D

HCCNH t_3-acquisition period, the preserved ^{13}Cα magnetization is used in the remaining part of the 3D HNCACONH experiment.

Provided that the amino acid type information is available from conventional experiments, e.g., CBCACONH, the sequential 3D HCCNH / HNCACONH data set provides sufficient information for unambiguous sequential resonance assignment of the backbone ^{15}N and ^{1}H^N nuclei as well as the side-chain protons. A similar approach is used in the sequential 3D HNCOCANH / HNCACONH pulse scheme, [96] and experiments designed for medium-size protein studies – 3D HA(CA)NH / HA(CACO)NH, 3D HA(CA)NH / H(N)CAHA and 3D H(N)CAHA / H(CC)NH [95].

It is worth noting that, in general, storing non-equilibrium magnetization as longitudinal magnetization for prolonged periods of time is subject to differential relaxation effects. In solids, T_1 relaxation is typically considerably slower than in solutions (liquids) whereas the duration of the FIDs is typically significantly shorter. Therefore, parking the relevant coherences as longitudinal magnetization during the FID in solids experiments is more efficient. In liquids the same approach is prone to signal losses due to longer acquisition times and differences in the relaxation rates of non-equilibrium states for different sites within the molecule, as observed in the NOAH experiments for small molecules [70,86]. This problem can be tackled by reducing acquisition times in the directly detected dimension, which combined with linear prediction can improve the performance of 3D experiments [96].

3.2. Experiments with multi-nuclear detection

3.2.1. Small molecule experiments

Over the past decade, multi-receiver technology has been gradually introduced to NMR on commercial NMR systems, initially as a special accessory and more recently as a standard feature making simultaneous detection of multiple FIDs from various nuclear species routine. On state-of-the-art NMR systems every channel is fitted with a dedicated receiver, enabling simultaneous detection of as many nuclear species as the number of channels, typically up to four (see Fig. 12). This opens up new avenues in multi-dimensional NMR experiment design, leading to development of new types of NMR experiments [100,101].

3.2.1.1. H/F COSY at Earth's magnetic field. At magnetic field strengths as low as Earth's field (*ca.* 60 μT), the resonance frequencies of some nuclear species become sufficiently close to enable simultaneous detection of their resonances in the same NMR spec-
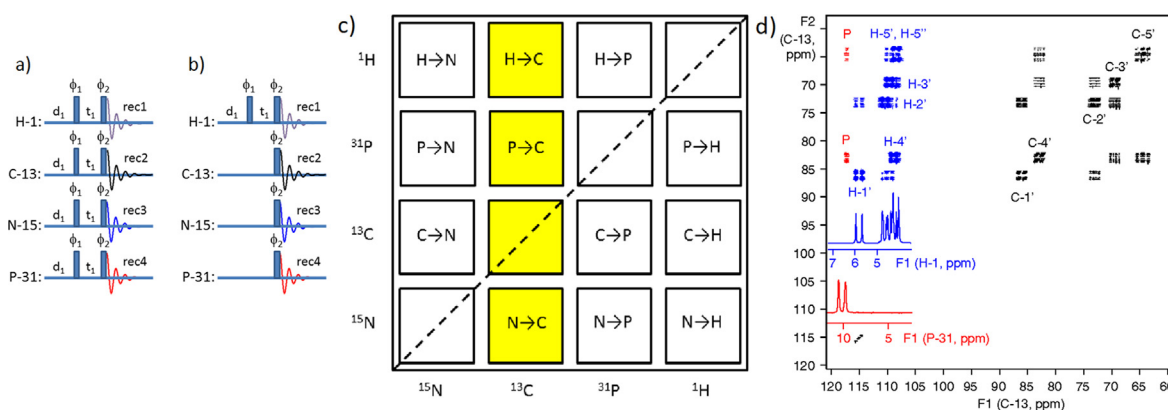
Fig. 14. a) Quadruple-COSY pulse sequence consisting of four conventional COSY pulse sequences applied in parallel; b) PANSY COSY pulse scheme involving four parallel receivers; c) the correlations that are expected in experiment (a), where the arrows indicate direction of the polarization flow; d) the ^{13}C-detected 2D plane recorded in receiver 2 shows correlations highlighted in (c). The spectra were acquired using the quadruple COSY pulse scheme shown in (a) on a 600 MHz Varian NMR system equipped with four receivers and a 5 mm HCNP probe. The insets show the chemical shift scales and the corresponding 1D spectra of the indirectly detected ^{1}H (in blue) and ^{31}P (in red) nuclei. The sample is CN-labelled guanosine triphosphate in DMSO d_6. Reproduced from Ref. [101] with permission.
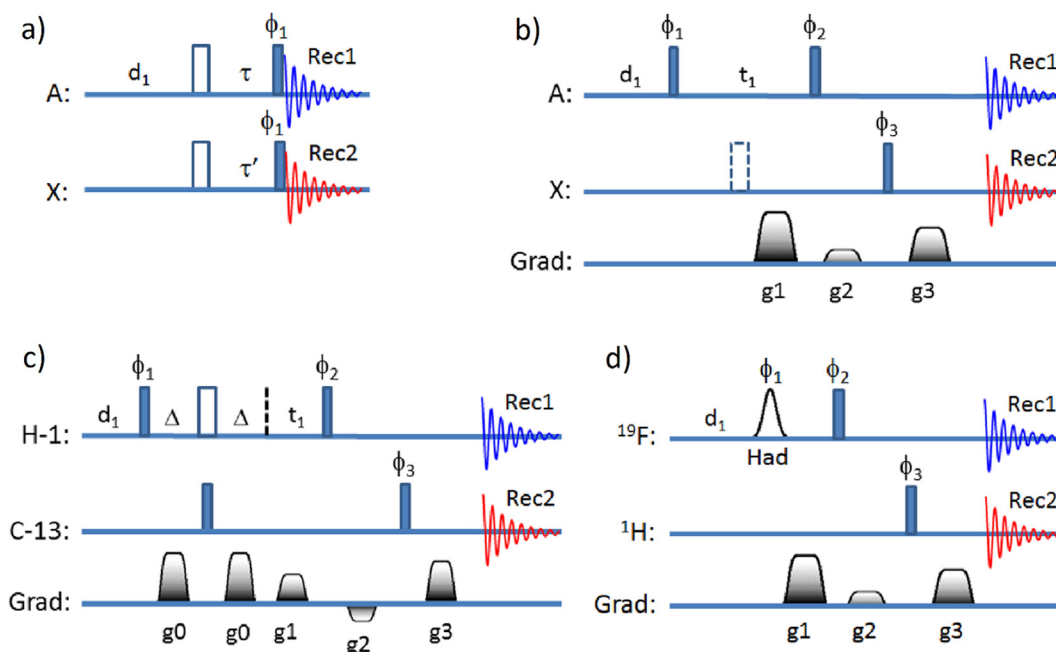
Fig. 15. a) Parallel inversion-recovery experiment where *A* and *X* represent different types of nucleus. The open rectangles are π pulses that for H/F measurements were replaced with adiabatic CA WURST pulses; b) the gradient version of the basic PANSY-COSY pulse scheme, where the dotted rectangle represents an optional decoupling π pulse; c) the pulse sequence with suppression of one-bond ^{13}C-^{1}H correlations; d) the Hadamard version of the PANSY-COSY experiment. Phase cycling: $\phi_1 = x, -x$, $\phi_2 = \phi_3 = 2x, 2(-x)$, *Rec1 = x, -x, Rec2 = x, -x*; gradients (G/cm, ms): g0 = (7, 1), g1 = (5, 1), g2 + g3 = g1, g3/g1 = γX/γA (in b), γH/γF (in b) and γC/γH (in d). Adapted from Ref. [105] with permission.

trum. While at a suitably low magnetic field strength homonuclear chemical shifts essentially vanish, resonances from different nuclear species can still be sufficiently separated and easily observed. Callaghan *et al.* have acquired 2D COSY spectra of fluorinated compounds – trifluoroethanol and para-difluorobenzene – showing that the ^{1}H and ^{19}F diagonal peaks and the corresponding H/F cross-peaks appear in the same spectrum (see Fig. 13) [102].

Zhu *et al.* described simultaneous ^{1}H and ^{19}F detection of nuclear spin optical rotation (NSOR) in a single NMR spectrum at sub-millitesla field [103]. The simultaneously acquired optical signal allowed calculation of the NSOR constants that depend on the hyperfine interaction between nuclear spins and electrons.

Heteronuclear ^{1}H-^{19}F *J*-coupling was also observable in the NSOR signal.

3.2.1.2. Quadruple COSY with 4 receivers. At the magnetic field strengths of commercial high-resolution NMR spectrometers, observing the resonance frequencies of several nuclear species in the same 2D spectrum is not normally feasible as the tuning bandwidth of NMR probes is quite narrow. A notable exception to this is a non-resonant planar microcoil able to detect nuclei across a 61–400 MHz bandwidth [104]. However, state-of-the-art multinuclear NMR probes are typically tuned simultaneously and selectively to resonance frequencies of several nuclei. For instance, probes typi-
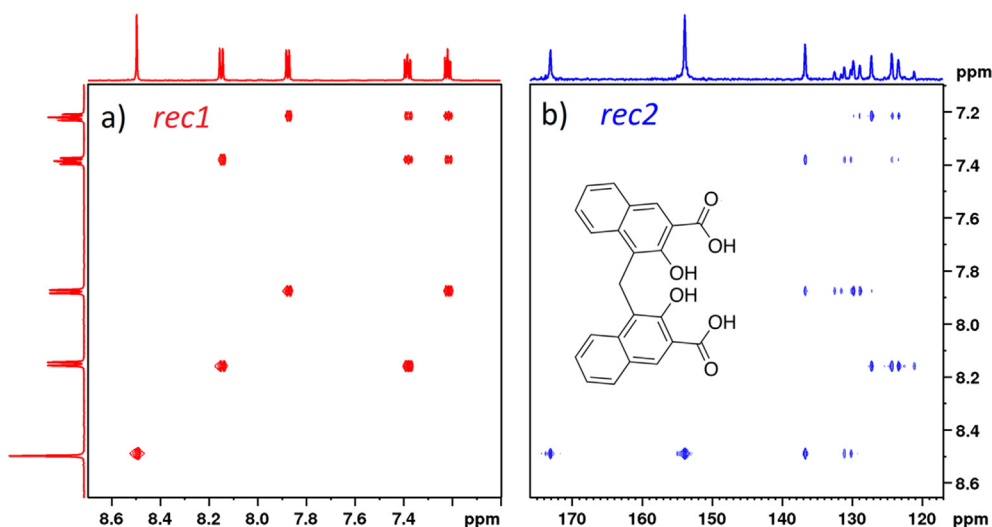
Fig. 16. Spectra of pamoic acid in DMSO d_6 recorded with the pulse scheme of Fig. 15c on a 500 MHz (^{1}H) Bruker Avance III HD system equipped with two receivers; a) the ^{1}H-^{1}H COSY spectrum acquired in ^{1}H receiver and (b) the ^{1}H-^{13}C COSY spectrum (akin to ^{13}C HMBC) acquired with ^{1}J(^{1}H,^{13}C) suppression in the F_1 domain by the second (^{13}C) receiver [105].
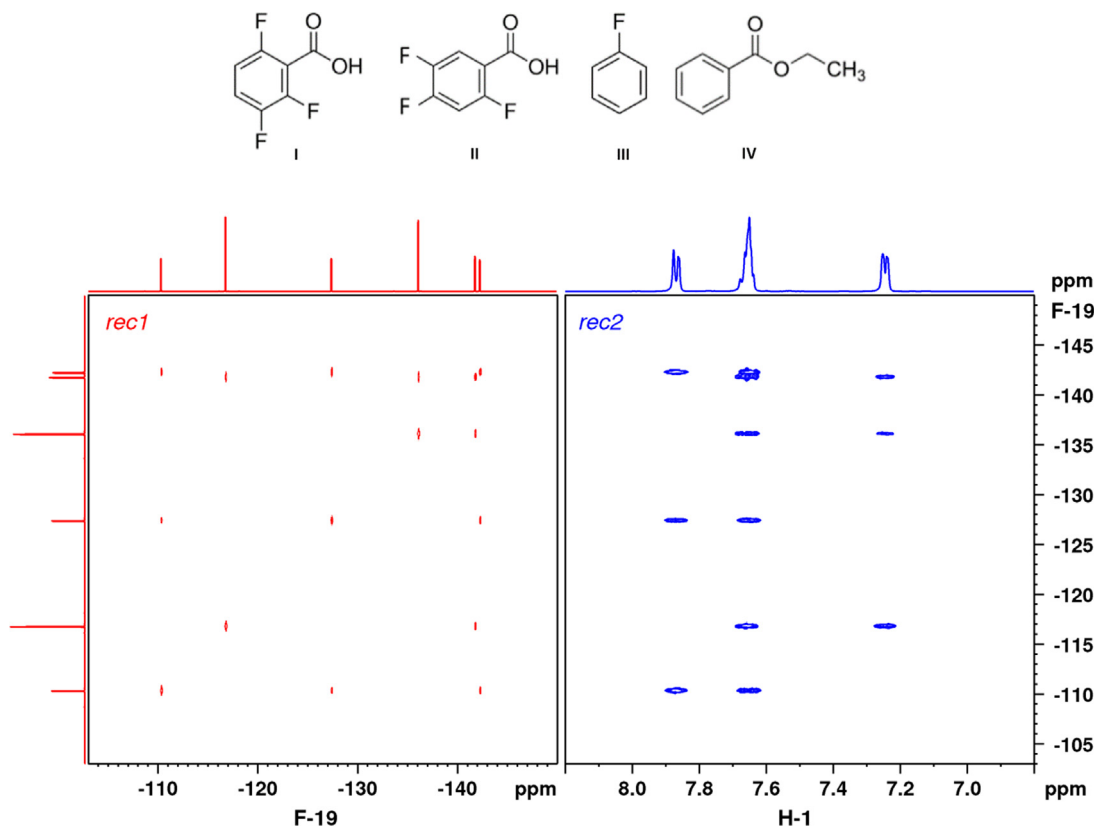
Fig. 17. The 2D Hadamard (**H$_8$** encoding matrix) ^{19}F-^{19}F COSY (left panel) and ^{19}F-^{1}H COSY (right panel) spectra of a mixture of fluorinated compounds (I, II and III) recorded in parallel using the pulse scheme of Fig. 15d on an Avance III HD 700 MHz (^{1}H) spectrometer equipped with two receivers and QCIF CryoProbe; the raw data matrix size was 8 × 1024 data points, one scan per increment, repetition delay d_1 = 0.2 s. The total experiment time was 3 s. Reproduced from Ref. [38] with permission.

cally used in biomolecular applications are simultaneously tuned to nuclei such as ^{1}H, ^{13}C, ^{15}N and ^{31}P. This allows simultaneous irradiation of several nuclear species, and on NMR systems equipped with multiple receivers, simultaneous detection of FIDs from several nuclear species. An example of a 2D quadruple COSY spectrum recorded by simultaneously pulsing on and detecting FIDs from four nuclear species is shown in Fig. 14. Note that in the four 2D COSY spectra, asymmetric off-diagonal cross-peaks due to heteronuclear COSY correlations appear simultaneously with homonuclear cross-peaks that are symmetric with respect to the diagonal peaks. Furthermore, the intensities of the heteronuclear correlations depend on the gyromagnetic ratios, γ, of the indirectly detected nuclei serving as the polarization source. As expected, polarization transfer from low-γ nuclei such as ^{15}N to high-γ nuclei is inefficient and the corresponding cross-peaks in this spectrum are too weak to be visible. In practice, the first (excitation) 90° pulses on low-γ nuclei are often omitted (see Fig. 14), leading to a simplified version of the quadruple-COSY named PANSY-COSY (PANSY - Parallel Acquisition Nmr SpectroscopY) [24].

3.2.1.3. Parallel acquisition experiments – PANSY. PANSY experiments involve simultaneous (parallel) acquisition of FIDs from several nuclear species (see Fig. 2) [24]. Apart from the basic pulse and acquire experiment, one of the simplest parallel acquisition experiments is the simultaneous inversion-recovery T_1 relaxation measurement [38]. In this, two inversion-recovery pulse sequences are executed in parallel (see Fig. 15a), but an interleaved version of the experiment is also feasible. In both cases the recovery time depends on the T_1 of the most slowly relaxing nucleus. It should
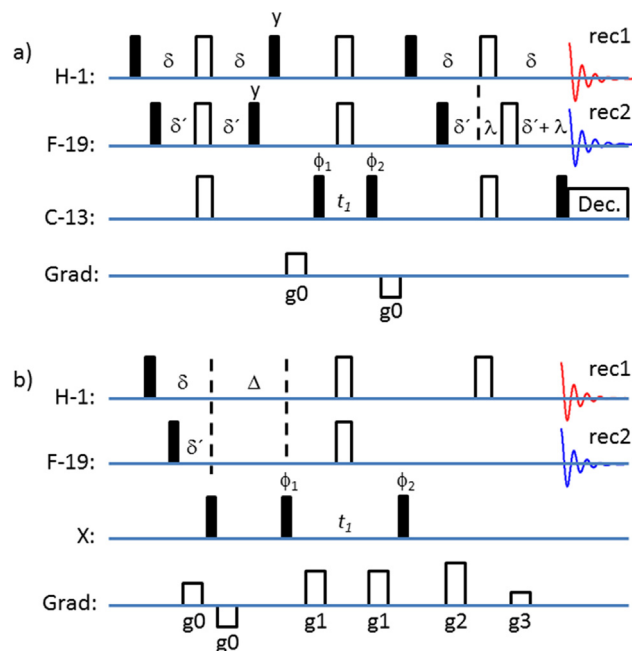
Fig. 18. a) ^{1}H/^{19}F-^{13}C PANSY HSQC sequence; b) ^{1}H/^{19}F-X PANSY HMBC sequence; delays: δ = 0.5/^{1}J(^{1}H-^{13}C), δ = 0.5/^{1}J(^{19}F-^{13}C), Δ = 0.5/^{n}J(^{1}H-X), the λ delay is adjusted to ensure simultaneous refocusing of the ^{1}H and ^{19}F magnetization; all pulses were applied with phase 'x', unless indicated otherwise, ϕ_1 = x, $-x$, ϕ_2 = x, x, $-x$, $-x$; $rec1$ = $rec2$ = x, $-x$, $-x$, x; gradients (G/cm, ms): g0 = (33.0, 1), g1 = (20, 1), 2 g1/ (g2 + g3) = γF/γX, 2 g1/(g2 - g3) = γH/γX; the amplitudes of the g1 gradient pulses were inverted every second scan for echo/anti-echo data in F_1.

be noted that the relaxation dynamics are slightly different in these two types of experiments.

The PANSY-COSY experiment [24] is perhaps one of the more versatile experiments, particularly in high-γ / high natural abundance situations. The basic pulse scheme for the gradient (echo - anti-echo) version of the PANSY-COSY experiment involving two receivers is shown in Fig. 15b. It starts with an excitation pulse on the A nuclei (typically high γ nuclei, such as ^{1}H, ^{19}F or ^{31}P) and is followed by a t_1 evolution period and an optional X-decoupling pulse (X = ^{13}C, ^{15}N, ^{19}F, ^{29}Si, ^{31}P or other magnetically active nuclei). Coherence selection gradient pulses are applied with $g3/g1 = \gamma X/\gamma A$ and $g1 = g2 + g3$ such that A nuclei experience the sum of $g2$ and $g3$ while the X nuclei 'see' only the $g3$ gradient [97,101]. Notably, in isotopically dilute spin systems (e.g., ^{13}C, ^{15}N, ^{29}Si) the homonuclear and heteronuclear COSY correlation spectra originate from different molecules (isotopomers). In abundant spin systems this is not the case and a reduced (e.g., 45°) flip-angle ^{1}H read pulse may be applied to avoid bleaching of some of the cross-peaks in the ^{1}H -^{1}H COSY spectra [38].

^{13}C-detected ^{1}H-^{13}C COSY spectra can be simplified by suppressing the one-bond C-H correlations using a $^1J(^{13}$C-^{1}H$)$ filter, as shown in Fig. 15c [105]. ^{1}H/^{13}C PANSY-COSY spectra of pamoic acid recorded with the pulse sequence of Fig. 15c deliver ^{1}H-^{1}H COSY and long-range ^{1}H-^{13}C correlated spectra (akin to ^{13}C HMBC) in a single 2D experiment (see Fig. 16).

^{1}H/^{19}F PANSY-COSY experiments involve parallel acquisition of homonuclear ^{1}H-^{1}H COSY and heteronuclear ^{1}H-^{19}F COSY, while ^{19}F/^{1}H PANSY-COSY produces ^{19}F-^{19}F COSY and ^{19}F-^{1}H COSY spectra. The gradient version of the PANSY-COSY pulse sequence for abundant nuclei is shown in Fig. 15b. The ^{19}F bandwidth is often much wider than the ^{1}H bandwidth. Therefore, more t_1-increments are generally required in the ^{19}F/^{1}H PANSY-COSY experiment (F_1 = ^{19}F) than the ^{1}H/^{19}F PANSY-COSY (F_1 = ^{1}H) to achieve similar spectral resolution. On the other hand, in samples with $T_1(^{19}$F$) < T_1(^1$H$)$ a shorter repetition time can be used in the ^{19}F/^{1}H PANSY-COSY experiment in contrast with the interleaved experiments. Therefore, the choice of experiment largely depends on the properties of the sample.

Hadamard encoding [19] can be used to circumvent the problem with wide ^{19}F bandwidths, as long as the ^{19}F spectra are sparse. Furthermore, the Hadamard version of the ^{19}F/^{1}H PANSY-COSY experiment exploits the shorter ^{19}F relaxation times, producing ^{19}F-^{19}F COSY and ^{19}F-^{1}H COSY spectra in as little as 3 s, as compared to the 3 min required to record the same spectrum with conventional sampling and the same repetition rate (see Fig. 17).

Significant time savings and sensitivity improvement in PANSY experiments can be achieved if polarization is transferred from high-γ, relatively rapidly relaxing nuclei such as ^{1}H and ^{19}F, to low-γ nuclei, such as ^{13}C or ^{15}N, with much slower T_1 relaxation. Mutual decoupling of the directly observed nuclei during acquisition using conventional decoupling methods is generally not possible. Therefore, parallel acquisition experiments are usually applied to spin systems with small and/or unresolved mutual J couplings. Spectral simplification by various types of 'virtual' decoupling remains a possibility.

As an example, the PANSY ^{1}H/^{19}F-^{13}C HSQC pulse sequence is shown in Fig. 18a [106]. Essentially, two HSQC sequences are simply executed in parallel, sharing the indirect ^{13}C (or ^{15}N) dimension, in this experiment. The INEPT delays in the two subsequences are adjusted to account for the differences between the $^1J(^1$H-^{13}C$)$ and $^1J(^{19}$F-^{13}C$)$ couplings. The repetition rate in this case is determined by the longest relaxation time of the two types of the high-γ nuclei, usually ^{1}H. The sensitivity advantages with respect to the conventional data acquisition approach are similar to those in time-shared experiments.

The ^{1}H/^{19}F-X (X = ^{13}C or ^{15}N) PANSY-HMBC pulse sequence shown in Fig. 18b serves as an example of a parallel heteronuclear correlation experiment that employs coherence selection gradient pulses. The difference in gyromagnetic ratio between ^{1}H and ^{19}F nuclei is accounted for by inserting a proton refocusing pulse and a pair of balancing gradient pulses just before the parallel acquisition stage. In this arrangement the protons are affected by the difference between the two gradient pulses, while ^{19}F nuclei experience the sum. The difference between the $^1J(^1$H-^{13}C$)$ and $^1J(^{19}$F-^{13}C$)$ couplings involved in the respective ^1J filters is taken care of by delaying the starting point of the ^{19}F-^{13}C HMBC pulse
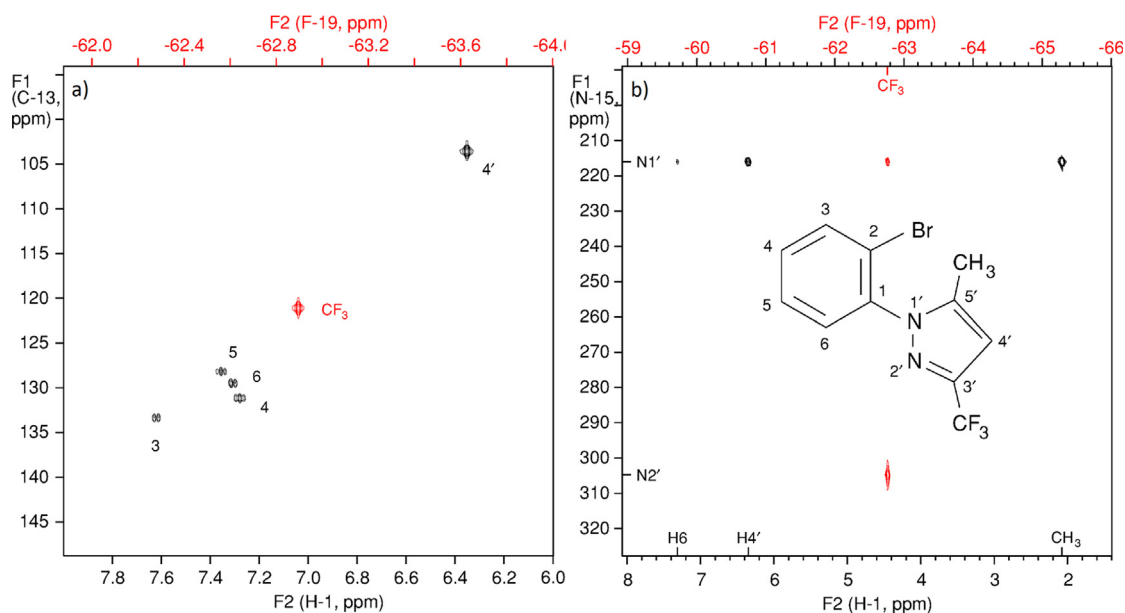
Fig. 19. Superposition of the ^{1}H/^{19}F-X PANSY spectra of 2-bromophenyl-3-trifluoromethyl-5-methylpyrazole recorded on Varian 600 MHz spectrometer using the pulse sequences of Fig. 18; ^{1}H-X cross-peaks are shown in black and ^{19}F-X cross-peaks and ^{19}F scale are shown in red. a) The PANSY-HSQC spectra recorded using the pulse sequence of Fig. 18a, X = ^{13}C; only the aromatic region is shown; experiment time was 22 min. b) The PANSY-HMBC spectra recorded using the pulse sequence of Fig. 18b, X = ^{15}N; the experiment time was 3 h 8 min. Reproduced from Ref. [106] with permission.
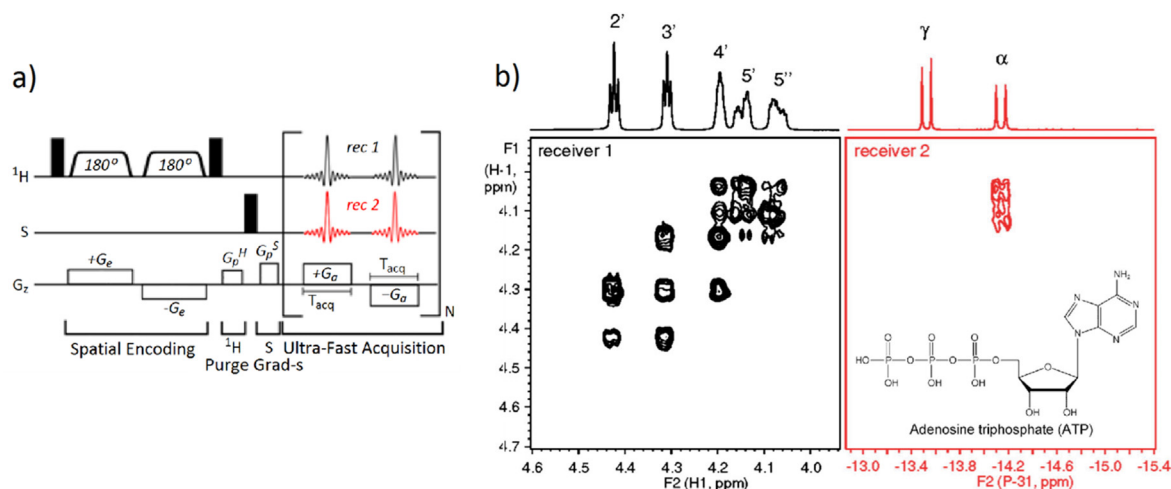
Fig. 20. a) The PUFSY-COSY pulse sequence for simultaneous acquisition of ^{1}H-^{1}H COSY and ^{1}H-X COSY in a single scan. b) ^{1}H/^{31}P PUFSY-COSY spectra recorded using the pulse sequence in panel (a) and $S = {}^{31}$P. The ^{1}H-^{1}H correlations detected in receiver 1 are shown in black while the ^{1}H-^{31}P spectrum acquired in receiver 2 is shown in red. Independently recorded 1D spectra are shown above the 2D spectra; $G_e = \pm10$ G/cm, $G_a = \pm9.6$ G/cm; $T_e = 30$ ms, $T_{acq} = 90$ μs and $N = 125$. Reproduced from Ref. [108] with permission.
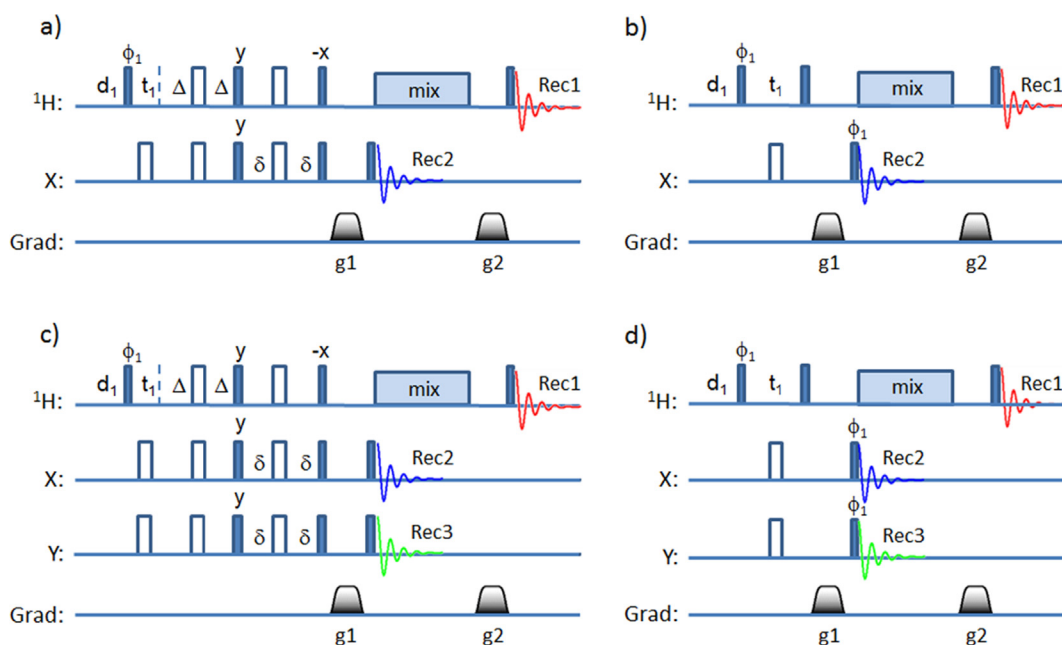
Fig. 21. Multi-receiver TOCSY/HETCOR pulse schemes designed for (a, b) two and (c, d) three receivers. Schemes (a) and (c) record 2D ^{1}H-^{1}H TOCSY and 2D ^{1}H-X,Y HETCOR spectra provided that the $^1J(^1$H-$X)$ and $^1J(^1$H-$Y)$ couplings in (c) are not very different and a good compromise for the INEPT delays $\varDelta$ and δ can be found; alternatively the X and Y refocusing pulses can be displaced so as to satisfy the polarization transfer requirements for both ^{1}H-X and X-Y spin systems. Phase cycling: $\phi_1 = x, -x$, Rec (all) = x, $-x$; spoiler gradient pulses $g1$ and $g2$ are of arbitrary strength. The pulse sequences (b) and (d) record 2D ^{1}H-^{1}H TOCSY and 1D spectra of any magnetically active nuclei, X and Y.

sequence by a short time, λ. In the ^{1}H/^{19}F-^{15}N PANSY HMBC experiment the $^1J(^{19}$F-^{15}N) filter is usually not required, allowing for more flexibility in setting the ^nJ-evolution delays.

The two 2D ^{1}H-^{13}C and ^{19}F-^{13}C HMBC spectra are overlaid in Fig. 19, emphasizing the shared F_1 dimension. This requires two different F_2 scales for the directly detected ^{1}H and ^{19}F dimensions, that are color coded along with the cross-peaks from the two 2D spectra. Thus the experiment essentially provides three-dimensional ^{1}H-^{19}F-^{13}C information and can be thought of as a reduced dimensionality experiment.

While interleaved versions of the experiments shown in Fig. 18 exist, not all PANSY sequences can be converted into inter-

leaved sequences, and vice versa. For instance, parallel acquisition experiments often involve a polarization transfer step between directly detected nuclei (see Fig. 2a) and, therefore, such pulse sequences have to be designed "from scratch" as opposed to using interleaved pulse schemes which are simply concatenated. Furthermore, parallel detection experiments typically involve a shared t_1 evolution period and therefore a joint F_1 axis. For this reason, PANSY spectra can also be seen as reduced dimensionality experiments, because they share one or more indirectly detected frequency domains [107]. Generally, PANSY experiments provide a different type of spectral information compared to interleaved experiments.
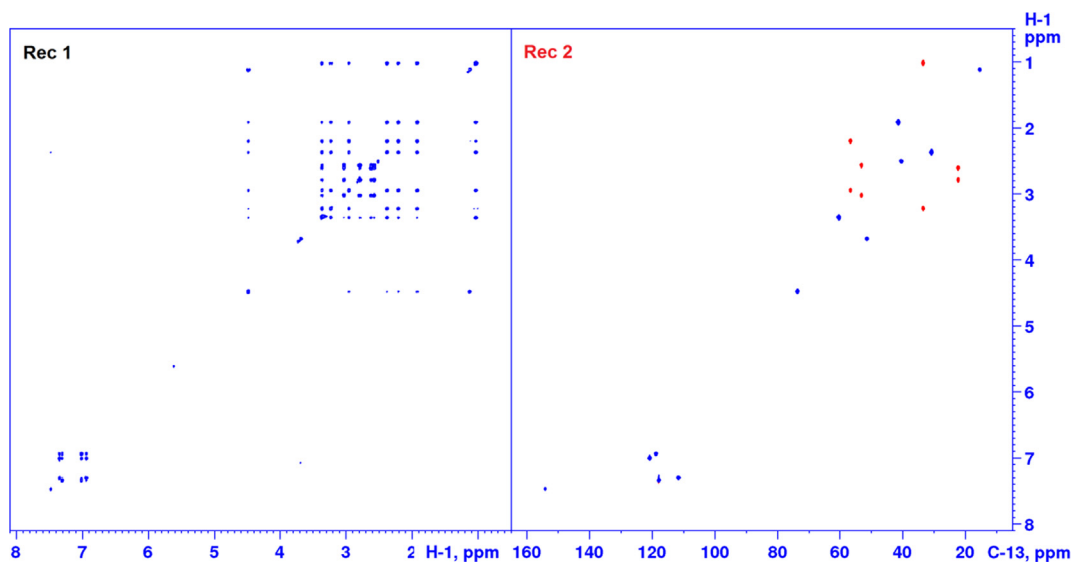
Fig. 22. TOCSY (receiver 1) and 2D multiplicity edited ^{1}H-^{13}C HETCOR (receiver 2) spectra of ajmalicine in DMSO d_6 (10 mg/600 μl) recorded on a Bruker NEO 800 MHz instrument in 12 min using the pulse sequence of Fig. 21a; 256 increments, 2 scans per increment; negative CH$_2$ peaks in the HETCOR spectra are shown in red, positive (CH and CH$_3$) peaks are shown in blue.

3.2.1.4. Ultrafast ^{1}H/^{19}F and ^{1}H/^{31}P PANSY experiments, PUFSY. Ultra-fast (UF) NMR spectroscopy is based on spatiotemporal encoding principles and has a unique capability to deliver multi-dimensional NMR spectra in a single scan, provided the sensitivity is sufficient [6–8]. One of the possible ways to combine this unique methodology with parallel acquisition is illustrated by the PUFSY (Parallel UltraFast SpectroscopY) pulse scheme shown in Fig. 20a [108]. The first hard ^{1}H 90° pulse is followed by two adiabatic CA-WURST pulses in the presence of a bipolar gradient, ±G_e, that form the spatiotemporal encoding element. The two coherence selection gradient pulses flanking the X read pulse prepare the required ^{1}H and X coherence components for the subsequent decoding and detection. Note that the ^{1}H nuclei are affected by the sum of the two gradient pulses, while the X nuclei only experience the gradient pulse that follows the X read pulse providing the desired γ-based coherence selection. The required 2D data matrix is generated by N loops of data acquisition period in the presence of bipolar decoding gradient, ±G_a. Just like in the conventional PANSY-COSY experiments, the F_1 (^{1}H) dimension is shared in this PUFSY-COSY experiment.

The experiment has been demonstrated for X = ^{19}F in a mixture of fluorinated compounds and for X = ^{31}P in adenosine triphosphate (ATP). ^{1}H/^{31}P PUFSY-COSY spectra of ATP solution in D$_2$O are shown in Fig. 20b. The ^{1}H-^{1}H COSY part of the spectrum shows ^{1}H-^{1}H correlations in the sugar (ribose) moiety, while the ^{31}P-^{1}H COSY spectrum reveals two nearest (three-bond) ^{31}P correlations, with H$_5'$ and H$_5''$.

The PUFSY technique provides new opportunities for high-throughput analysis, chemical kinetics, and fast experiments on short-lived hyperpolarized solutions.

3.2.1.5. Sequential detection experiments with 2 and 3 receivers - TOCSY/HETCOR.. Sequential acquisition experiments occupy the middle ground between interleaved and parallel experiments. They take advantage of long J-evolution delays or other coherence transfer periods, such as TOCSY and NOESY mixing periods, to acquire additional spectra 'as soon as possible' (see Fig. 3a). Alternatively, the magnetization that is utilized in the experiment(s) that follow is stored as longitudinal magnetization during the data acquisition of the current experiment (Fig. 3b). A common feature

with parallel acquisition experiments is that they share some coherence transfer pathways and associated t_1-evolution period (s). A crucial difference with parallel acquisition experiments is that sequential data acquisition enables mutual decoupling of the directly detected nuclei.

Pulse sequences for TOCSY/HETCOR experiments designed for two receivers are shown in Fig. 21a, where X can be any spin ½ nucleus [24,105]. The experiment starts with a refocused ^{1}H-X INEPT transfer from protons bound to *dilute* X spins. The phase cycling is designed to preserve the bulk magnetization of protons not coupled to X spins. At the end of the refocused INEPT sequence, the bulk magnetization together, with the polarized X spin magnetization, is aligned with the Z axis. Following a purge gradient pulse and the X read pulse, TOCSY mixing is switched on. The ^{1}H-X HET-COR spectrum (see Fig. 22) with an optional multiplicity editing step is acquired during the TOCSY mixing period. The TOCSY (DIPSI-2) mixing also acts as a proton decoupling sequence.

The X-nuclei detection period completes the concurrent ^{1}H-X HETCOR experiment, and another purge gradient pulse is applied followed by a proton read pulse and acquisition of the 2D H-H TOCSY spectrum. Other modifications of this experiment include the 2D TOCSY/HETCOR-Q experiment, which acquires the 2D ^{1}H-^{13}C HETCOR and 1D ^{13}C spectra of non-protonated carbons in a time-shared manner [105]. The same paper describes the Hada-mard version of the 2D TOCSY/HETCOR experiment for fast acquisition of the ^{1}H-^{1}H TOCSY and ^{1}H-^{13}C HETCOR spectra.

Generally, protons can be replaced by other abundant (high-γ) spin ½ nuclei, such as ^{19}F or ^{31}P, however for such nuclei TOCSY experiments are not very common, not least because of the large bandwidth that needs to be covered by the TOCSY mixing sequences.

The 2D HETCOR sequence in the 2D ^{1}H-^{1}H TOCSY / HETCOR pulse scheme can be replaced with a simple 1D X experiment, where X can be any magnetically active nuclear species, as shown in Fig. 21b. For instance, a 1D ^{13}C spectrum can be recorded during the TOCSY mixing period, which also serves as a ^{1}H decoupling sequence for the 1D ^{13}C acquisition. 1D ^{13}C spectra are routinely recorded in small molecule NMR to obtain information about the number of ^{13}C atoms in the molecule, and to obtain preliminary information about the spectral windows of interest for subsequent
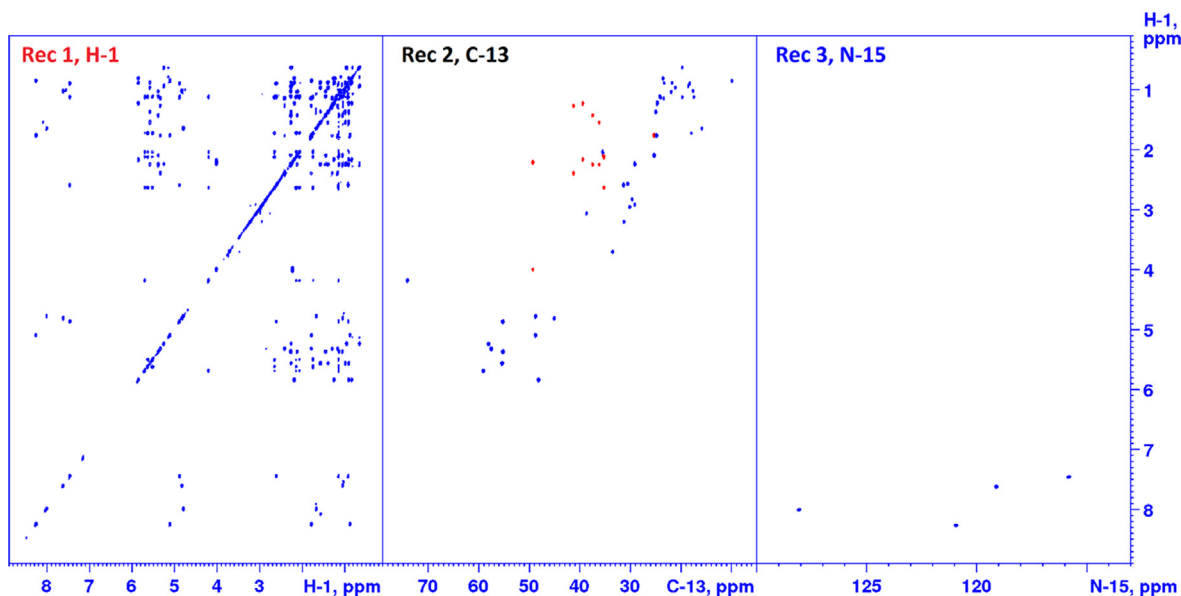
Fig. 23. ^{1}H-^{1}H TOCSY (Rec 1), ^{1}H-^{13}C HETCOR (Rec 2) and ^{1}H-^{15}N HETCOR (Rec 3) spectra recorded on a Bruker NEO 800 MHz instrument using the pulse sequence of Fig. 21c. The sample is 50 mM cyclosporine in C_6D_6; 256 increments, 4 scans per increment, experiment time 24 min; negative CH_2 peaks in the ^{1}H-^{13}C HETCOR spectra are shown in red, positive (CH and CH_3) peaks are shown in blue [111].
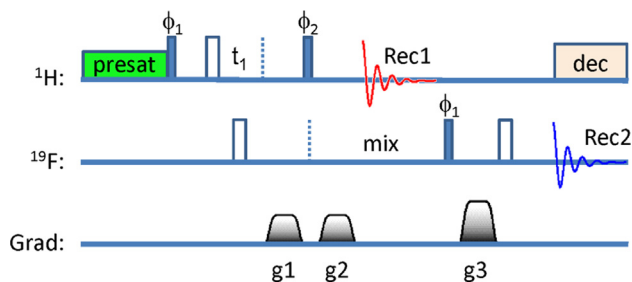
Fig. 24. Dual receiver 2D COSY/HOESY pulse sequence with optional ^{1}H presaturation for recording ^{1}H-^{1}H COSY and ^{1}H-^{19}F HOESY spectra; all pulses are applied with phase 'x' unless indicated otherwise; $\phi_1 = x, -x$, $\phi_2 = x, x, -x, -x$, $Rec1 = Rec2 = x, -x$; gradient pulses (ms, G/cm) $g1 = g2 = (1.0, 20.13)$, $g3 = (1.0, 21.40)$; phase sensitive HOESY spectra are obtained by inverting the polarity of the $g1$ gradient in every second increment according to the echo/anti-echo scheme. Reproduced from Ref. [38] with permission.

HSQC and HMBC experiments. Such information is also crucial for fast NMR techniques such as Hadamard NMR [19,105], UF NMR [6–8] and spectral folding [109].

Many basic heteronuclear multi-receiver experiments involve only one type of multi-receiver acquisition. More sophisticated experiments, such as PANACEA [110], involve both parallel and sequential multi-receiver data acquisition. In a similar way, the basic TOCSY/HETCOR pulse scheme of Fig. 21a can be extended to a triple resonance experiment involving three receivers and both sequential *and* parallel acquisition (see Fig. 21c). The basic pulse scheme of this three receiver H/C/N experiment is very similar to that for the two-receiver H/X version of the experiment, but involves two magnetically dilute spin ½ nuclear species, e.g., ^{13}C and ^{15}N, in addition to the abundant (proton) nuclei. The three 2D spectra, ^{1}H-^{1}H TOCSY, ^{1}H-^{13}C HETCOR and ^{1}H-^{15}N HETCOR recorded in the time needed for one conventional 2D experiment are shown in Fig. 23.

Depending on the availability of suitable probes, several proton decoupled 1D spectra of nuclei, such as ^{13}C, ^{15}N, ^{19}F, ^{31}P and similar, can be recorded during the TOCSY mixing time using the pulse

sequence shown in Fig. 21d. The scheme can easily include nuclei that are not coupled to protons, e.g., quadrupolar nuclei. In such cases the 1D data can also be acquired in parallel with the proton FID or by employing interleaved acquisition.

3.2.1.6. COCOHOSY - sequential COSY/HOESY experiment. The 2D dual receiver ^{1}H-^{19}F COSY/HOESY experiment [38] can be seen as a heteronuclear version of the COCONOSY experiment [30,31]. The pulse sequence (see Fig. 24) includes a joint ^{1}H t_1-evolution period and ^{1}H decoupling during the ^{19}F (^{1}H-^{19}F HOESY) acquisition period. The ^{1}H FID of the ^{1}H-^{1}H COSY experiment is acquired during the HOESY mixing time and thus does not contribute to the total duration of the ^{1}H-^{19}F HOESY experiment.

2D ^{1}H-^{1}H COSY and 2D ^{1}H-^{19}F HOESY spectra of a mixture of α- and β- 2-fluoro-2-deoxy- glucose in D_2O are shown in Fig. 25. The intrinsic alignment of peaks in the shared F_1 (proton) dimension allows easy signal assignment of the two isomers.

3.2.1.7. Interleaved multinuclear experiments. Pulse schemes for interleaved experiments are typically constructed by simply concatenating pulse schemes of conventional experiments, occasionally with some minor adjustments. Therefore these pulse schemes are often shown as simple block diagrams. The radiofrequency (RF) pulses in the two individual interleaved experiments are applied exclusively to one type of nuclear species so as not to perturb the recovering alternate nuclear species. As an example, interleaved ^{1}H/^{19}F 2D DOSY (Diffusion-Ordered SpectroscopY) experiments and spectra are shown in Fig. 26.

DOSY experiments are extensively used for NMR analysis of mixtures based on the diffusion coefficients of different molecules [112]. Such experiments are typically recorded with ^{1}H detection, to take advantage of the high proton sensitivity. The accuracy and resolving power of DOSY measurements are severely affected by signal overlap, which is often the case in ^{1}H NMR, as is evident in Fig. 26b. The trifluorobenzoic acids have the same diffusion coefficients and line up perfectly in the ^{19}F DOSY spectrum while monofluorobenzene has much higher mobility and is easily distinguished. The ^{1}H and ^{19}F DOSY spectra provide complementary information, not least because these spectra were recorded in
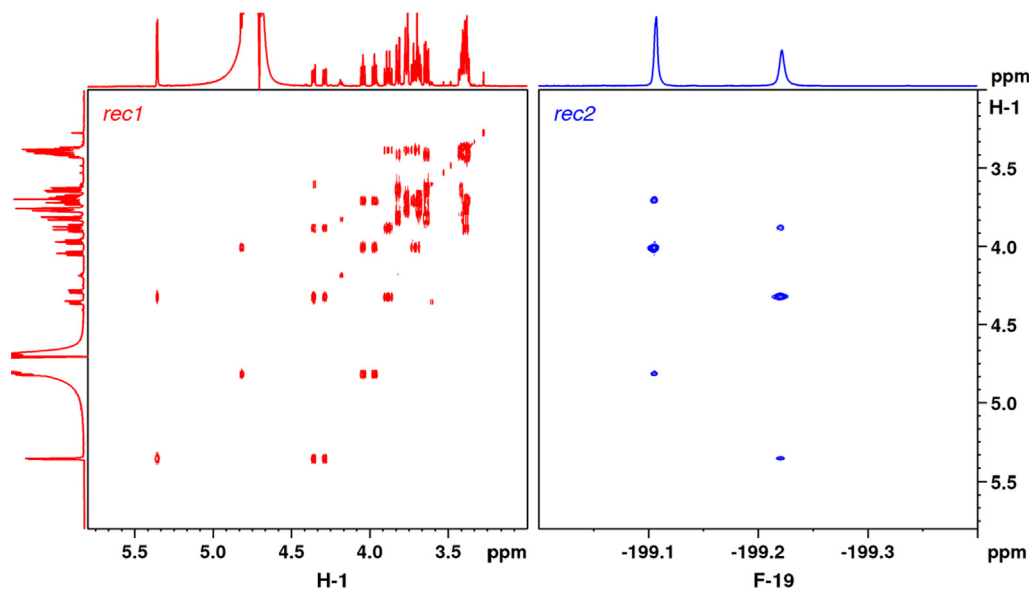
Fig. 25. ^{1}H-^{1}H COSY and ^{19}F-^{1}H HOESY spectra of a mixture of α- and β-2-fluoro-2-deoxy-glucose, recorded using the COCOHOSY pulse sequence of Fig. 24. The acquisition times were 0.366 (^{1}H) and 0.623 s (^{19}F); the spectral widths ($F_1 \times F_2$) were 4 × 4 ppm (COSY) and 4 × 10 ppm (HOESY); 256 increments, one scan per increment, 1.5 s recovery delay, total experiment time was 13 min 8 s. Reproduced from Ref. [38] with permission.
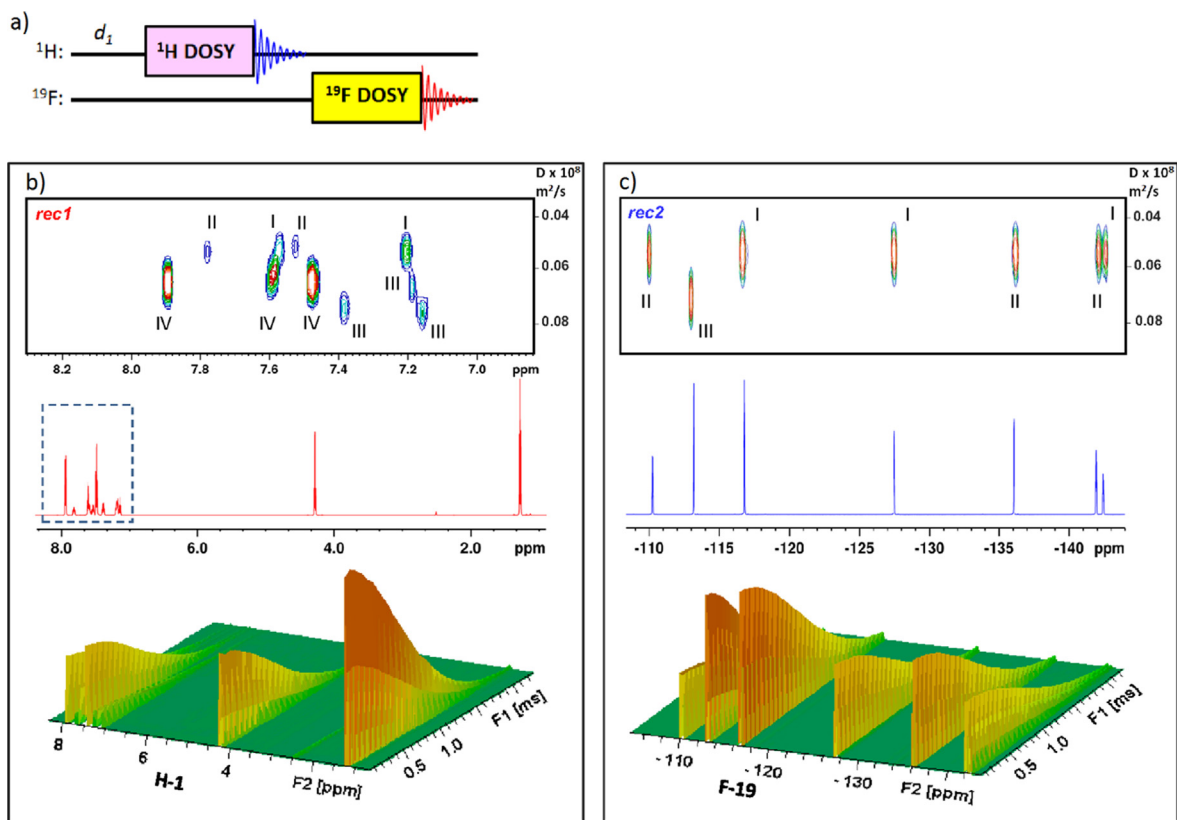
Fig. 26. a) Block diagram of the interleaved ^{1}H/^{19}F DOSY experiment; b) ^{1}H and c) ^{19}F DOSY spectra of a mixture containing four compounds − 2,3,6-trifluorobenzoic acid (I), 2,4,5-trifluorobenzoic acid (II), monofluorobenzene (III) and ethyl benzoate (IV) in DMSO d_6 recorded in an interleaved experiment as shown in (a) on a Bruker 700 MHz (^{1}H) Avance III HD spectrometer equipped with two receivers and a QCIF CryoProbe, with d_1 = 3 s, 32 increments and 8 scans per increment. Reproduced from Ref. [38] with permission.

exactly the same experimental and environmental conditions, in particular at the same temperature.

Interleaved ^{1}H-^{1}H and ^{19}F-^{19}F 2D COSY experiments [38,113] that are based on the conventional homonuclear 2D COSY

sequence applied to either ^{1}H or ^{19}F in alternate scans are shown in more detail in Fig. 27. As in the previous example, the experiment duration is reduced by recording COSY data for one nuclear species (^{19}F) during the recovery period of the COSY experiment
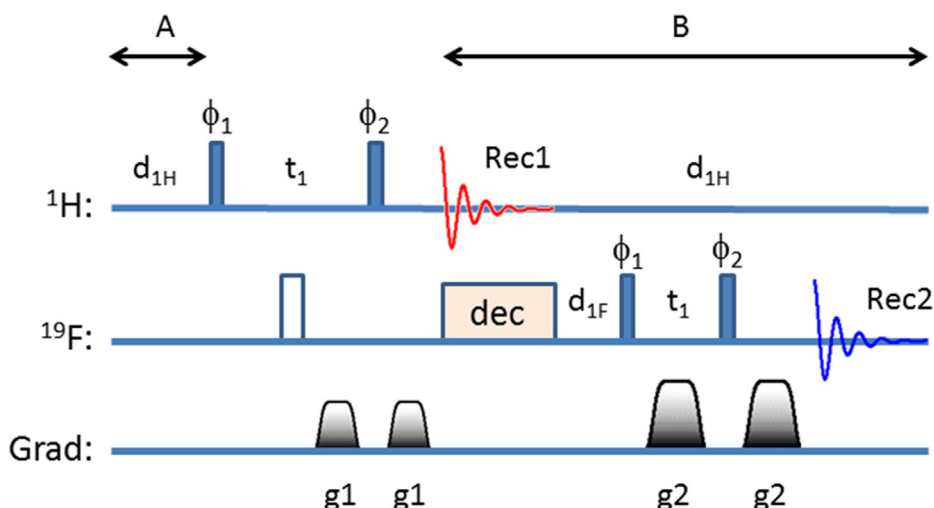
Fig. 27. Interleaved 2D ^{19}F-^{19}F COSY and ^{19}F-decoupled ^1H-^1H COSY pulse sequence. The gradient amplitudes, $g1$ and $g2$ can be set independently and typically are in the range 10–20 G/cm for 1 ms long gradient pulses; the t_1 evolution periods are also set independently for ^1H and ^{19}F nuclei; phase cycling: $\phi_1 = x, -x, \phi_2 = x, x, -x -x,$ $Rec1 = Rec2 = x, -x$. The ^1H recovery time is a combination of periods A and B. The ^{19}F recovery period, d_{1F}, is anticipated to be significantly shorter than the ^1H recovery time. The recovery interval A is therefore adjusted to achieve the desired combined duration (A + B) of the ^1H recovery in d_{1H}. Decoupling ^1H in the 2D ^{19}F-^{19}F part of the experiment would reduce the total d_{1H} recovery time to the interval A, nullifying any time advantage of the interleaved experiment as compared to conventional acquisition.
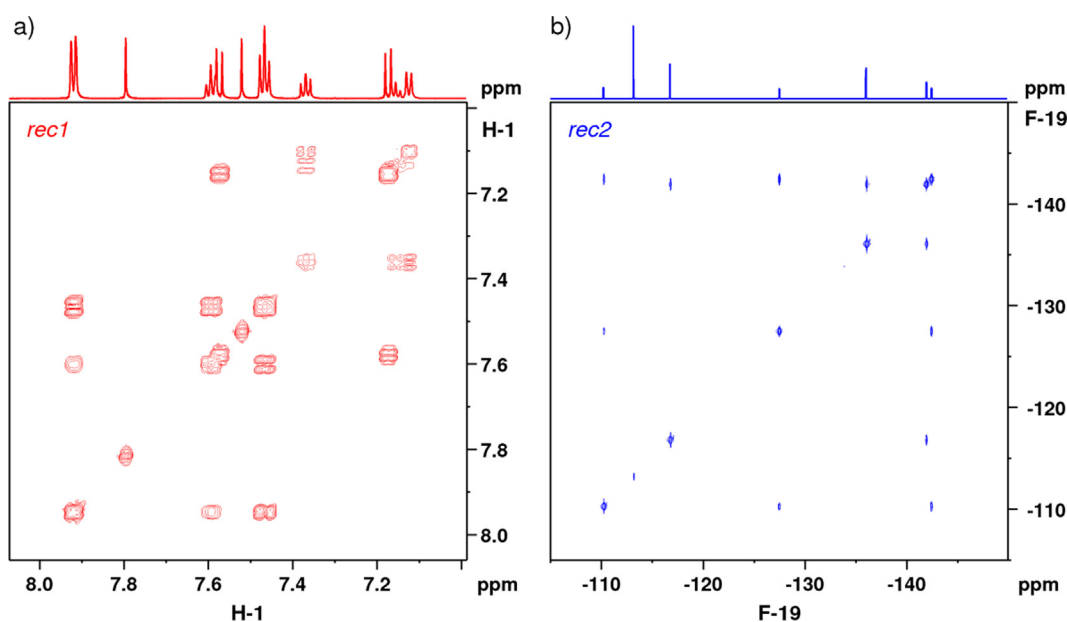
Fig. 28. (a) ^1H-^1H COSY and (b) ^{19}F-^{19}F COSY spectra of the same mixture of fluorinated compounds I, II, III and IV in DMSO d_6 as in Fig. 26, recorded as interleaved experiments on a 700 MHz Avance III HD spectrometer equipped with two receivers using the pulse sequence shown in Fig. 27. The raw data matrix size was 1024 (complex) × 512 × 512 data points, one scan per increment; experiment time was 25 min.

on the other nuclear species (^1H). Note that the strengths of the gradient pulses can be set independently in the two interleaved pulse sequences. The repetition time in interleaved experiments is determined by the most slowly relaxing nuclear species, typically ^1H in this case. Significant contributions from the chemical shift anisotropy (CSA) mechanism can substantially reduce the T_1 relaxation time of ^{19}F nuclei in asymmetric environments [37]. This often means that in interleaved ^1H/^{19}F experiments ^{19}F decoupling can be employed because there is ample time for ^{19}F nuclei to recover (see Fig. 4b). Note that such interleaved experiments are *cyclic*. Therefore, in practice it does not matter in which order the pulse sequence is coded. Spectra recorded using this pulse scheme are shown in Fig. 28.

Interleaved ^1H-^{13}C and ^1H-^{13}C HMQC experiments are recorded in a very similar fashion. Once again, ^{19}F decoupling can be used in the ^1H-^{13}C HMQC part of the experiment provided $T_1(^{19}F) < T_1(^1H)$ (see Fig. 29). ^1H decoupling in F_1 of ^1H-^{13}C HMQC can be achieved by using a pair of π pulses that return the ^1H magnetization to the equilibrium state. ^1H decoupling during the direct ^{19}F detection is not feasible as it would cancel any experiment time advantages of the interleaved experiment as compared to conventional acquisition. In samples where the two recovery periods are comparable, the ^{19}F decoupling must be omitted and a compensating ^{19}F π pulse must be added to account for the inversion pulse in the middle of the t_1 period. An important advantage of interleaved experiments is that the gradient amplitudes, offsets and spectral
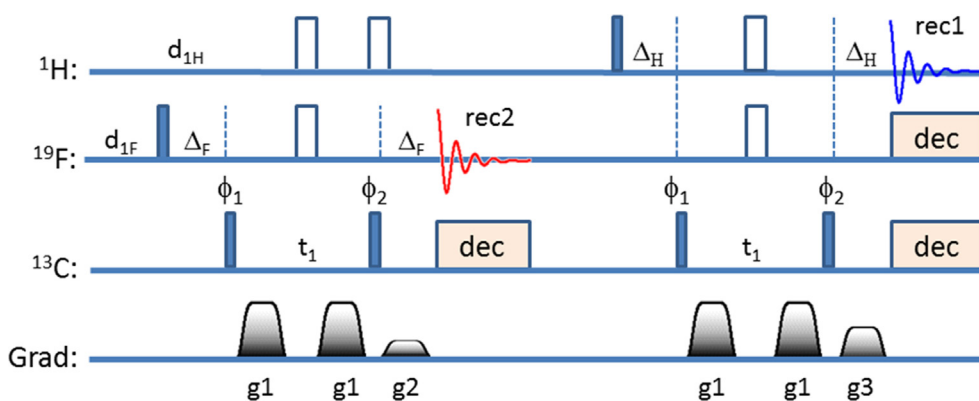
Fig. 29. The interleaved ^{19}F-^{13}C (left) and ^{1}H-^{13}C (right) HMQC experiment; delays: $\Delta_F = 0.5/^1J(^{19}$F-^{13}C$)$, $\Delta_H = 0.5/^1J(^1$H-^{13}C$)$, all pulses were applied with phase '*x*', unless indicated otherwise, $\phi_1 = x, -x$, $\phi_2 = x, x, -x, -x$; $rec1 = rec2 = x, -x, -x, x$; gradient pulses (G/cm, ms): $g1 = (21.4, 1)$, $g2 = (10.75, 1)$, $g3 = (11.44, 1)$; the amplitude of the $g1$ gradient pulses was inverted every second scan for echo/anti-echo data in F_1; for further experimental details see Ref. [38].
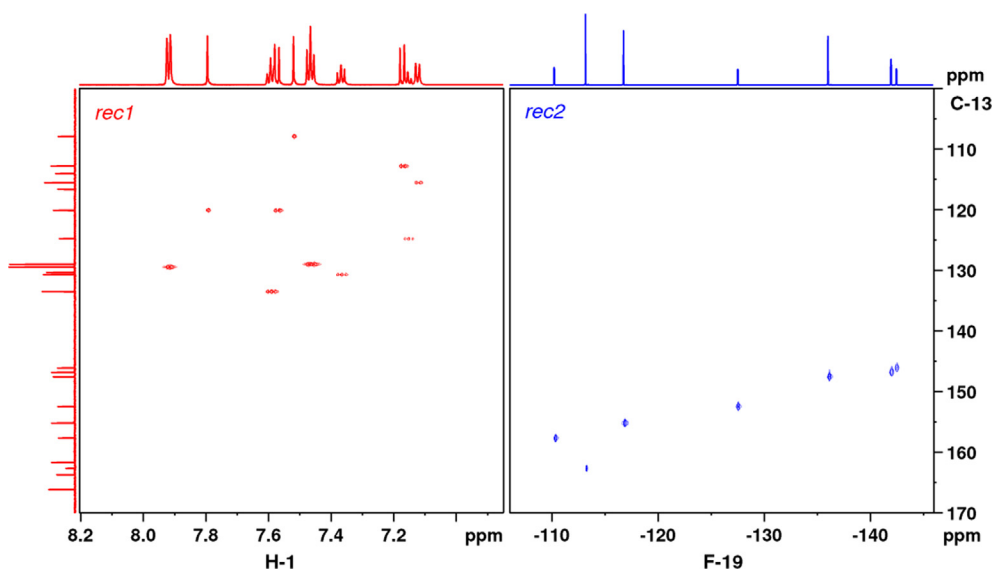
Fig. 30. Spectra of the mixture of fluorinated compounds I, II, III and IV in DMSO d_6 as in Fig. 26 recorded using the pulse sequence depicted in Fig. 29; (a) ^{1}H-^{13}C HMQC and (b) ^{19}F-^{13}C HMQC, recorded simultaneously in 7 min; one scan per increment; $^1J(^1$H-^{13}C$) = 170$ Hz and $^1J(^{19}$F-^{13}C$) = 250$ Hz were used to calculate the Δ_H and Δ_F delays; both d_1 recovery delays were 0.5 s, the acquisition times were 0.366 s (^{1}H) and 0.156 s (^{19}F) resulting in a total recovery period of *ca* 1.5 s for ^{1}H and 0.5 s for ^{19}F. The spectral width was 4 ppm (^{1}H), 40 ppm (^{19}F) and 80 ppm (^{13}C), and the corresponding raw data matrix size was 2×8 k $\times 256$ data points.

windows can be set independently for the ^{1}H and ^{19}F HMQC segments of the pulse scheme. A pair of spectra recorded with this pulse sequence is shown in Fig. 30. In a similar way the corresponding HSQC and HMBC experiments can be implemented.

Examples involving direct ^{1}H and ^{19}F detection demonstrate the great flexibility of this technique, particularly in situations that involve nuclei with high sensitivity and high natural abundance. Many other experiments such as TOCSY, NOESY, DQF-COSY, HSQC, HMBC and similar can be recorded as interleaved experiments. Such experiments do not necessarily have to be of the same type. Combining different pulse schemes with direct ^{1}H and ^{19}F detection is also feasible. For instance, ^{19}F-^{13}C HMBC and ^{1}H-^{1}H COSY can be recorded as interleaved experiments.

3.2.2. Molecular structure from a single supersequence
3.2.2.1. The PANACEA experiment.
In its basic configuration the PANACEA (Parallel Acquisition Nmr, an All-in-one Combination of Experimental Applications) scheme (see Fig. 31a) delivers ^{13}C-^{13}C INADEQUATE, ^{1}H-^{13}C HSQC and ^{1}H-^{13}C HMBC spectra from a single measurement, thus providing all information needed for structure

elucidation of small organic molecules in a single measurement [110,114,115]. It is based on the ^{13}C-^{13}C INADEQUATE experiment, [116–118] which is one of the most powerful NMR techniques for structure elucidation of small molecules. However, this is also the least sensitive module in the PANACEA supersequence. Therefore, the experiment starts with a ^{13}C detected 2D ^{13}C-^{13}C INADEQUATE pulse scheme that is active for the whole duration of the PANACEA experiment, and followed by various versions of the more sensitive 2D ^{1}H-^{13}C HSQC and 2D HMBC or 3D *J*-HMBC pulse schemes, incorporated in a sequential manner (see Fig. 31). These ^{1}H-detected modules of the PANACEA supersequence utilize the 99% of the ^{13}C magnetization that remains unused in the INADEQUATE experiment. This single quantum (SQ) magnetization is typically destroyed by gradient pulses and/or suppressed by phase cycling in conventional INADEQUATE pulse schemes.

A minor phase cycle modification in the INADEQUATE sequence enables the recording of 1D ^{13}C spectra in parallel with the 2D INADEQUATE spectra in a time-shared manner. The 1D ^{13}C spectra help to keep track of the total number of ^{13}C atoms in samples that give poor SNR in the INADEQUATE spectra. Moreover, the signal
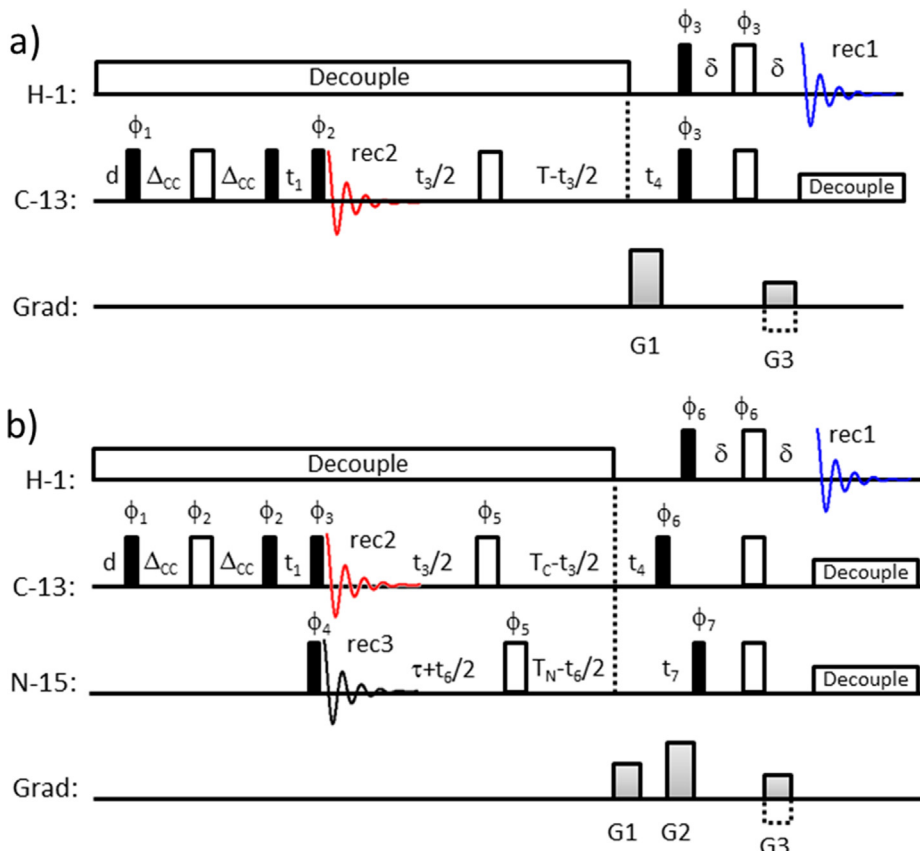
Fig. 31. PANACEA pulse sequences for a) two and b) three receivers; all pulses are applied with phase 'x', unless indicated otherwise; phase cycling (a): $\phi_1 = x, -x$; $\phi_2 = x, x, -x, -x$; $\phi_3 = y, y, -y -y$; $rec1 = rec2 = x, -x, -x, x$; phase cycling (b): $\phi_1 = 4(x, -x) \, 4(-x, x)$; $\phi_2 = x$; $\phi_3 = 2x, 2(-x)$; $\phi_5 = x$; $\phi_6 = \phi_7 = y, y, -y -y$; $\phi_4 = rec(all) \, x, -x, -x, x, -x, x, x, -x$; delays: $\Delta_{CC} = 0.25/^1J(^{13}C\text{-}^{13}C)$, $T_C = t_2 - t_4$, where t_2 is the acquisition time for the ^{13}C receiver; $T_N = t_2 - t_7$ where t_7 is the $^nJ(^{15}N\text{-}^1H)$ evolution delay; gradients pulses, (G/cm, ms) (a): G1(40, 1) and G2(10, 1); (b): G1(20, 1), G2(20.5, 1) and G3(5, 1). Adapted from Ref. [110] with permission.
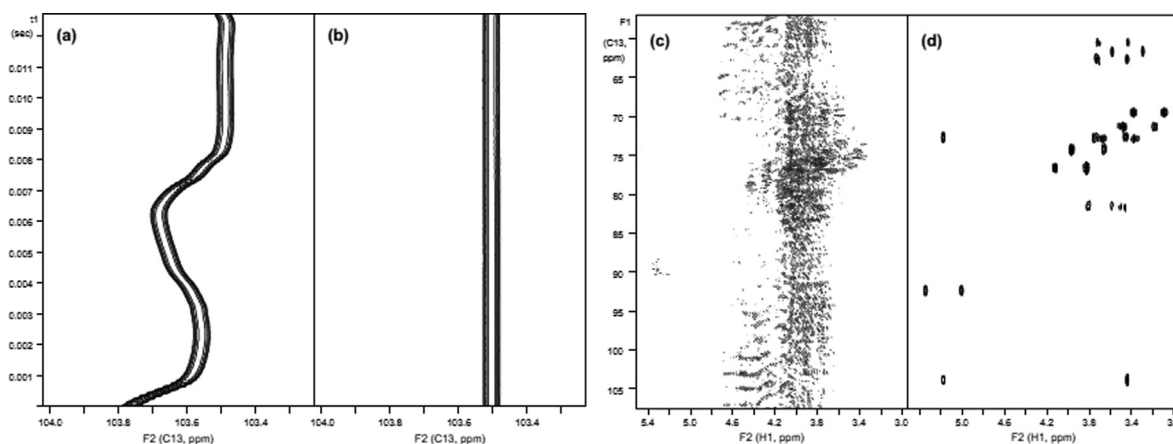
Fig. 32. (a) Instabilities due to disabled deuterium field/frequency lock and temperature regulation as detected in 1D ^{13}C spectra of 1 M sucrose in D_2O recorded with the PANACEA pulse scheme of Fig. 31a. (b) The corrected 1D ^{13}C spectrum; (c) the corrupted PANACEA-HMBC spectrum without ^2H lock and temperature regulation; (d) the same spectrum following post-acquisition field/frequency correction using the 1D ^{13}C spectrum. Reproduced from Ref. [114] with permission.

positions in the 1D ^{13}C spectra allow the S/N ratio in the 2D INADE-QUATE spectra to be improved by a factor of 2 using double symmetrization techniques [110]. Finally, as in techniques used for motion correction in multinuclear MRI, [119] the 1D ^{13}C spectra of the PANACEA experiment enable post-acquisition field/frequency correction of all spectra acquired in this experiment, thus potentially replacing the functionality of the conventional deuterium field/frequency lock (see Fig. 32). This enables the recording

of PANACEA spectra in neat liquids [114]. For instance, two major components - oleic acid (56.6%) and linoleic acid (26.7%) - were observed in PANACEA spectra of neat peanut oil without field/frequency lock.

The single quantum ^{13}C magnetization that remains at the output of the ^{13}C-^{13}C INADEQUATE module is refocused and frequency encoded in a constant time manner before being transferred via the $^1J(^1H\text{-}^{13}C)$ coupling to protons for detection. By incrementing the ^1J
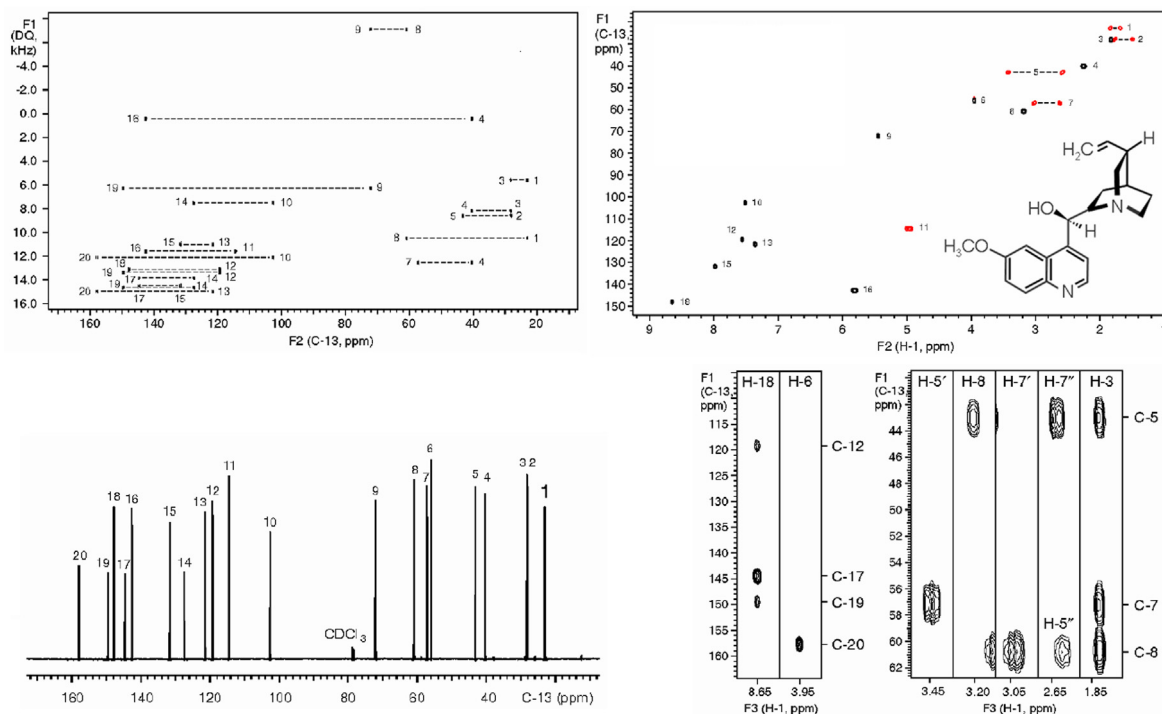
Fig. 33. PANACEA spectra of quinine in CDCl$_3$ recorded on a 600 MHz (^{1}H) Varian direct drive NMR system equipped with a triple resonance HCN room temperature probe; a) 2D ^{13}C-^{13}C INADEQUATE spectrum, b) multiplicity edited 2D ^{13}C HSQC spectrum, c) 1D ^{13}C spectrum and d) strip plot of long-range correlations from the 3D ^{13}C *J*-HMBC spectrum. Experiment time was 12 h. Reproduced from Ref. [110] with permission.
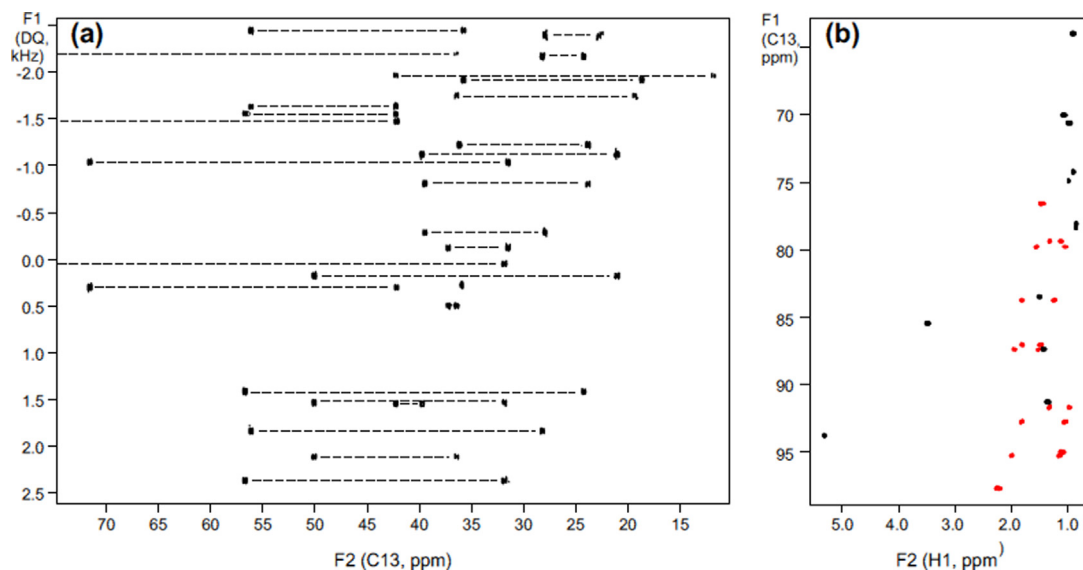
Fig. 34. The PANACEA spectra of 1 M cholesterol in CDCl$_3$ recorded in 23-min; a) 2D ^{13}C-^{13}C INADEQUATE spectrum recorded with four-fold folding, b) multiplicity-edited HSQC spectrum; negative (red) peaks belong to CH$_2$ groups and black peaks represent CH and CH$_3$ groups. Reproduced from Ref. [114] with permission.

(^{1}H-^{13}C) evolution delay, t_4, in steps of 0.25/^{1}*J*(^{1}H-^{13}C) three versions of the 2D H-C HSQC spectra can be recorded - (i) with all peaks positive, (ii) with positive CH and CH$_3$ and negative CH$_2$ signals, and (iii) with CH and CH$_3$ peaks only. This can be exploited as an extra dimension to provide more resolution in samples with overlapping cross-peaks.

In the PANACEA experiment the 2D HSQC spectra are usually collected with 1 or 2 scans per increment whereas the INADE-QUATE spectra require many more scans, typically at least 32 or

more. Hence, all the HSQC spectra can be recorded in a much shorter period of time. Once the HSQC spectra have been collected the ^{13}C decoupling is switched off and the t_4 delay is readjusted for recording the ^{13}C HMBC spectra. This seems to be a rather unusual construct among multi-FID detected experiments. As with the HSQC experiment, it is possible to record several ^{13}C HMBC spectra using different settings of the t_4 delay, so as to cover a range of long-range ^{n}*J*(^{1}H-^{13}C) couplings. Alternatively, the t_4 delay can be incremented in 3D fashion to record a 3D *J*-HMBC spectrum that
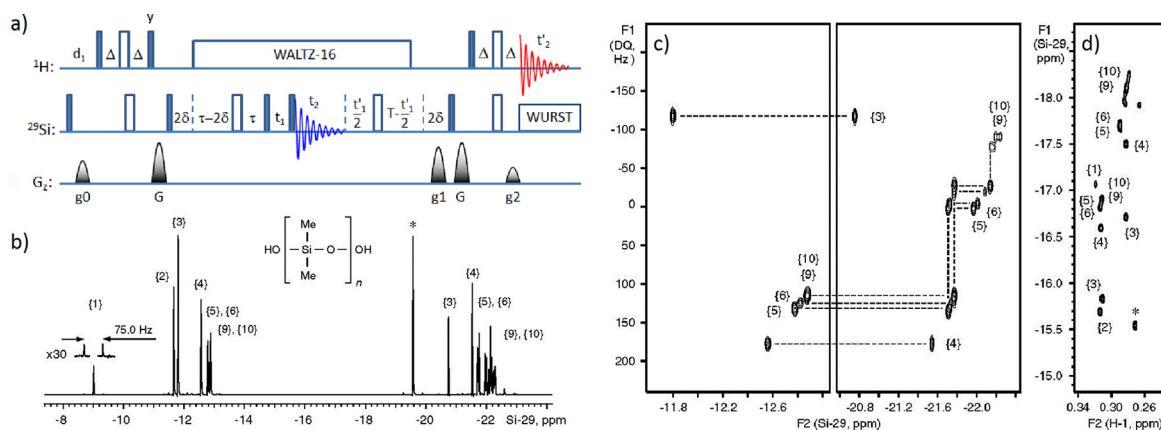
Fig. 35. a) The INEPT version of the PANACEA pulse sequence adapted for ^{29}Si NMR; coherence selection gradient ratio was g1:g2 ≈ 5:1; the spoiler gradients, g0 = 5 G/cm, G = 15 G/cm; the INEPT delays, Δ and δ were tuned to $^2J(^{29}$Si-^{1}H) = 7.4 Hz and the τ delay was set to $0.25/^2J(^{29}$Si-^{29}Si) = 125 ms. b) – d) PANACEA spectra of OH-terminated silicone oil recorded using computer optimized folding and the pulse sequence shown in (a). Reproduced from Ref. [120] with permission.

can be analyzed either as a series of 2D HMBC spectra, or processed as a 3D experiment to take the full advantage of multiplex sensitivity improvement. PANACEA spectra of quinine are shown in Fig. 33.

The versatility of the PANACEA pulse scheme is further enhanced by incorporating ^{15}N-correlated HSQC and HMBC experiments in a time-shared manner. Furthermore, on a system equipped with three receivers an optional 1D ^{15}N spectrum can be acquired in parallel with the 1D ^{13}C spectrum (see Fig. 31b). Thus, the triple-resonance PANACEA experiment delivers 11 spectra in a single measurement – 6 HSQC-s, 2 J-HMBC-s, 2 1D spectra and one INADEQUATE spectrum. Arguably, multiplicity edited ^{15}N spectra are seldom of any interest. However, the PANACEA experiment has been designed to provide all the essential correlations required for small molecule structure elucidation without any need for retrospective measurements. Furthermore, the long range ^{13}C-^{1}H couplings can be extracted from the HMBC spectra with high accuracy providing further stereospecific information about the 3D structure of the molecules [115].

The total duration of the PANACEA experiment is determined by the sensitivity of the INADEQUATE part while the number of the additional HMBC and HSQC spectra can be adjusted accordingly. For instance, in high concentration high sensitivity samples the PANACEA spectra can be recorded in as little as 23 min (see Fig. 34). Hadamard encoding [18,19] can reduce the measurement time even further. For instance, the PANACEA spectrum of the 30% menthol sample was recorded in just 56 s employing a Hadamard matrix of H_{16} [114].

The PANACEA experiment is not limited to organic molecules, and has been applied to organosilicon compounds [120]. Two-bond ^{1}H-^{29}Si INEPT polarization transfer was used to enhance the sensitivity of the ^{29}Si-^{29}Si INADEQUATE module to study polysiloxanes (see Fig. 35). Considering that there are no direct Si-H bonds in siloxanes and the two-bond $^2J(^{29}$Si-^{1}H) couplings are very uniform in polysiloxanes, the ^{29}Si PANACEA experiment can be simplified. Namely, the HMBC experiment is omitted and a two-bond ^{1}H-decoupled HSQC experiment is recorded without the multiplicity editing steps. Due to the natural abundance of the ^{29}Si isotope (ca 4.7%) and efficient INEPT enhancement, the ^{29}Si PANACEA experiment can be recorded in a relatively short time. Along with the PANACEA experiment the utility of 2D ^{29}Si/^{1}H PANSY-COSY and TOCSY/HETCOR experiments was also explored [120].

3.2.2.2. NOAH supersequences for structure elucidation. The PANACEA pulse scheme described in the previous section relies on the ^{13}C–^{13}C INADEQUATE experiment to provide the C-C connectivities

for mapping out the carbon skeleta of organic molecules. However, the notoriously low sensitivity of the INADEQUATE experiment means that high sample concentrations and/or long acquisition times are necessary. In the vast majority of small organic molecules, the structure can be established from three basic ^{1}H-detected 2D NMR experiments [121–125] – HSQC, HMBC and COSY. As discussed in the previous section, the HSQC, HMBC and COSY modules can be linked into multiple NOAH supersequences, such as NOAH-3 SBC, NOAH-3 BSC, NOAH-4 SBCN, NOAH-4 BSCN, NOAH-4 MSBC, NOAH-5 MSBCN and similar. Such supersequences can provide all the information necessary for structure elucidation of small molecules in a single measurement (akin to other analytical techniques based on a single experiment, such as X-ray crystallography) [70]. For instance, the NOAH-3 BSC supersequence and the spectra of 1,2:3,4-O-isopropylidene-α-D-galactopyranose recorded using this experiment are shown in Fig. 36. These 2D spectra were used as input to a computer-assisted structure elucidation (CASE) protocol from which the correct structure showed highest ranking of those compatible with the data (Fig. 36e), attesting to the spectral quality obtained. Most significantly, the NOAH data were recorded in 20 min whereas the three conventionally recorded spectra required a total of 46 min.

Moreover, NOAH experiments that include the NOESY (N) or ROESY (R) module additionally provide further stereospecific information about the 3D structures of small molecules [70]. For instance, the NOAH-4 BSCN supersequence is derived from the NOAH-3 BSC pulse scheme, providing the 2D NOESY spectrum in the same experiment. Likewise, the NOAH-4 BMSC and NOAH-5 BMSCN supersequences have been complemented with an additional ^{15}N HMQC or HSQC module for structure elucidation of nitrogen-containing organic molecules [33].

In cases of strong signal overlap in proton spectra, the structure elucidation process using these data may nevertheless fail, especially when attempted with CASE methods. For instance, the CASE procedure failed to establish the structure of gibberellic acid in DMSO d_6, but the structure could be solved in acetone d_6 [70]. In such instances, the adoption of additional heteronuclear correlation methods can be beneficial and the H2BC experiment is one such example that can be usefully exploited within the NOAH methodology. This experiment, a variation of HMQC-COSY, identifies two-bond ^{1}H-^{13}C connections through the exploitation of ^1J (^{13}C-^{1}H) and $^3J(^1$H-^{1}H) couplings and can be acquired in parallel with a multiplicity-edited $^1J(^{13}$C-^{1}H) HMQC spectrum using the time-shared methodology, as in the 2BOB (2-Bond, One-Bond) experiment [126]. Since 2BOB employs only $^1J(^{13}$C-^{1}H) correlations,
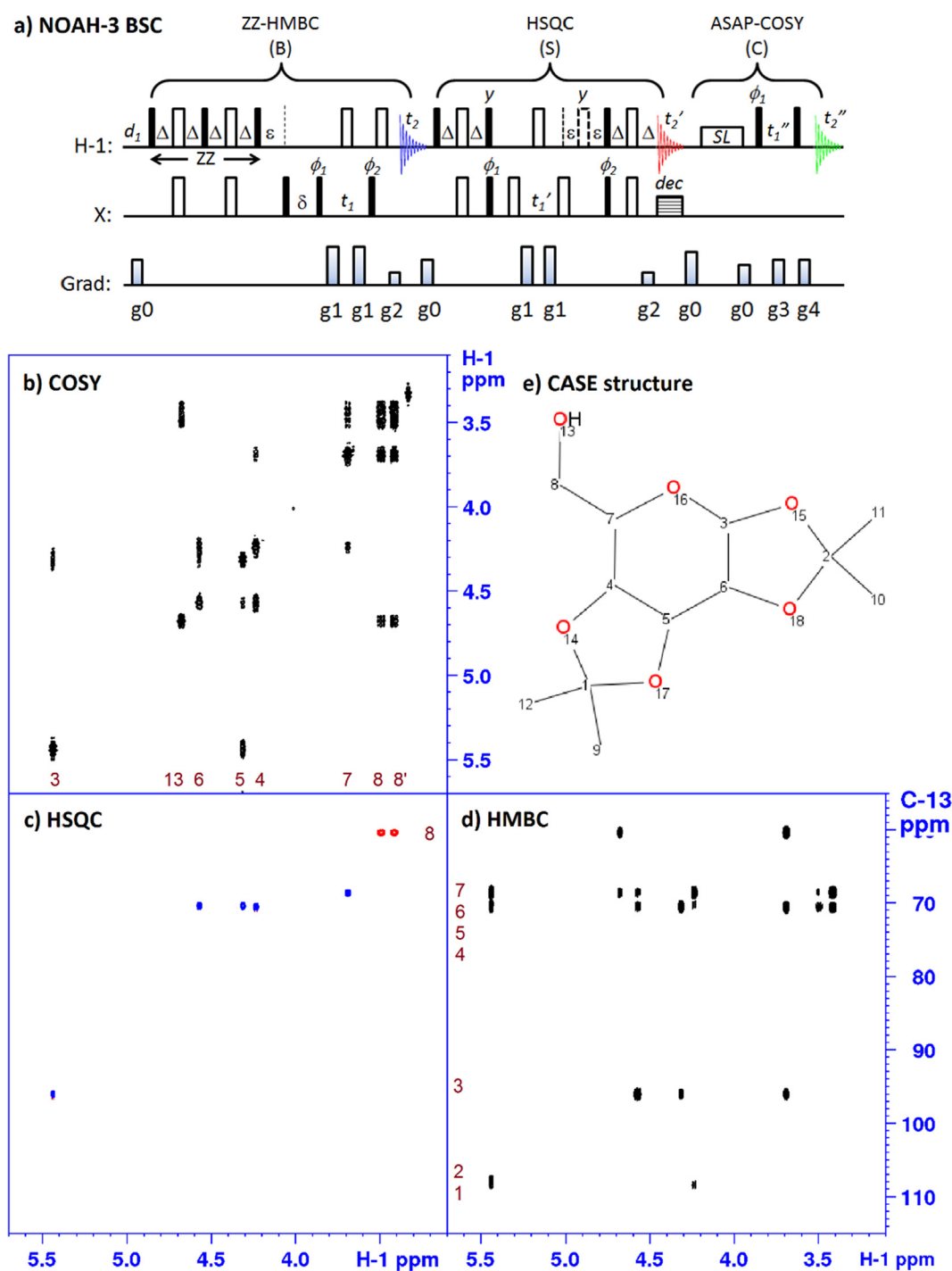
Fig. 36. a) the NOAH-3 BSC supersequence, consisting of ZZ-HMBC (B), HSQC (S) and ASAP-COSY (C) modules; *SL* represents a short spin-lock of 40–60 ms; all pulses are applied with phase '*x*' unless indicated otherwise and all gradient pulses are of 1 ms duration; phase cycles: $\phi_1 = x, -x$; $\phi_2 = x, x, -x, -x$; *Rec* $(t_2, t_2') = x, -x, -x, x$; *Rec* $(t_2') = x, -x$; the dotted rectangle in the HSQC module is an optional 180°pulse providing multiplicity edited HSQC spectra; delays $\Delta = 0.25/{}^1J({}^{13}C\text{-}{}^1H)$, $\varepsilon = 2\Delta$, $\delta = 0.5/{}^nJ({}^{13}C\text{-}{}^1H)$; gradient pulses: g0 are spoiler gradient pulses of arbitrary intensities, g1 and g2 are coherence selection gradient pulses applied with a ratio of 2 : 1; the sign of the g2 gradients is inverted in alternate increments for echo – anti–echo encoding; g3 : g4 = 1 : 1; (b–d) NOAH-3 BSC spectra recorded on a 700 MHz Bruker AVANCE III NMR spectrometer equipped with a TCI CryoProbe; b) 2D ^{1}H COSY, c) multiplicity-edited 2D ^{13}C HSQC and d) 2D ^{13}C HMBC spectra - all recorded in the same experiment; the sample is 1,2:3,4-O-isopropylidene-α-D-galactopyranose in 500 μl of DMSO d_6; e) the highest ranked structure of the molecule generated by the Bruker CMCse structure elucidation software [125] based on spectra (b–d). Reproduced from Ref. [70] with permission from The Royal Society of Chemistry.

it may be preceded by ZZ-HMBC in the NOAH-2 supersequence to ultimately yield multiplicity-edited ^{1}H-^{13}C HMQC, HMBC and H2BC data sets which provide a complete map of one-, two- and three-bond H-C connectivities within a molecule (see Fig. 37) [33]. The marriage of HMBC with 2BOB is especially well matched since all modules have comparable sensitivities, each exploiting ^{13}C coupled ^{1}H magnetization.

In a similar approach, Nagy *et al.* combined HMBC (or the related SEA-XLOC method, which is designed to distinguish between two- and three-bond ^{13}C-^{1}H correlations) with a H2OBC module (a variant of 2BOB in which HSQC-type and H2BC peaks appear in the same spectrum with different phases) to also yield complete heteronuclear connectivity maps [127]. In this scheme, the initial separation of the directly ^{13}C-coupled and non-coupled
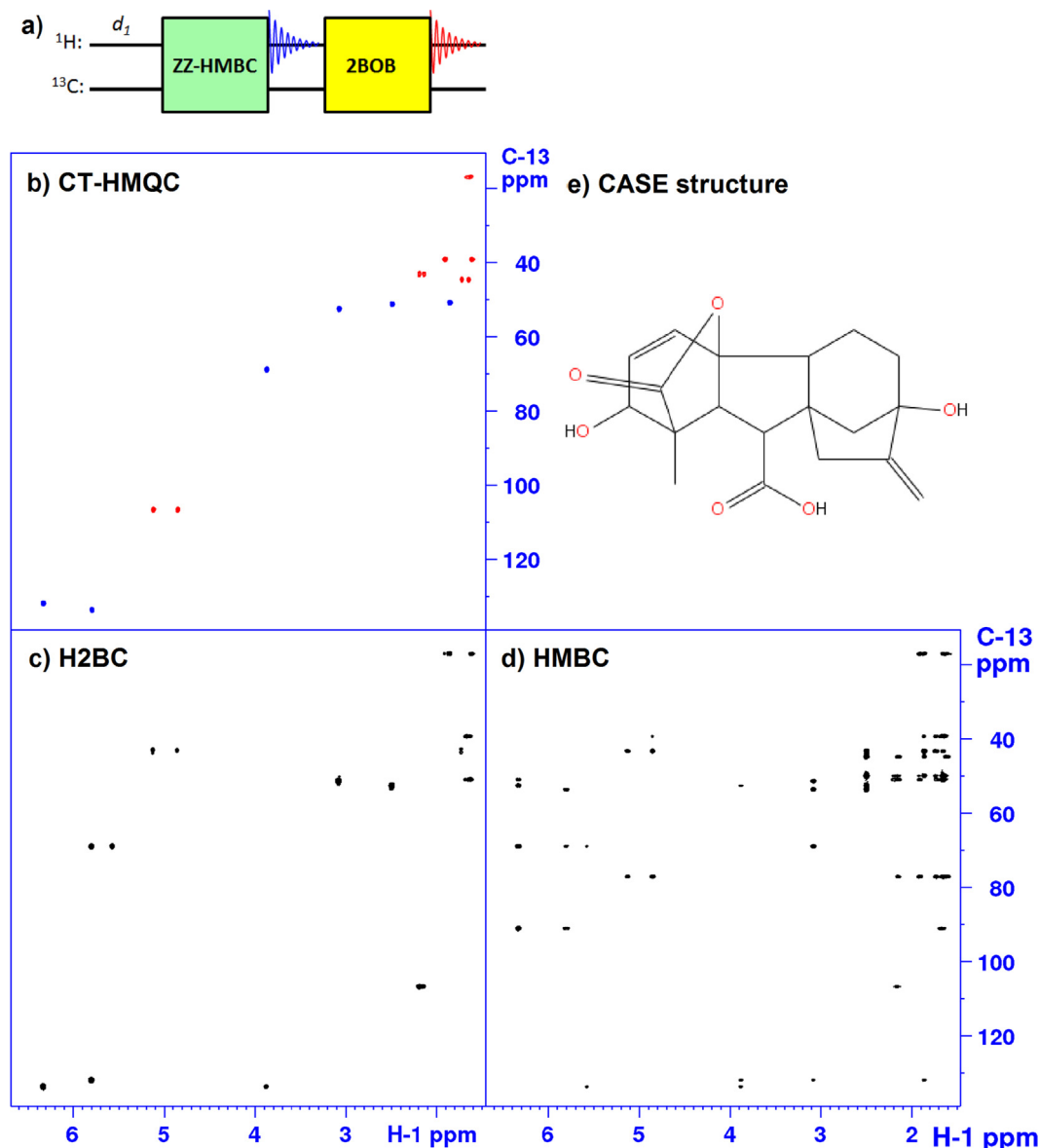
Fig. 37. a) Schematic representation of the NOAH-2 BO supersequence, consisting of ZZ-HMBC and 2BOB modules; b) – d) the NOAH-2 BO spectra of gibberellic acid 20 mM solution in DMSO d_6 recorded on a 700 MHz Avance III HD spectrometer in 17 min 34 s using the NOAH-2 BO supersequence shown in (a); raw data size was 2048 × 512 (2048 × 256 per module), 2 scans per increment, 4 dummy scans, spectral widths were 6250 Hz (^{1}H) and 32 kHz (^{13}C); (e) the CASE structure obtained with the CMCse software. Reproduced from Ref. [33] with permission.

proton magnetization pools was achieved through the use of the BANGO element [128] rather than a ZZ-filter, which, as implemented, inverts the magnetization of ^{1}H that are coupled to ^{13}C through one-bond couplings, and excites the rest of ^{1}H magnetization. An alternative use of the BANGO element has been to split a single pool of magnetization into two separate pools for exploitation in concatenated modules [129]. Through adjustment of the pulse angles within the BANGO sequence it was possible to achieve partial excitation of ^{1}H magnetization that has a long-range coupling to ^{13}C whilst leaving the remaining fraction stored along the Z axis (alongside that originating from one-bond ^{1}H-^{13}C pairs). The initially excited magnetization pool was utilized immediately in the SEA-XLOC long-range correlation experiment, whilst the second pool was used in the following HMBC, and finally the one-bond magnetization pool was sampled in a H2OBC or 2BOB sequence. The price paid in the double BANGO approach is the splitting of the initial long-range ^{1}H-^{13}C coupled magnetization into two pools, so this method sacrifices sensitivity. It was also demonstrated that

greater tolerance to $^1J(^{13}$C-^{1}H) mismatch and ^{13}C off-resonance effects in the BANGO editing element could be achieved through the use of adiabatic carbon pulses [130,131].

A somewhat different approach to defining molecular connectivity, that has found occasional use when sensitivity permits, uses the direct identification of ^{13}C-^{13}C coupled pairs within molecules. This was originally carried out by the INADEQUATE experiment introduced previously, [116–118] and subsequently by its proton-detected counterpart ADEQUATE [132,133]. The latter has been employed in combination with edited-HSQC and TOCSY experiments in the NOAH-AST supersequence (A = 1,1-ADEQUATE) for complete structure elucidation [134]. The initial A module samples only ^{1}H magnetisation associated with molecules containing ^{13}C-^{13}C pairs (a mere 0.01% of molecules at natural abundance), leaving the bulk of the magnetization for the subsequent S and T modules. The very small initial magnetisation pool that is exploited places severe limits on sensitivity, and the use of cryogenic microprobes was suggested to address this. The
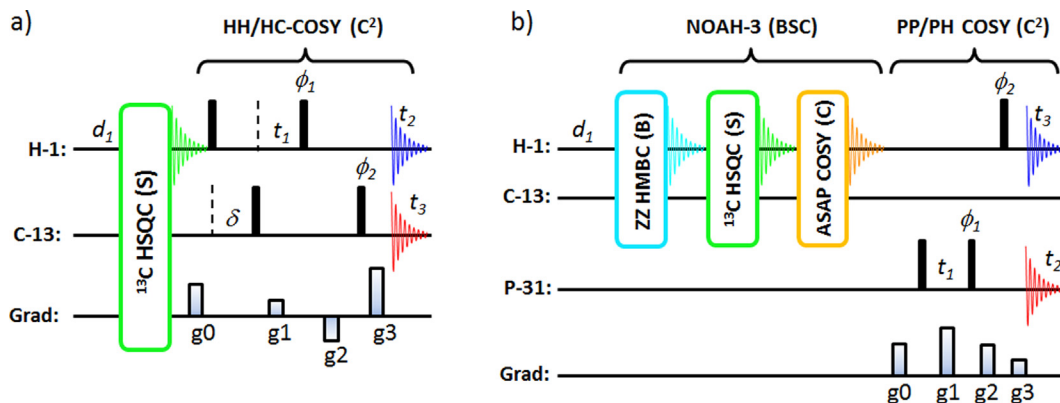
Fig. 38. NOAH supersequences augmented with multi-receiver modules; (a) NOAH-2 SC² supersequence that incorporates the dual receiver ¹H-¹H/¹H-¹³C COSY module (PANSY-COSY); all pulses are applied with phase 'x' unless specified otherwise and all gradients are 1 ms duration; phases: ϕ_1 = Rec(all) = x, -x; delays: δ = 0.5/¹Jₐᵥ(CH); gradient pulses (G/cm): g0 = 17.1, g1 = 7.5; gradient ratios for coherence selection: g3/g1 = γH/γC, g1 = g2 + g3; the polarity of the gradient pulse g1 and the receiver phase were inverted for all even increments; (b) NOAH-4 BSCC²-BSC supersequence where the NOAH3-BSC construct is extended with the parallel ³¹P-³¹P/³¹P-¹H COSY module (PANSY-COSY); all pulses are applied with phase 'x' unless specified otherwise and all gradients are 1 ms duration; phases: ϕ_1 = Rec(all) = x, -x; gradient pulses (G/cm): g0 = 17.1, g1 = 27.5; gradient ratios for coherence selection: g3/g1 = γP/γH, g1 = g2 + g3; the polarity of the gradient pulse g1 and the receiver phase were inverted for all even increments. Reproduced from Ref. [33] with permission.
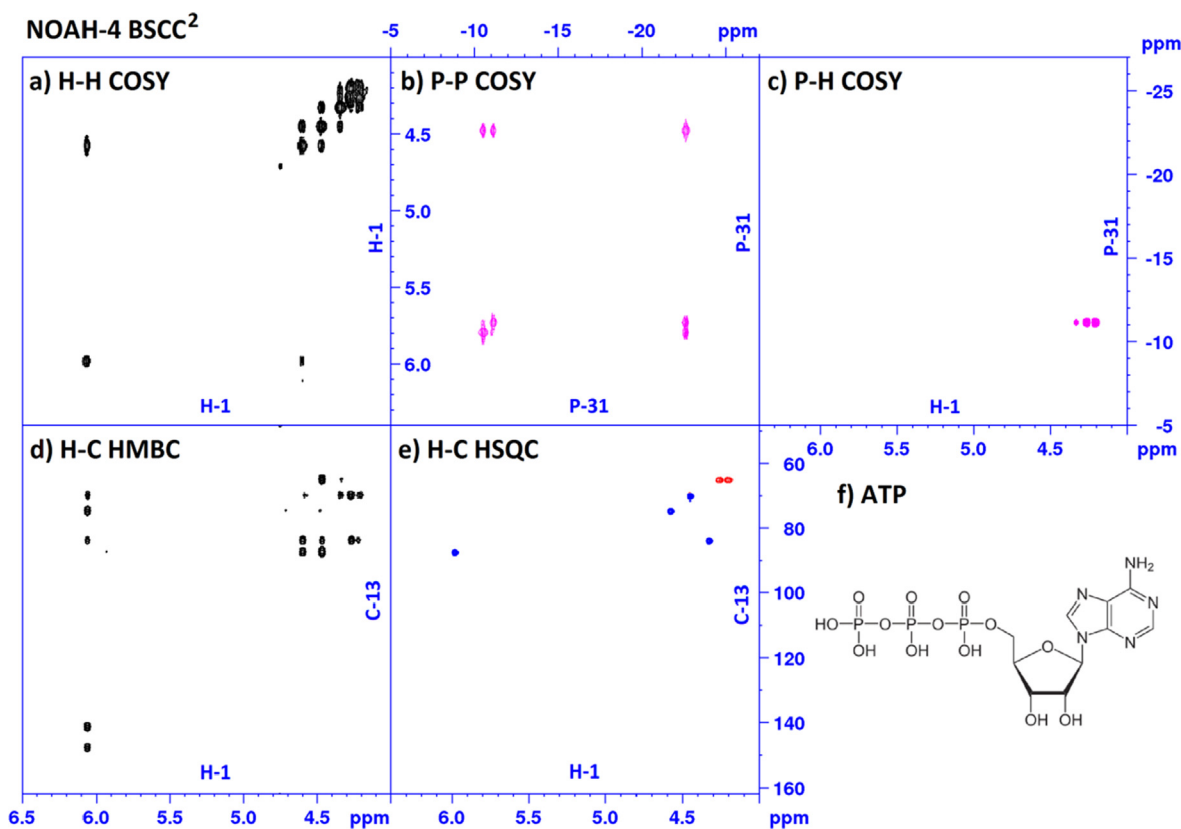
Fig. 39. NOAH-4 BSCC² spectra (a–e) of the ribose part of ATP, adenosine triphosphate (f), (50 mM in D₂O) recorded with a four channel 700 MHz NMR system (Bruker NEO) equipped with four receivers and a helium-cooled QCIP cryoprobe. In the multiplicity-edited HSQC spectra negative peaks are shown in red and positive peaks in blue; correlation spectra involving ³¹P are in pink and the magnitude COSY and HMBC spectra are shown in black. Reproduced from Ref. [33] with permission.

need for high sample concentrations and/or high detection sensitivity to enable the collection of ADEQUATE data also enables the optional use of F_1 pure shift PSYCHE decoupling in the TOCSY module (NOAH-AST$_{PS}$), since the sensitivity penalty associated with homodecoupling can be tolerated.

3.2.2.3. NOAH supersequences and multiple receivers. The combination of multi-receiver detection with NOAH supersequences offers new avenues for the development of time-efficient and

information-rich techniques. For instance, a single 2D ¹H/¹³C PANSY-COSY experiment (see Fig. 15b) provides as much information as the NOAH-3 BSC supersequence. However, due to the complexity of the peak patterns of ¹H-¹³C COSY spectra the basic ¹H/¹³C PANSY-COSY experiment is not very practical. On the other hand, the ¹J-filtered version of the experiment (Fig. 15c) can be a useful replacement for the HMBC module. For example, combining the HSQC experiment (S) with the ¹H-¹H/¹H-¹³C PANSY-COSY (C²), which utilises dual ¹H and ¹³C detection, in place of the standard
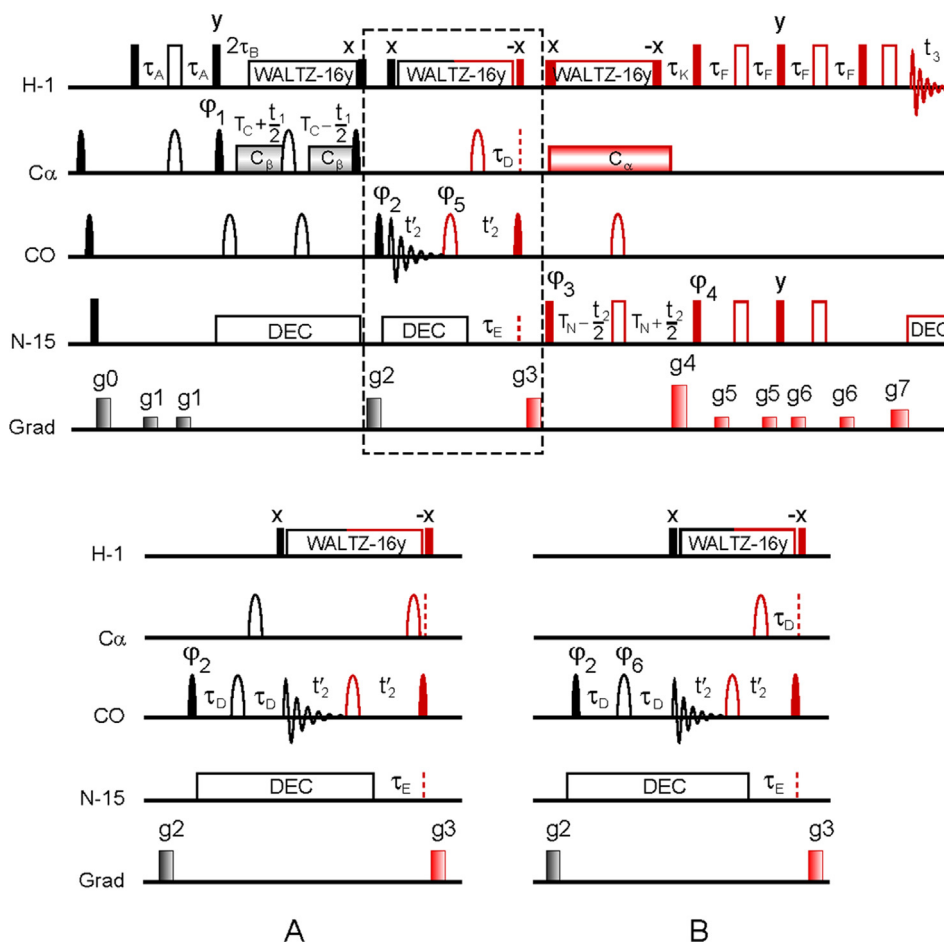
Fig. 40. Pulse scheme for recording 2D (HA)CACO (black)/3D (HA)CA(CO)NNH (black + red) with sequential detection of ^{13}CO and ^{1}H^N FIDs. The antiphase doublet CO peaks in F2′ are "collapsed" to singlets using the IPAP scheme - the dashed box is replaced by panels A and B in alternate scans. Delays: τ_A = 1.7 *ms*, τ_B = 1.8 *ms*, τ_D = 4.625 *ms*, τ_E = 24 *ms*, τ_F = 2.3 *ms*, τ_K = 5.5 *ms*, T_C = 4 *ms*, T_N = 12.4 *ms*. Phase cycling: φ_1 = x, −x; φ_2 = 2(x), 2(−x); φ_3 = 4(x), 4(−x); φ_4 = x; Rec(^{13}C) = x,−x,−x,x; Rec(^{1}H) = x,2(−x),x,−x,2(x),−x. Phases φ_5 (top scheme), φ_6 (scheme B) are adjusted to compensate for Bloch-Siegert phase shifts introduced by the Cα pulse. Quadrature detection in F_1 is achieved by incrementing φ_1 by 90°. Quadrature detection in F_2 is achieved by recording a pair of data sets for each t_2 point with (g4, φ_4) and (-g4,-φ_4). To apply the IPAP scheme sequence, A is implemented for (g4, φ_4), and scheme B for (-g4,-φ_4), thereby reducing the experiment time by a factor of two. Gradient pulses (G/cm, ms): g0 = (10, 0.5), g1 = (8, 0.5), g2 = (20, 1), g3 = (-15, 1), g4 = (30, 1.25), g5 = (3, 0.3), g6 = (2.5, 0.4), g7 = (29.5, 0.125). Reproduced from Ref. [138] with permission.

COSY, yields NOAH-2 SC^2 (see Fig. 38a). The C^2 combination provides both ^{1}H-^{1}H COSY and long-range ^{1}H-^{13}C correlation spectra, which are most valuable for identifying connectivities to non-protonated ^{13}C centres. Thus, the shorter two-module NOAH-2 SC^2 supersequence provides the same information as the three-module NOAH-3 BSC that in principle is sufficient for structure elucidation of small molecules [33]. However, the direct detection of ^{13}C in the PANSY-COSY module places greater demands on sensitivity, requiring higher sample concentrations than those experiments employing proton detection only. Greater utility may be found in the parallel detection of more sensitive high-γ nuclei such as ^{31}P or ^{19}F, as exemplified in the use of the ^{31}P/^{1}H PANSY COSY module within the NOAH-4 BSCC^2 supersequence (see Fig. 38b) [33]. This augments the previously described NOAH-3 BSC experiment (Fig. 36) to yield additional ^{31}P-^{31}P and long-range ^{31}P-^{1}H correlation data for phosphorus-containing molecules. Unlike the NOAH experiments described previously that rely solely upon ^{1}H source magnetization, the phosphorus correlation modules here exploit the unused ^{31}P magnetization pool for the ^{31}P-^{31}P and ^{31}P-^{1}H PANSY-COSY spectra, which nevertheless have greater sensitivity than the initial HMBC module. Five spectra recorded for adenosine triphosphate (ATP) in *ca* 23 min are shown in Fig. 39.

3.2.3. Biomolecular experiments

There is considerable interest in direct detection of low-γ nuclei in biomolecular NMR. For instance, it has been shown that ^{15}N and ^{13}C NMR spectra are less susceptible to broadening by paramagnetic species than ^{1}H spectra [135]. The substantial increase in the cryoprobe sensitivity for direct observation of low-γ nuclei in the last decade, and the fact that in biomolecular NMR the samples are typically enriched with ^{13}C and ^{15}N isotopes, make direct detection of low-γ nuclei suitable for multi-receiver experiments. The introduction of multi-receiver capability on the latest generation commercial spectrometers opens up new possibilities to design better and more efficient optimized NMR experiments.

In many modern biomolecular NMR experiments the magnetization is typically channeled *via* several different coherence pathways and usually only one of the pathways is utilized to record the desired multi-dimensional spectrum. With multiple receivers, detection of coherences from several pathways in the same experiment can be achieved much more efficiently. Therefore, the new technology opens up new ways of simultaneously recording several multi-dimensional spectra in the same experiment. Such experiments provide more information in a single measurement than conventional techniques for recording NMR spectra.
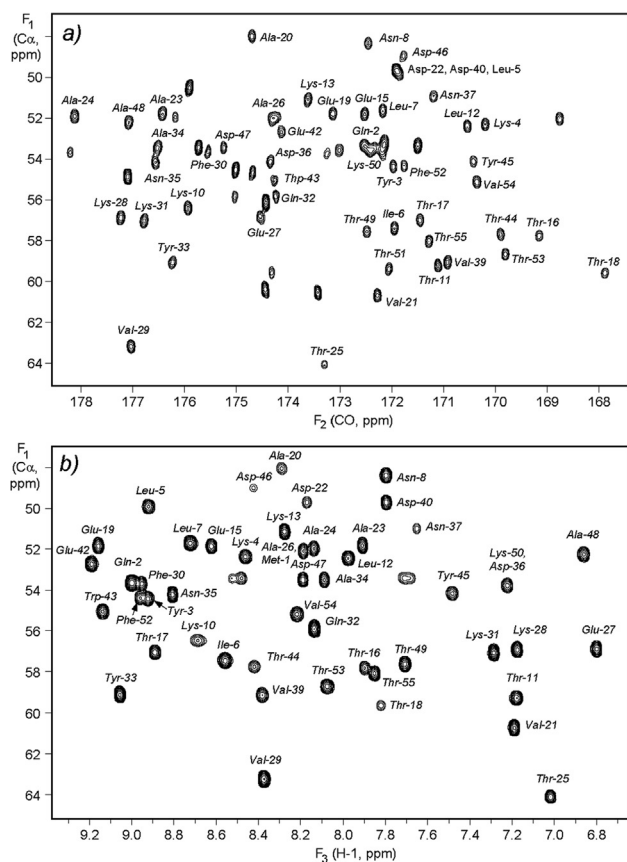
Fig. 41. (a) The ^{13}C-detected 2D (HA)CACO spectrum of a 1.0 mM aqueous solution of GB1 (90% H$_2$O, 10% D$_2$O) recorded simultaneously with (b) the ^{1}H-detected 3D (HA)CA(CO)NNH experiment in 190 min. The acquisition times of the directly detected FIDs of ^{13}C and ^{1}H nuclei were 42.6 ms. Panel (b) shows the F_1F_3 projection of the 3D experiment. Reproduced from Ref. [138] with permission.

3.2.3.1. Sequential acquisition schemes - detecting the 'afterglow' of low-γ nuclei.

A significant advantage of sequential acquisition experiments is that mutual decoupling of directly observed nuclei is usually feasible. For sensitivity reasons it is beneficial to start sequential multi-receiver experiments by recording the spectra of the least sensitive nuclear species (e.g., ^{15}N). The remaining mag-

netization is then transferred to more sensitive nuclear species for further detection (e.g., ^{13}C), and then the experiment finishes by recording the spectra of the most sensitive nuclei (^{1}H). As an example, consider the ^{13}C-detected two-dimensional 2D (HA)CACO experiment that correlates the Cα and CO chemical shifts in F_1 and F_2, respectively [136]. A similar coherence transfer pathway is employed by the 3D ^{1}H-detected (HA)CA(CO)NNH experiment [137]. Therefore, these two experiments can be combined and recorded sequentially in the same experiment (see Fig. 40) [138]. The combined 2D (HA)CACO/3D (HA)CA(CO)NNH experiment starts with a ^{13}C-detected 2D (HA)CACO pulse sequence (Fig. 40, black). The residual ^{13}C magnetization that is left over following the acquisition period of the (HA)CACO experiment (the "afterglow") will have decayed too much for direct ^{13}C detection. However, in this dual receiver experiment it is refocused, and transferred to protons for detection (Fig. 40, red) to take advantage of the higher proton sensitivity. Thus *ca.* 10% of the ^{13}C signal originating on CO at the start of the ^{13}C detected 2D (HA)CACO acquisition is used to record 3D (HA)CA(CO)NNH experiment, with essentially no penalty in spectrometer time.

The magnetization flow during the 2D (HA)CACO (black)/3D (HA)CA(CO)NNH (black + red) experiment is summarized as follows:

$$^1\text{Ha} \xrightarrow{J_{HC}} {}^{13}\text{C}\alpha, t_1 \xrightarrow{J_{C\alpha CO}} {}^{13}\text{CO}, acq(t_2)$$
$$\textcolor{red}{\xrightarrow{J_{CON}} {}^{15}\text{N}, t_2' \xrightarrow{J_{NH}} {}^1\text{H}_N, acq(t_3)}$$
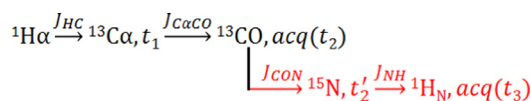
Note that the 3D experiment shares the first t_1 (Cα) evolution period with the 2D data set. Once the FID of the 2D (HA)CACO experiment has been acquired, the CO chemical shift is refocused and ^{15}N decoupling is switched off to allow evolution under the $^1J(^{13}\text{CO}-^{15}\text{N})$ coupling during the τ_E delay (Fig. 40). The antiphase ^{13}CO magnetization, C'_YN_Z, is subsequently transferred to ^{15}N, and following a constant-time evolution period t_2 is then transferred to the protons for detection. The ^{13}C-detected 2D (HA)CACO spectrum and F_1F_3 projection of the ^{1}H-detected 3D (HA)CA(CO)NNH spectrum of the protein GB1 are shown in Fig. 41a,b, respectively.

In samples not limited by sensitivity, unconventional sampling methodology such as radial sampling and the projection-reconstruction (PR) technique can be invoked to further reduce
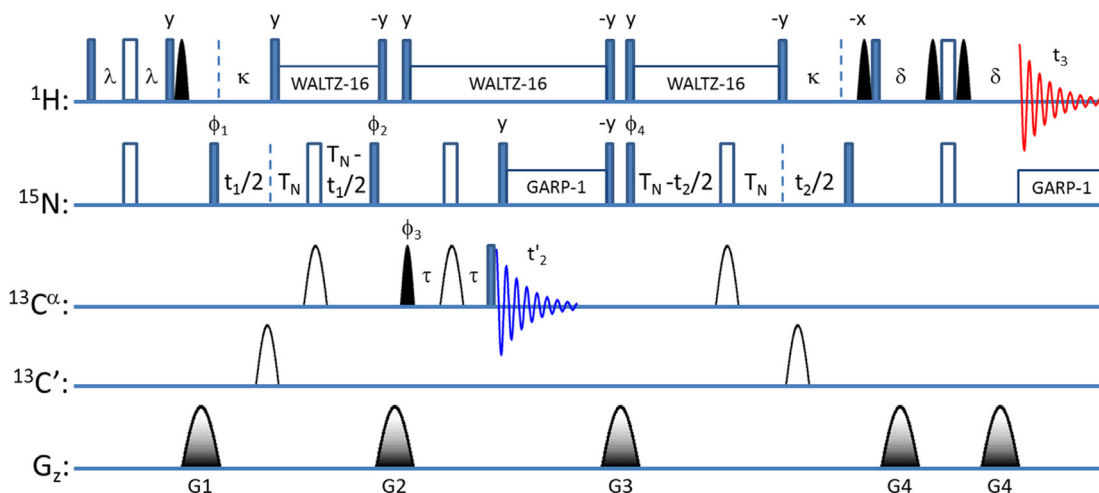
Fig. 42. The 2D (H)NCA/3D HNN pulse scheme [141]. Delays: λ = 2.7 ms, κ = 5.4 ms, δ = 2.7 ms, T_N = 15 ms, τ = 12–16 ms (to be optimized), phase cycling: ϕ_1 = x, x, −x, −x, $\phi_2 = \phi_3$ = x, −x, ϕ_4 = 4x, 4(−x), Rec(^{1}H) = x, x, −x, −x, −x, −x, x, x, Rec(^{13}C) = x, x, −x, −x; States-TPPI scheme applied to ϕ_1 and ϕ_4; gradients (1 ms, G/cm): G1 = G2 = G3 = 16, G4 = 42.
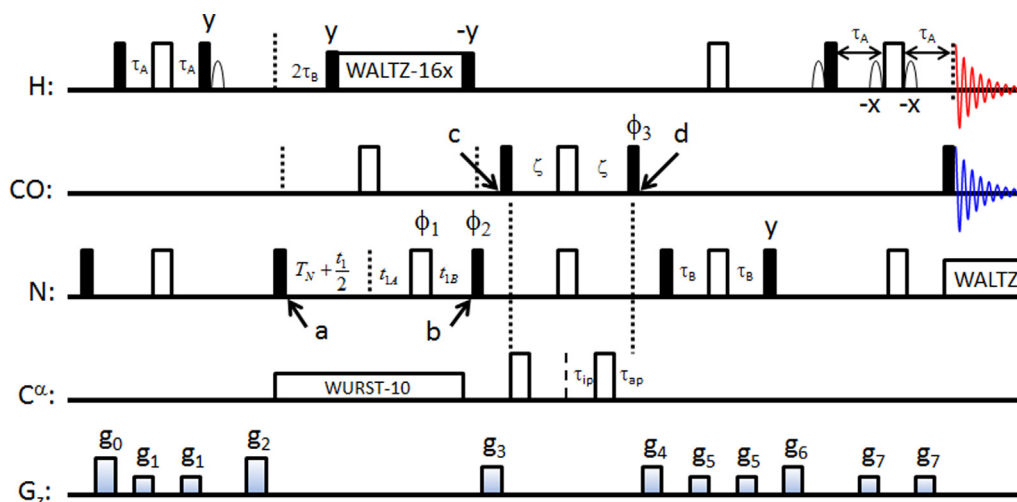
Fig. 43. Pulse scheme for a parallel ^{15}N HSQC experiment with simultaneous detection of ^{1}H^{N} and ^{13}CO FIDs. Delays: τ_A = 2.5 ms, τ_B = 2.75 ms, T_N = ≈15 ms (adjusted to achieve similar sensitivity for ^{1}H and ^{13}CO), ζ = 12.4 ms; if $T_N \geq$ t1/2 then t_{1A} = 0 and t_{1B} = T_N − t1/2, otherwise t_{1A} = t1/2 − T_N and t_{1B} = T_{CO} (^{13}CO 180° pulse duration). Phase cycling: ϕ_1 = $x, y, -x, -y$; $Rec(^{1}H)$ = $Rec(^{13}C)$ = $x, -x$; States-TPPI applied to ϕ_2; the IPAP scheme is implemented by setting ϕ_3 = y, τ_{ip} = ζ and τ_{ap} = 0 for the IP component and ϕ_3 = $-x$, τ_{ip} = ζ − τ_{ap} and τ_{ap} = 4.86 ms for the AP component. A small angle phase shift is applied to the ^{13}CO 180° pulse between points c and d compensates for the differences in power used for this pulse and the flanking 90° pulses. Gradient pulses (G/cm, ms): g0 = (10,0.5), g1 = (5,0.5), g2 = (15,1), g3 = (11,1), g4 = (7,0.8), g5 = (−3,0.3), g6 = (5,0.6), g7 = (24,0.4). Reproduced from Ref. [107] with permission.

the measurement time [21,139,140]. For instance, the sequentially recorded 3D (HA)CA(CO)NNH spectrum of a sample of the protein GB1 was reconstructed from just three planes – the orthogonal planes F_1F_3 (t_2 = 0; recorded in 2 min) and F_2F_3 (t_1 = 0; 4 min), and a tilted plane (t_1/t_2, 9 min). This experiment is expected to have utility for small- to moderately-sized proteins as well as for intrinsically disordered proteins.

Chakraborty *et al.* have reported a conceptually similar experiment for sequential acquisition of ^{13}Cα–^{15}N and ^{1}H–^{15}N–^{15}N correlations in proteins [141]. The standard 3D HNN pulse sequence [142] is modified to allow for multinuclear detection using two receivers (see Fig. 42). The experiment starts with an INEPT transfer of magnetization from the amide protons to the directly attached ^{15}N spins via the one-bond $^{1}J(^{15}$N-^{1}H) coupling (90–95 Hz). The polarization transfer is followed by a constant time evolution period during which the ^{15}N magnetization evolves under $^{1}J(^{15}$N-^{13}Cα) (7–11 Hz) and $^{2}J(^{15}$N-^{13}Cα) (4–9 Hz) couplings. At the end of this period, ^{15}N$_i$ magnetization which is antiphase with respect to ^{13}Cα is transferred to both ^{13}Cα$_i$ and the neighboring ^{13}Cα$_{i-1}$ by a pair of 90° pulses on ^{15}N and ^{13}Cα. The transfer is followed by a $^{n}J(^{15}$N-^{13}C) refocusing period, 2τ, that ends with a hard ^{13}C pulse. At this point a detectable ^{13}Cα magnetization is created along with N_zC_z coherence. Following the ^{13}C acquisition period, a second ^{15}N constant time evolution and INEPT transfer of the ^{15}N coherence back to the amide protons for detection complete the HNN experiment. Thus, the magnetization that is destroyed by gradient pulses in the conventional 3D HNN experiment is detected in the second receiver to produce the 2D ^{15}N-^{13}Cα correlation spectrum.

The magnetization transfer pathways for this experiment are summarized below:

$$^{1}H_i \xrightarrow{J_{HN}} {}^{15}N_i, t_1 \xrightarrow{J_{NC\alpha}} \begin{array}{l} {}^{13}C^{\alpha}_{i,i-1}, acq(t_2) \\ (N_zC_z^{\alpha})_{i,i+1} \xrightarrow{J_{NC\alpha}} {}^{15}N_{i,i+1}, t_2 \xrightarrow{J_{NH}} {}^{1}H_{i,i+1}, acq(t_3) \end{array}$$
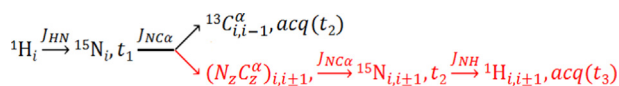
In this experiment it is the ^{13}Cα magnetization that is used for the direct detection of sequential ^{13}Cα–^{15}N correlations, thus facilitating the protein backbone assignment by providing directional-

ity to the sequential walk in the 3D HNN spectrum that is recorded in the same experiment. Specifically, the 2D ^{13}Cα–^{15}N correlation spectrum provides connectivity between consecutive residues $i −$ 1 and i, while the HNN spectrum reveals ^{1}H^{N} and ^{15}N correlations between three consecutive residues, $i − 1$, i, and $i + 1$. The benefits of the 2D ^{13}Cα–^{15}N sequential correlations obtained from this 3D experiment include – (a) the *Gly* peaks appear negative; serving as check points during sequential walk; (b) the 2D ^{13}Cα–^{15}N correlation spectrum connects only the $i − 1$ and i residues, providing directionality in the HNN backbone walk; and (c) the large chemical shift dispersion in both ^{13}Cα and ^{15}N dimensions facilitates assignments in regions with poor ^{1}H chemical shift dispersion. The experiment provided complete assignment of resonances for a protein sample (ubiquitin) in a single measurement [141].

3.2.3.2. Pulse schemes with parallel multinuclear detection. One of the advantages of parallel detection experiments is that the duration of the acquisition periods is not limited. Furthermore, the parallel detection experiments in biomolecular applications typically employ a joint recovery period, d_1 which must be adapted to the fastest relaxing nuclei (typically ^{1}H). Consequently, the parallel acquisition experiments are also somewhat more efficient in terms of the experiment duration as compared to similar interleaved and sequential experiments.

As mentioned previously, in parallel detection experiments the directly detected nuclei cannot be mutually decoupled using classical decoupling techniques. Therefore, these experiments are most efficient in situations where the mutual coupling between the nuclear species of interest is insignificant or unresolved, as, for instance, in molecules or mixtures with no direct bonds between the relevant atoms.

Consider, for example, an ^{15}N HSQC pulse sequence employing parallel detection of ^{1}H^{N} and ^{13}CO (see Fig. 43) [107]. The two-bond scalar couplings between ^{1}H^{N} and ^{13}CO nuclei are small (<5 Hz) and usually remain unresolved, so that mutual decoupling of these nuclei is unnecessary and parallel acquisition can be used. The experiment starts with the usual INEPT transfer from protons to ^{15}N. During the subsequent time period between the points a and b transverse ^{15}N magnetization evolves with respect to the one-bond $^{1}J(^{15}$N-^{13}CO) and $^{1}J(^{15}$N-^{1}H) scalar couplings and ^{15}N chemical shift. From point b onwards the two components N_z and
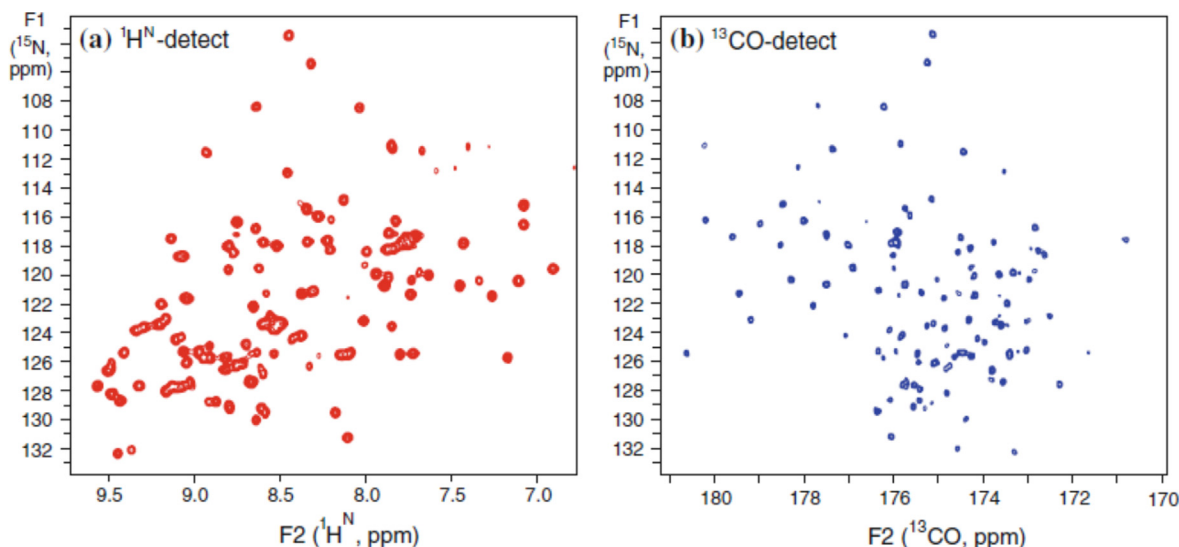
Fig. 44. $^1H^N$ (a) and ^{13}CO (b) detected 2D ^{15}N HSQC spectra of the chicken liver fatty acid binding protein, Lb-FABP (Asla Biotech), 1 mM in 9:1 H_2O/D_2O, 25 °C) recorded in parallel using the pulse sequence of Fig. 43 on an Agilent 800 MHz DDR2 NMR system equipped with two receivers and a cryogenic ^{13}C and ^1H enhanced sensitivity probe. The duration of the FIDs for both ^{13}CO and $^1H^N$ nuclei was 82 ms. Reproduced from Ref. [107] with permission.
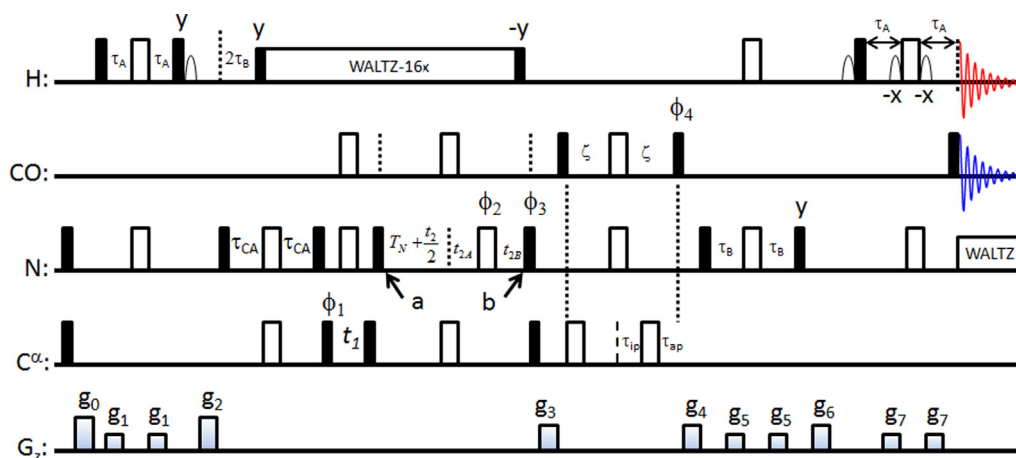
Fig. 45. Pulse scheme for a parallel 3D HNCA experiment with simultaneous $^1H^N$ and ^{13}CO detection. Delays: $\tau_{CA} = 14$ ms. Phase cycling: $\phi_1 = x, -x$; $\phi_2 = x, x, y, y, -x, -x, -y, -y$; $Rec(^1H) = Rec(^{13}C) = x, -x, -x, x$. States-TPPI applied to ϕ_1 (F_1) and ϕ_3 (F_2); $\phi_4 = y$, $\tau_{ip} = \zeta$ and $\tau_{ap} = 0$ to record the IP component and $\phi_4 = -x$, $\tau_{ip} = \zeta - \tau_{ap}$ and $\tau_{ap} = 4.86$ ms to record the AP component. Gradient pulses (G/cm, ms): g0 = (10, 0.5), g1 = (5.0, 0.5), g2 = (15.0, 1.0), g3 = (10.0, 1.0), g4 = (7.0, 0.8), g5 = (-5.0, 0.3), g6 = (5.0, 0.6), g7 = (24.0, 0.5). Other experimental details are the same as in the caption to Fig. 43. Reproduced from Ref. [107] with permission.

$2N_ZCO_Z$ follow separate coherence pathways *en route* to detection. Typically, the T_N delay is adjusted so that the cosine and sine coefficients are approximately 0.174 and 0.985, thus balancing the sensitivity of the ^1H and ^{13}C detected spectra. This can be optimized on a case by case basis. A shared constant-time approach is used to ensure that t_1(max) is not limited by the value of T_N. Consequently, the relative sensitivities of the ^1H and ^{13}C detected spectra can be adjusted independently of the resolution required in F_1.

The N_Z component is kept longitudinal between points c and d. Following point d the ^{15}N coherence is transferred back to protons for detection, yielding the 2D ^1H-^{15}N HSQC spectrum. In contrast, $2N_ZCO_Z$ is manipulated by the scheme between the points c and d to generate a ^{13}CO-detected 2D ^{13}C-^{15}N HSQC data set. The ^1J (^{13}CO-$^{13}C\alpha$) scalar coupling is suppressed using the IPAP scheme [63,64]. The 2D ^{15}N-$^1H^N$ and ^{15}N-^{13}CO correlated spectra of $^{15}N,^{13}C$ labelled Lb-FABP protein (chicken liver fatty acid binding protein, 125 residues, 1 mM) recorded in parallel in approximately 20 min are shown in Fig. 44.

The parallel 2D $^1H/^{13}CO$-detected ^{15}N HSQC experiment can be recorded in just 20 min providing the resonance frequencies of three nuclei, ^{13}CO, ^{15}N and $^1H^N$, as in a 3D HNCO experiment [136]. The two detection schemes employed in this experiment share a common t_1 (^{15}N) evolution period. Consequently, the two 2D spectra share the same F_1 frequency axis. In fact, the two spectra are equivalent to orthogonal $^{15}N,^{13}CO$ and $^{15}N,^1H^N$ projections of the 3D HNCO spectrum and can, in principle, be used together to reconstruct the 3D HNCO spectrum [107]. Not only are the 2D spectra recorded in a considerably shorter period of time, but also with higher resolution than 3D data. Thus, the two parallel data sets provide complementary information and can help to resolve ambiguities caused by signal overlap in a conventional 3D HNCO experiment.

The design features of the parallel 2D $^1H/^{13}CO$ ^{15}N HSQC experiment can be applied to 3D and higher dimensionality experiments. As an example, a parallel $^1H^N$ and ^{13}CO detected 3D HNCA pulse scheme is shown in Fig. 45. As in the conventional HNCA
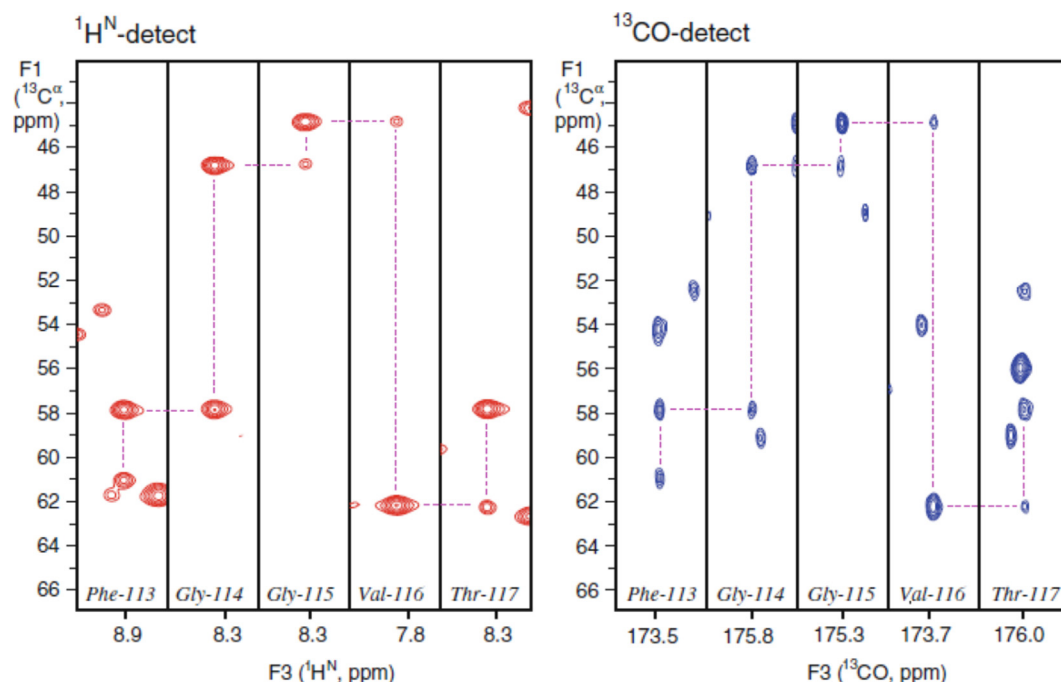
Fig. 46. F_1F_3 strip plots of $^1H^N$- (left) and ^{13}CO- (right) detected 3D HNCA spectra of 1 mM Lb-FABP protein (9:1 H_2O/D_2O, 25° C), recorded using the pulse scheme of Fig. 45 on an Agilent 800 MHz DDR2 NMR system equipped with two receivers and a cryogenic ^{13}C and ^1H sensitivity-enhanced probe. The $^1J(^{13}C\alpha-^{13}CO)$ coupling was suppressed using the IPAP scheme. The total experiment time was 11 h 20 min. Reproduced from Ref. [107] with permission.
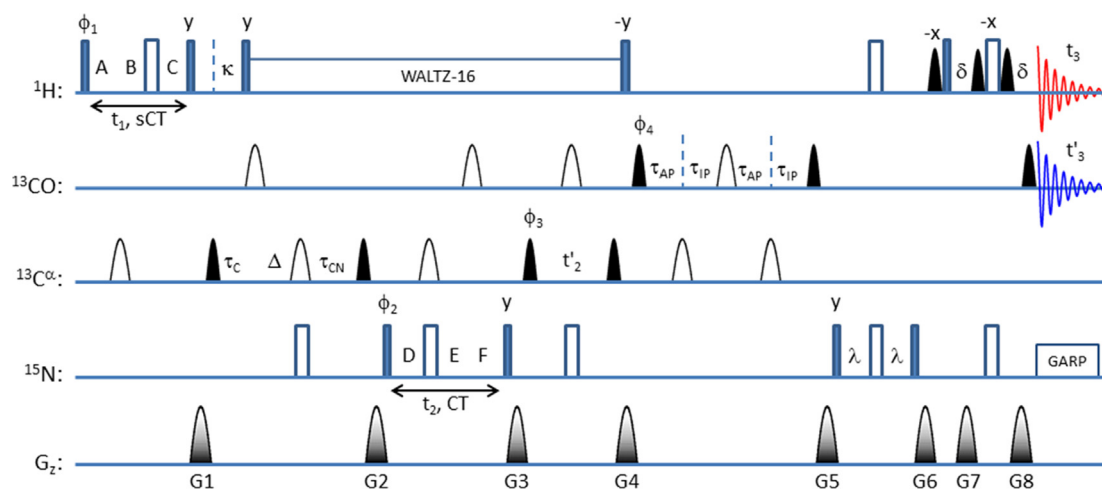
Fig. 47. 3D-HA(CA)NH / 3D-HACACO pulse scheme with parallel acquisition of $^1H^N$ and ^{13}CO nuclei. Phase cycling: $\phi_1 = x, -x$; $\phi_2 = \phi_3 = 2(x), 2(-x)$ and $\phi_{rec} = x, 2(-x), x$; all other pulses are applied with phase 'x' unless indicated otherwise. States-TPPI applied to phases ϕ_1 and ϕ_2/ϕ_3 along with phase of the corresponding receivers, ϕ_{rec}. The ^{13}C carrier frequency is initially set at 54 ppm and after gradient pulse G4 is switched to 176 ppm. Gradient pulses (G/cm, 1 ms): G1 = 25, G2 = G3 = G4 = 15, G5 = G6 = 40 and G7 = G8 = 30. Delays: $\kappa = 2.2$ *ms*, $\tau_C = 3.5$ *ms* (to be optimized), $\tau_{CN} = 12.5$ ms, $T_N = 14$ ms, $\lambda = \delta = 2.7$ ms, and $\Delta = \tau_{CN} - \tau_C$; A, B and C are semi-constant t_1-evolution (Hα) delays, D, E and F are constant time t_2 evolution (^{15}N) delays. The IPAP scheme is employed for recording 3D-HACACO data set by setting $\phi_4 = y$, $\tau_{IP} = 4.5$ ms, $\tau_{AP} = 0$ ms for the IP component and $\phi_4 = -x$, $\tau_{AP} = \tau_{IP} = 2.25$ ms for the AP component.

pulse sequence, [136] magnetization is transferred according to the pathway:

$$H_z \xrightarrow{J_{NH}} 2H_zN_z \xrightarrow{J_{NH} J_{NCa}, t_1} 2N_zC_z^a \cos(\omega_{Ca}t_1)$$

with $2N_zC\alpha_z$ present immediately after the t_1 period. During the period between points *a* and *b*, ^{15}N coherence is refocused with respect to $^{13}C\alpha$, allowed to evolve (partially) due to the scalar ^1J ($^{15}N-^{13}CO$) coupling, while it remains encoded by the ^{15}N chemical shift. After point *b* the magnetization pathways for $^1H^N$ (N_z) and ^{13}CO ($2N_zC_z$) detection diverge, and the remaining portion of the sequence is identical to that already described for the 2D $^1H/^{13}CO$

^{15}N HSQC experiment shown in Fig. 43. Thus, a pair of 3D data sets correlating $^{13}C\alpha – ^{15}N – ^1H^N$ and $^{13}C\alpha – ^{15}N – ^{13}CO$ is obtained in a single measurement. Note that the two 3D data sets share two indirect evolution periods, t_1 and t_2, and, therefore, have a joint F_1F_2 plane ($^{13}C\alpha$, ^{15}N). Therefore, the experiment provides information about four nuclei, $^1H^N$, ^{15}N, $^{13}C\alpha$ and ^{13}CO, as in the 4D HNCACO experiment. As such it can be regarded as a reduced dimensionality experiment.

Fig. 46 compares strip plots from a pair of parallel $^1H/^{13}CO$ detected 3D HNCA data sets. High quality data sets of Lb-FABP protein (125 residues) were obtained, with 119 intra- and inter-residue correlations and 116 intra-, 109 inter-residue cross-peaks
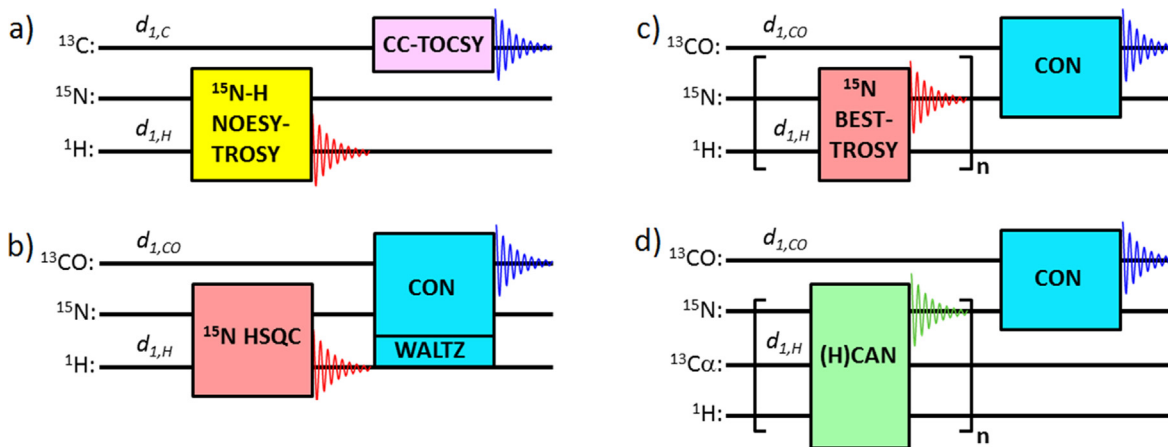
Fig. 48. Interleaved correlation experiments with dual detection of ^{1}H/^{13}C and ^{13}C/^{15}N FID-s [150]. In (b) proton decoupling can be afforded due to the shorter ^{1}H recovery delay; in (c) and (d) the ^{15}N-detected experiments can be repeated 3–4 times due to the fast proton recovery.

observed in the ^{1}H^N and ^{13}CO detect experiments, respectively (out of a possible 122) [107]. A comparison of the two data sets makes it very easy to link ^{1}H^N and ^{13}CO chemical shifts, and because the ^{13}CO chemical shift is recorded directly much higher resolution can be obtained than from conventional HNCO data sets. This demonstrates the feasibility of obtaining the backbone assignment of a small to medium-size protein (except for prolines) from a single 3D dual receiver experiment.

An alternative scheme – a parallel HA(CA)NH / HACACO experiment for backbone assignment from a single measurement with magnetization originating from ^{1}Hα – has been proposed by Reddy and Hosur [143]:
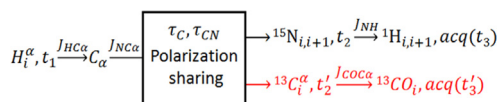
Following the ^{1}Hα evolution the proton magnetization is transferred to ^{13}Cα, where it is split into two pathways – part of the magnetization (in black) is transferred to the ^{15}N nuclei, and the other part (in red) remains on the Cα nuclei (see Fig. 47). As in the dr-HNCA experiment, [107] this step is used to balance the sensitivities of the ^{1}H^N and ^{13}CO detected spectra of this dual receiver experiment. However, in this experiment two independent evolution periods (t_2 and t_2') are used before the magnetization is transferred to ^{1}H^N and ^{13}CO for detection. Thus, two 3D experiments - HA(CA)NH and HACACO, with a joint ^{1}Hα frequency axis – are recorded in parallel. This experiment involves five evolution periods and therefore can be regarded as a 5D reduced dimensionality experiment. Notably, the joint frequency space connecting the two 3D experiments, HA(CA)NH and HACACO, is one-dimensional (^{1}Hα axis), limiting the resolution that can be achieved in protein samples.

This pulse sequence has been extended to parallel 3D HBHA(CA)NH / 3D HBHACACO and 3D-(HB)CB-CANH / 3D-(HB)CBCACO experiments that include also the sidechain resonances, to further facilitate resonance assignments [144].

3.2.3.3. Interleaved experiments. Just like the sequential and parallel detection experiments described in the previous sections, interleaved experiments offer significant time savings compared to the conventional way of recording experiments, provided distur-

bance of the magnetization pools used in the alternating pulse schemes can be avoided. Initially interleaved experiments were introduced in MRS [145] and MRI, [146] and more recently they have been employed in NMR of small molecules in liquids [38,113,147] and in solids [148]. Design of the interleaved experiments is much simpler than that of sequential and parallel detection experiments. It is often possible to simply concatenate the alternating pulse programs. As in the case of NOAH supersequences, such experiments can be represented by simple block diagrams. In situations that require use of an inversion pulse on the recovering spins, e.g., for decoupling purposes, an appropriately spaced pair of such pulses can be used to return the disturbed spins to equilibrium.

A simple and rather obvious example is the interleaved 2D ^{1}H-^{15}N NOESY-TROSY / ^{13}C-^{13}C TOCSY experiment for deuterated samples (Fig. 48a). A ^{1}H-^{15}N NOESY-TROSY pulse scheme that applies pulses only to ^{1}H and ^{15}N can be concatenated with a ^{13}C-^{13}C TOCSY sequence, as deuterated samples do not require ^{1}H decoupling and only employ ^{13}C RF pulses. The two pulse schemes are based on largely independent coherence transfer pathways. This experiment has been named UTOPIA (Unified
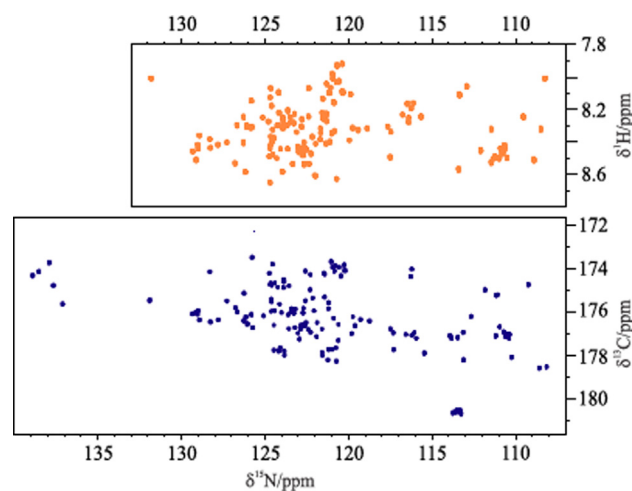
Fig. 49. 2D spectra of 1 mM ^{13}C,^{15}N labelled α-synuclein recorded at 285 K and pH 6.5 using the interleaved CON/BEST-TROSY pulse scheme incorporating direct detection of ^{13}C and ^{15}N resonances. Reproduced from Ref. [150] with permission

Time-OPtimized Interleaved Acquisition) [149]. In perdeuterated proteins, such as the U-[^{2}H,^{13}C,^{15}N] labelled (fully ^{1}H back-exchanged) soluble Bcl-x$_L$ protein (21 kDa) that was used for tests, the signal intensities in the UTOPIA experiments were essentially the same (95%) as in the corresponding spectra recorded using the conventional approach.

As pointed out by Viegas et al. it is possible to reorganize parallel detection experiments to allow sequential acquisition of FIDs on single receiver systems, albeit at the price of some sensitivity loss [149]. One such example is the interleaved version of the parallel 2D ^{15}N HSQC experiment named HN/CO (see Fig. 48b) [150]. The 2D CON experiment does not benefit from the ^{1}H polarization transfer and faster ^{1}H relaxation and, therefore, is less sensitive, but it allows the recording of correlations to proline residues. The ^{1}H-^{15}N HSQC experiment is acquired during the lengthy ^{13}CO recovery time of $d_1 = 2$ s. Decoupling ^{15}N from ^{13}C during the ^{15}N evolution period of the ^{15}N HSQC experiment was achieved by a pair of 180° ^{13}C pulses, thus minimizing the disturbance of the ^{13}CO recovery process. Hence, the sensitivity of the ^{15}N-^{1}H and ^{13}CO-^{15}N correlation experiments is largely unaffected compared to the stand-alone modules. A slightly higher sensitivity loss (15%) in the ^{15}N-^{1}H correlation spectra as compared to that in the CON spectra (5%) is partially due to the need to use ^{1}H composite pulse decoupling throughout the whole CON experiment, to minimize possible effects of exchange processes between solvent and amide protons. These are known to reduce signal intensities, especially when approaching the pH of physiological conditions. The slight loss in sensitivity of the ^{1}H detected ^{15}N HSQC experiment is of little consequence due to its significantly higher overall sensitivity compared to the ^{13}CO-^{15}N correlation experiment. Decoupling of ^{15}N from ^{13}C during the ^{15}N evolution period of ^{1}H-^{15}N HSQC could be achieved by a combination of two 180° pulses in appropriate positions, to restore the CO magnetization to equilibrium as a starting polarization source for the CON experiment. A very similar approach is used in the interleaved 3D HNCA / 2D NCO experiment [149]. The versatility of multi-receiver experiments becomes particularly important for samples that have limited lifetimes, such as cell lysates. For instance, the much more pronounced increase in ^{1}H linewidth compared to that of ^{13}C in in-cell spectra indicates that this is not due to possible differences in experimental conditions or in-cell sample quality but is rather an effect of in-cell processes.

The number of experiments with completely independent coherence transfer pathways in biomolecular NMR is rather limited, since almost all such experiments involve RF pulses on all three major nuclear species – ^{1}H, ^{13}C and ^{15}N. Schiavina et al. have overcome this problem by using protons only as a polarization source, avoiding direct ^{1}H detection and instead focussing only on pulse schemes with direct ^{13}C and ^{15}N detection [150]. For instance, the CON experiment can be interleaved with pulse schemes based on direct ^{15}N detection, such as the BEST-TROSY experiment [151]. Furthermore, the very efficient T_1 relaxation of amide protons in intrinsically disordered proteins (IDPs) enables repetition of the ^{15}N-detected version of the BEST-TROSY experiment 3–4 times during the ^{13}CO recovery period (Fig. 48c). This significantly reduces the imbalance in sensitivity between experiments with direct detection of ^{13}C and ^{15}N resonances. To avoid disturbing ^{13}CO recovery, broad-band ^{13}C decoupling during the direct ^{15}N detection period was replaced by virtual ^{13}CO decoupling based on the IPAP scheme and band-selective ^{13}Cα decoupling. Likewise, to aid ^{1}H recovery proton CPD decoupling during the CON experiment was omitted and a pair of ^{1}H^N band-selective inversion pulses was used during the ^{15}N t_1-evolution period for N-H decoupling purposes. This reintroduced susceptibility to solvent exchange processes and couplings to ^{1}H during the direct ^{13}CO detection period, reducing the sensitivity of the CON experiment. However, this was found to be of little consequence since the sensitivity of the CON experiment was still much higher than the ^{15}N detected BEST-TROSY (see Fig. 49).

A similar experiment involving direct detection of ^{15}N and ^{13}CO FIDs is the interleaved CON/(HA)CAN pulse scheme (Fig. 48d) [150]. In the (H)CAN pulse sequence polarization is sourced from ^{1}Hα, making this experiment less vulnerable to amide proton exchange processes [152]. This is followed by frequency encoding of Cα resonances during the t_1 evolution period. The magnetization is then transferred via $^1J(^{13}$C-^{15}N) coupling to ^{15}N^i of the same residue, and via the $^2J(^{13}$C-^{15}N) coupling to ^{15}N^{i-1} of the previous residue. The latter provides information that is complementary to that from the interleaved CON experiment. The relatively short Hα recovery time enables the recording of several (H)CAN scans during the ^{13}CO recovery period. The compromises made in the CON pulse scheme are very similar to those in the interleaved CON / BEST-TROSY experiment. Approximately 113 out of 139 inter-residue connections were observed in the ^{15}N,^{13}C-labelled α-
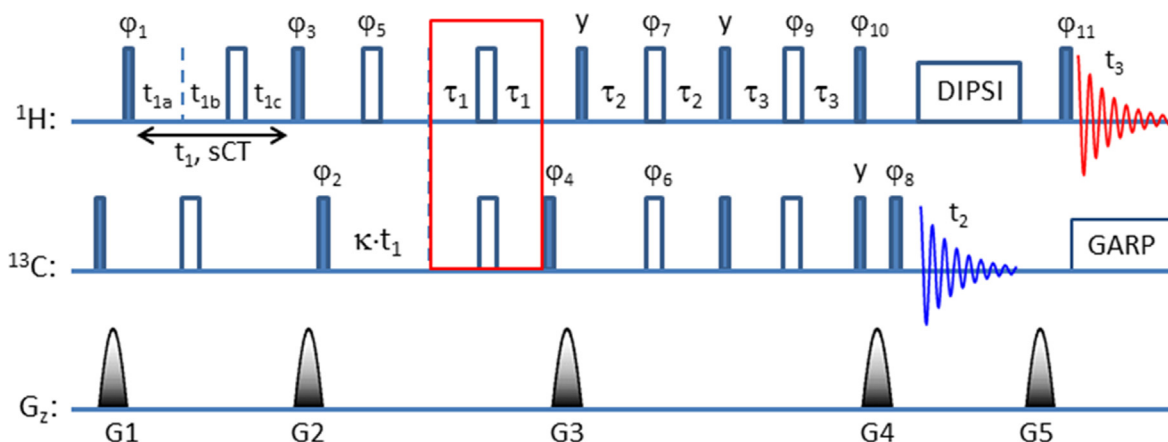
Fig. 50. Multiplicity-edited ^{13}C (3, 2)D HSQC-TOCSY / HETCOR / TOCSY pulse sequence [156]. All pulses are applied with phase 'x' unless indicated otherwise; phase cycling: $\varphi_1 = \varphi_2 = x$ (incremented according to the States method); $\varphi_3 = y$, $-y$; $\varphi_4 = \varphi_7 = \varphi_{10} = x$, $-x$; φ_4 is alternated for TS encoding; $\varphi_5 = \varphi_6 = \varphi_8 = \varphi_9 = \varphi_{11} = x$, x, $-x$, $-x$; $Rec(^{13}$C) = x, x, $-x$, $-x$; $Rec(^1$H) = x, $-x$, $-x$, x. Delays: $\tau_1 = 3.6$ ms, $\tau_2 = 1.79$ ms, $\tau_3 = 0.893$ ms; the ^{1}H t_1-evolution period is implemented in a semi-constant time manner; at $t_1 = 0$ the delays t_{1a}, t_{1b} and t_{1c} are set to 0.9 ms, 3 µs and 0.9 ms, respectively such that $T_{CT} = t_{1a} + t_{1b} + t_{1c} = 0.25/^1J(^{13}$C-^{1}H). The ^{13}C t_1-evolution period is co-incremented with that of ^{1}H with a relative scaling factor (κ). The DIPSI mixing time was 80 ms. Gradient pulses (1 ms): G1 = G2 = G3 = G4 = 19 G/cm, G5 = 11 G/cm; the red box indicates an optional ^{13}C multiplicity editing block.
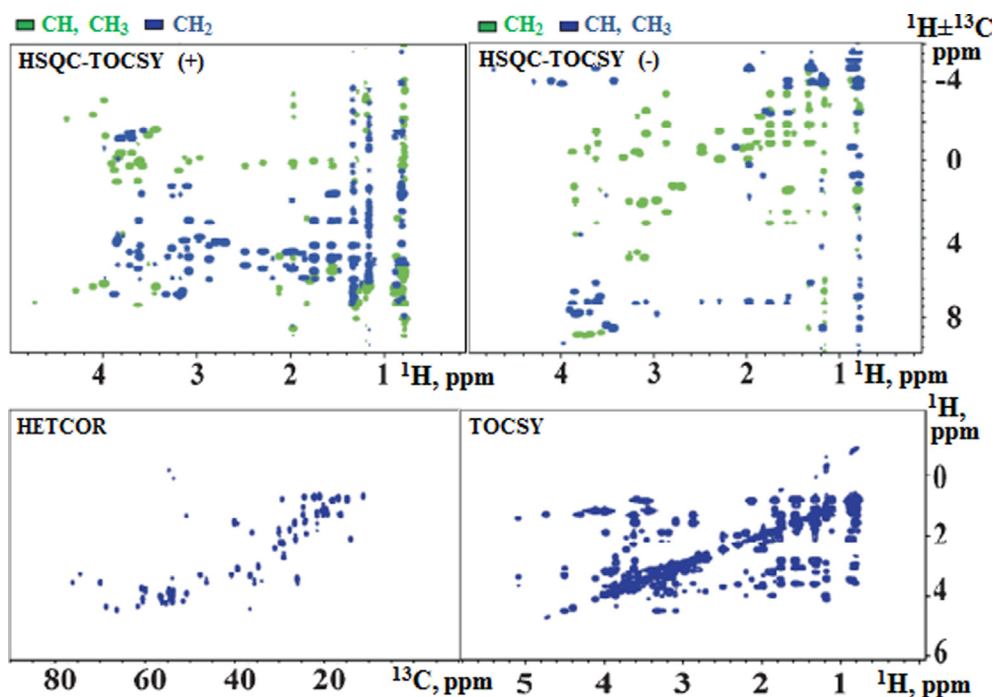
Fig. 51. 2D H-C HETCOR, 2D TOCSY and ^{13}C multiplicity-edited (3, 2)D HSQC-TOCSY spectra of a 21 metabolite mixture in D$_2$O recorded at 25° C on a Bruker Avance spectrometer operating at 800 MHz (^{1}H) frequency and equipped with cryogenically cooled probe and two receivers. The components of the mixture were alanine, arginine, asparagine, cysteine, glucose, glutamine, histidine, lactate, lysine, isoleucine, leucine, methionine, phenylalanine, proline, pyruvate, serine, taurine, threonine, tryptophan, tyrosine and valine. Reproduced from Ref. [156] with permission.

synuclein sample, but only a fraction of the resonances were resolved in these 2D spectra. The authors conclude that the possibility to acquire the two spectra simultaneously is very important, particularly in samples of limited lifetime [150]. The availability of cryoprobes optimized for direct detection of heteronuclei is paramount in such experiments.

3.2.4. Multi-receiver experiments in metabolomics

NMR spectra in metabolomics research typically suffer from strong signal overlap, making resonance assignment problematic. Therefore, the use of multidimensional techniques and spectral simplification techniques for unambiguous identification of metabolites in mixtures is essential. The multidimensional NMR methods that are most often used in metabolomics include 2D COSY, 2D TOCSY, 2D ^{13}C HSQC, 2D and 3D TOCSY-HSQC and 2D ^{13}C HMBC [153]. Recording such experiments is often very time-consuming. Atreya *et al.* have combined the sequential dual-receive 2D TOCSY / HETCOR [24] experiment with a reduced dimensionality (TILT [154]) 3D HSQC-TOCSY pulse scheme for metabolomics applications (see Fig. 50) [155,156]. Magnetization of protons bound to ^{12}C and ^{13}C is channelled through separate coherence pathways as schematically summarized below:
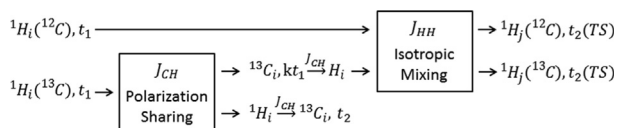
The experiment begins with a ^{1}H excitation pulse and a joint constant time t_1 evolution period. One of the two orthogonal components of the ^{1}H magnetization bound to ^{13}C is transferred to ^{13}C, while the ^{12}C bound proton magnetization is preserved and used solely for the 2D TOCSY experiment. The ^{13}C magnetization is then

frequency labelled jointly with the proton t_1 period, except that a scaling factor, κ, is applied to the ^{13}C t_1 increments, to obtain two tilted projections of the 3D HSQC-TOCSY experiment. This is followed by an optional multiplicity editing segment (red box in Fig. 50) and a reverse INEPT transfer back to protons for TOCSY mixing and detection. At the same time the second orthogonal component of protons bound to ^{13}C is transferred to ^{13}C for direct detection to produce the HETCOR spectrum. The 2D TOCSY and the two tilted planes of the 3D HSQC-TOCSY spectra are detected in parallel in time-shared fashion. Thus, the experiment offers a wealth of information. In addition to spectra recorded with the two receivers, 3D HSQC-TOCSY spectral information is obtained from the two orthogonal (H-H TOCSY and H-C HETCOR) planes and two HSQC-TOCSY planes tilted at an angle $\alpha = \pm \arctan(\kappa)$.

The pulse scheme has been used to record spectra of a mixture containing 21 metabolites in the 1 mM concentration range (see Fig. 51). Spectra were acquired on an 800 MHz NMR system equipped with a cryogenic probe that provided sufficient sensitivity for use of non-uniform sampling to further reduce the measurement time [15–17,23].

4. Multiple-FID experiments in solids

The use of multiple acquisitions (loosely defined as acquisition of multiple FIDs before the delay for T_1 recovery) has a long history in solid-state NMR. The first example of such a sequence was the pioneering work on cross-polarization by Pines and Waugh [41]. The detection of multiple FIDs after each of the sequentially implemented Cross-Polarization (CP) steps was first demonstrated here. This leads to a boost in sensitivity over that achieved by a single cross-polarization step. A critical requirement to perform such an experiment is the use of a highly efficient spin-lock on ^{1}H (during CP and during decoupling), to yield sufficiently long rotating-frame relaxation times, $T_{1\rho}$. The signal from all of the

detected FIDs is subsequently added up after normalizing the noise in each spectrum. This approach has, however, not been utilized often, most likely due to the development of phase- and amplitude-modulated ^{1}H decoupling sequences, which result in better decoupling, but often scramble the phase of the ^{1}H magnetization, as well as the technical challenge of using high-power RF pulses with increased duty cycles. Contemporary takes on this approach with multiple cross-polarization contact steps and a single direct acquisition have been demonstrated in oriented NMR [157] and in MAS (Magic-Angle Spinning) NMR [158]. Here, an additional requirement is fast T_1 relaxation of the attached ^{1}H or ^{2}H, to make repeated cross-polarization steps feasible. A direct implementation of the method of Pines and Waugh was also demonstrated on samples where CW decoupling suffices [159]. RELOAD-CP [160] uses a similar strategy of acquiring multiple spectra before the recycle delay, using fast T_1 relaxation in selective detection of ^{13}C nuclei due to fast spin diffusion from neighbouring ^{13}C nuclei.

Another class of experiments that can be classified under the umbrella of multiple acquisition is the echo-train acquisition scheme that uses a CPMG sequence [161,162]. The directly detected FIDs for many nuclei, especially those with quadrupolar spins, show large inhomogenous linewidths due to either high sample heterogeneity or very broad spectra in the frequency domain, or both. However, many of these samples can have narrow homogenous linewidths. One can apply spin-echo sequences and record several consecutive FIDs in such samples, resulting in a sensitivity boost. These experiments are routinely used for studying quadrupolar nuclei, as well as spin-1/2 nuclei in selected cases. Recent work from Grandinetti and co-workers [163] has shown that this experiment combined with selective 180° pulses can achieve sensitivity gains of over 1000 for isolated quadrupolar nuclei, allowing ^{17}O and ^{33}S spectra in samples with very narrow homogenous linewidths to be recorded at natural abundance within a very short time.

Although powerful, the two classes of examples given above are restricted in the sense that the multiple echoes or FIDs that are detected are finally combined (or processed together) to give a single spectrum. The current resurgence of multi-FID detection schemes in solids comes from a different direction: the need to record several multi-dimensional spectra for complete characterization of a single sample. This is especially true in the field of biomolecular solid-state NMR spectroscopy, where a single spectrum often does not suffice. The ability to design pulse sequences that combine complementary experiments in a straightforward and flexible manner is what makes these approaches useful. The following sections will outline the basic building blocks of these experiments, and provide a practical guide to implementing these sequences on spectrometers.

4.1. Creation of multiple coherences

Multi-FID detection techniques rely on two basic strategies: (i) generating multiple coherences which can be detected individually, and (ii) recovering coherences that are usually discarded in an experiment. The two examples described above - multiple contact times and echo-train acquisition sequences - in a sense serve as examples of these classes. Multiple cross-polarization steps generate new coherences that can be independently detected, while echo-train sequences recover and acquire signals that would have otherwise been lost. More flexible methods for generating multiple coherences in solids encompass methods that are similar those in solution NMR: one can either use simultaneous or staggered 90° pulses on different nuclei, simultaneous INEPT sequences, or simultaneous cross-polarization contacts. The first two are identical in implementation to their solution NMR counterparts,

although their implementation in solids has not yet been demonstrated to the best of our knowledge. Such a sequence is likely to be useful when 90°-pulse-detect sequences are required to characterize multiple nuclei [164]. The large difference in longitudinal relaxation times (T_1) between different nuclei in solids will then allow multiple scans to be recorded for the nuclei with a short T_1, before the next scan of a nuclei with a long T_1. Although INEPT transfers (using either scalar or dipolar couplings) can be implemented in solids, they are generally done at fast MAS frequencies where the spin-echo times are longer. A notable exception is the work by Opella and coworkers, who have demonstrated simultaneous dipolar-INEPT transfer using an R-symmetry based sequence in membrane proteins at 11.111 kHz MAS [56]. However, the overwhelming majority of sequences in solids use cross-polarization, and the implementation of simultaneous cross-polarization is discussed in detail in the next section.

Once generated, the individual coherences can be detected sequentially using appropriate pulse sequences, or simultaneously using multiplex phase cycling [165] to separate out different pathways. As long as individual FIDs are detected sequentially (i.e., not at the same time), a single physical receiver suffices to carry out all of these experiments on most modern hardware [149], as one can rapidly switch between different detection channels. A second physical receiver is required only if the detection on two or more nuclei is to be carried out simultaneously. Only a few experiments of this type have been explored in the literature [166–168], and even in these cases the experiment itself can often be rearranged so that the spectra are detected sequentially rather than simultaneously. As such, in this review, we do not make a distinction between the uses of detection with one or more physical receivers, unless specifically pointed out. This distinction is also expected to be rendered moot in the near future due to the availability of individual receivers on each RF channel from all the major manufacturers of NMR instrumentation. Nevertheless, it is possible that the use of multiple receivers will allow more flexibility in the implementation of some of these pulse sequences and allow one to reduce probe duty cycles. These aspects will be pointed out when important.

4.1.1. Simultaneous cross-polarization (Sim-CP)

The distinctive feature of multi-FID detection experiments in solids is the use of simultaneous CP, and it forms the basis of the majority of sequences that fall into this category. Most pulse sequences in biomolecular solid-state NMR start with CP from ^{1}H to ^{13}C or ^{15}N. In addition to the increase in sensitivity due to the higher gyromagnetic ratio of ^{1}H, CP also allows one to repeat an experiment more frequently due to the shorter T_1 (^{1}H) in most solid samples. A critical feature of CP in solids is that it is a bulk phenomenon, i.e., multiple ^{1}H nuclei contribute to the final polarization on the heteronucleus. However, dipole-dipole coupling, which mediates CP, has a steep distance dependence. Consequently, the final polarization on a heteronucleus is overwhelmingly from the directly attached ^{1}H, if such a ^{1}H nucleus exists. It follows that ^{13}C and ^{15}N nuclei in proteins that are connected to different ^{1}H nuclei can be independently cross-polarized and detected, without much loss in SNR. As these coherences can be detected independently before the recycle delay, such an experiment would be equivalent to a time saving of 50%, i.e., two different experiments that would each take a time "t" to record (total time 2 t), would now be done in time t. However, a small fraction of the polarization does come from the remote protons. This corresponds to a small but significant loss in SNR, and the time savings obtained using Sim-CP are typically only 30–40%. Nevertheless, these time savings can be substantial, as several weeks of NMR time are commonly required for assigning proteins in the solid state.
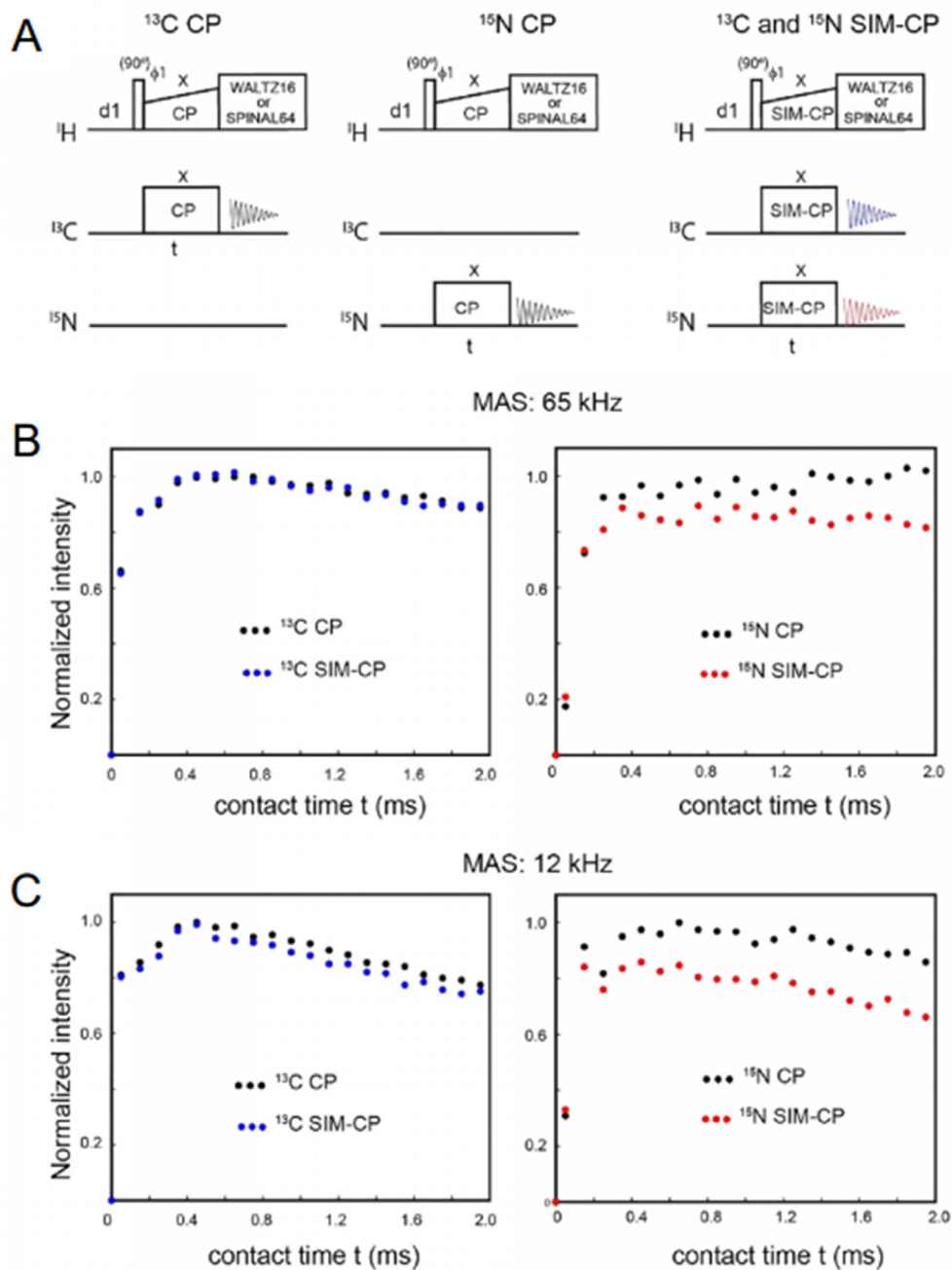
Fig. 52. Simultaneous cross-polarization from ^1H to ^{13}C and ^{15}N. (A) Pulse sequences used for the comparison of Sim-CP with standard CP. (B) Comparison of the sensitivity of ^{13}C and ^{15}N CP (black points) with ^{13}C Sim-CP (blue points) and ^{15}N Sim-CP (red points) at the MAS frequency of 65 kHz, as a function of the contact time of the cross-polarization element. (C) Same as that in B, except at the MAS frequency of 12 kHz, respectively. A-C adapted from Ref. [173] with permission.

4.1.2. Optimization of Sim-CP

Under slow to moderate MAS frequencies (<20 kHz), CP is usually done at the Hartmann-Hahn matching condition under magic-angle spinning: the RF amplitudes (ν_X) on ^{13}C and ^{15}N are ideally set at approx. 43–45 kHz [169], and the ^1H RF amplitude (ν_H) is swept around the n = 1 or n = 2 sideband matching condition ($\nu_H - \nu_X = n\nu_r$). At MAS frequencies greater than 8 kHz, the RF amplitude for ^1H must therefore be greater than or equal to 60 kHz. Note that higher RF amplitudes may be required on ^{13}C at higher magnetic fields (>1 GHz) to efficiently spin-lock all different types of ^{13}C spins in biomolecules, further increasing the RF on requirement on ^1H. Thus, an efficient spin lock can be obtained for virtually all ^1H nuclei in proteins even at the highest magnetic fields currently

commercially available (assuming a chemical shift range of ~10–12 ppm found for ^1H in most proteins). This allows cross-polarization to be done efficiently to both ^{13}C and ^{15}N nuclei. To the best of our knowledge, the first example of the use of Sim-CP for biomolecular samples in solids is the work by Ramachandran and co-workers [166], where it was used to cross-polarize ^{15}N and ^{13}C nuclei in RNA. It was later extended to protein samples by Reif and co-workers [170], who used it to cross-polarize the well-separated amide ^{15}N and methyl ^{13}C spin-systems in highly perdeuterated, amide-^1H -back-exchanged and selectively methyl-labelled proteins. Veglia and co-workers demonstrated the general applicability of Sim-CP in uniformly ^{13}C and ^{15}N labelled protonated proteins [97]. Fig. 52 shows the comparison
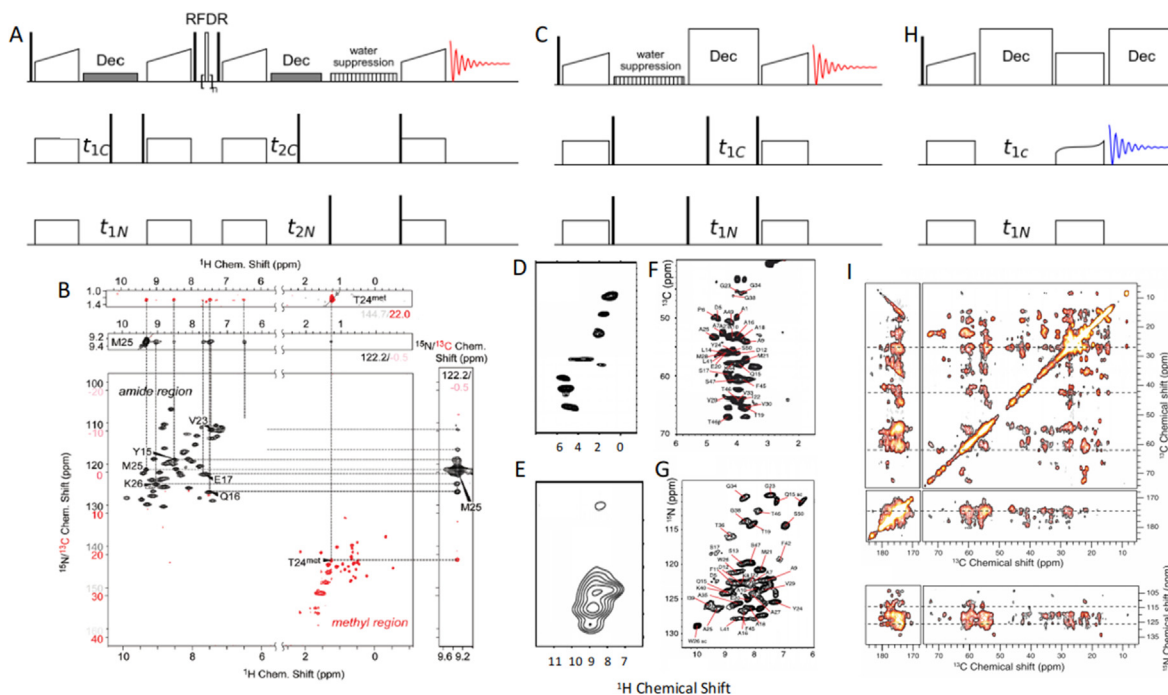
Fig. 53. Utilizing Sim-CP to perform two experiments. (A) Pulse sequence and (B) spectra for the simultaneous acquisition of CCH and NNH spectra using CHHC and NHHN transfers in a sample of perdeuterated, ^{1}H-back exchanged and selectively ^{13}C-^{1}H methyl labelled ubiquitin. (C) Pulse sequence for the simultaneous acquisition of CH and NH correlation spectra (D-E) Simultaneously acquired ^{13}C-^{1}H and ^{15}N -^{1}H spectra for a sample of selectively labelled Aβ$_{40}$ using windowed ^{1}H detection at 12.5 kHz MAS and (F-G) a uniformly ^{13}C and ^{15}N labelled membrane protein at 62.5 kHz. (H) Pulse sequence and (I) spectra for the simultaneous acquisition of PAR and PAIN experiments on a sample of ^{13}C and ^{15}N labelled ubiquitin. (B) adapted from Ref. [165] with permission. (D-E) adapted from Ref. [172] with permission. (F-G) adapted from Ref. [171] with permission. (I) adapted from Ref. [178] with permission.

of standard CP and Sim-CP in proteins at slow and fast MAS frequencies. It is seen that in uniformly ^{13}C, ^{15}N labelled samples, the efficiency of Sim-CP is close to 90–95% for ^{13}C, and 80–85% for ^{15}N. This comparison also holds at the fastest available MAS frequencies, where ^{13}C or ^{15}N-edited ^{1}H experiments can be acquired with a similar sensitivity (Fig. 52). This approach has since been used by a number of laboratories to generate multi-FID detection schemes at slow to moderate [98,167,171,172], and fast MAS frequencies [171,173–175].

Practically, the following approach has given optimal transfers to ^{13}C and ^{15}N in the hands of the authors at slow to moderate MAS frequencies: (i) Optimize cross-polarization conditions from ^{1}H to ^{15}N, keeping the ^{1}H offset at ~5 ppm. (ii) Keeping the RF at the optimized conditions on ^{1}H and ^{15}N, optimize the ^{13}C RF amplitude and the contact time near values close to the RF used for ^{15}N. Compared to the independently optimized transfers, Sim-CP gives ~100% and ~80% transfer on ^{13}C and ^{15}N, respectively [97]. Under fast MAS frequencies (60 kHz and above), either the zero-quantum or the double quantum recoupling condition ($v_H - v_X = nv_r$, usually with n = 1) can be utilized. Examples for both exist in the literature: double quantum recoupling conditions were used at MAS frequencies of 62.5 kHz [174] ($v_X \sim 40$ kHz, $v_X \sim 22$ kHz) whereas single-quantum recoupling conditions ($v_X \sim \ldots$ kHz, $v_X \sim \ldots$ kHz) were used at MAS frequencies of 60–65 kHz [171,173] and 107 kHz [175]. In all of these cases, the yields of the transfer to ^{13}C and ^{15}N were 90–95% and 80–84%, respectively, in independently optimized CP experiments, (Fig. 52).

Once simultaneous cross-polarization is established, the resulting transverse ^{13}C and ^{15}N magnetizations can be immediately detected, while decoupling the ^{1}H, giving the respective 1D spectra. Such an experiment requires two receivers, which is becoming increasingly common. Otherwise, one can allow the ^{13}C and ^{15}N magnetization to co-evolve in the indirect dimension and then

simultaneously transfer their polarizations back to ^{1}H for detection at sufficiently high MAS frequencies [170,171], or using homonuclear decoupling and windowed detection at slow to moderate MAS frequencies [172]. ^{13}C-^{1}H and ^{15}N-^{1}H correlation spectra acquired using this strategy are shown in Fig. 53 A-G. An alternative to this is the use of simultaneous proton-assisted recoupling (PAR) [176] and proton-assisted insensitive nuclei cross-polarization (PAIN-CP) [177] blocks for establishing ^{13}C-^{13}C and ^{15}N-^{13}C correlations respectively, which can then be detected simultaneously [178,179] (Fig. 53 H-I). This experiment requires choosing the RF amplitudes for the three nuclei so that the PAR and PAIN conditions are simultaneously satisfied [180]. The above strategies technically do not belong to the class of multiple acquisition, as only a single FID is detected in these experiments before the recycle delay. However, multiple coherence pathways are detected here. Furthermore, if desired, both these experiments can be conveniently converted into experiments that do acquire multiple FIDs (vide infra), and are thus classified in the same category. This will, however, come at the cost of increasing the decoupling time during the pulse sequence, which can cause significant sample heating, especially at slow to moderate MAS frequencies where high RF amplitudes are required for decoupling.

4.1.3. Storage of ^{15}N polarization

Although useful under many circumstances, the above strategies do not give spectroscopists much choice regarding the combination of experiments. The ^{13}C and ^{15}N polarizations generated must be used immediately by either detecting the FIDs or allowing the respective chemical shifts to evolve, or by immediately transfering these to other spins. The strategy of Veglia and co-workers, dubbed Dual-Acquisition Magic-Angle Spinning (DUMAS) [97], lifted this restriction by proposing the following way around this problem: ^{15}N T_1 relaxation times in proteins in the solid state
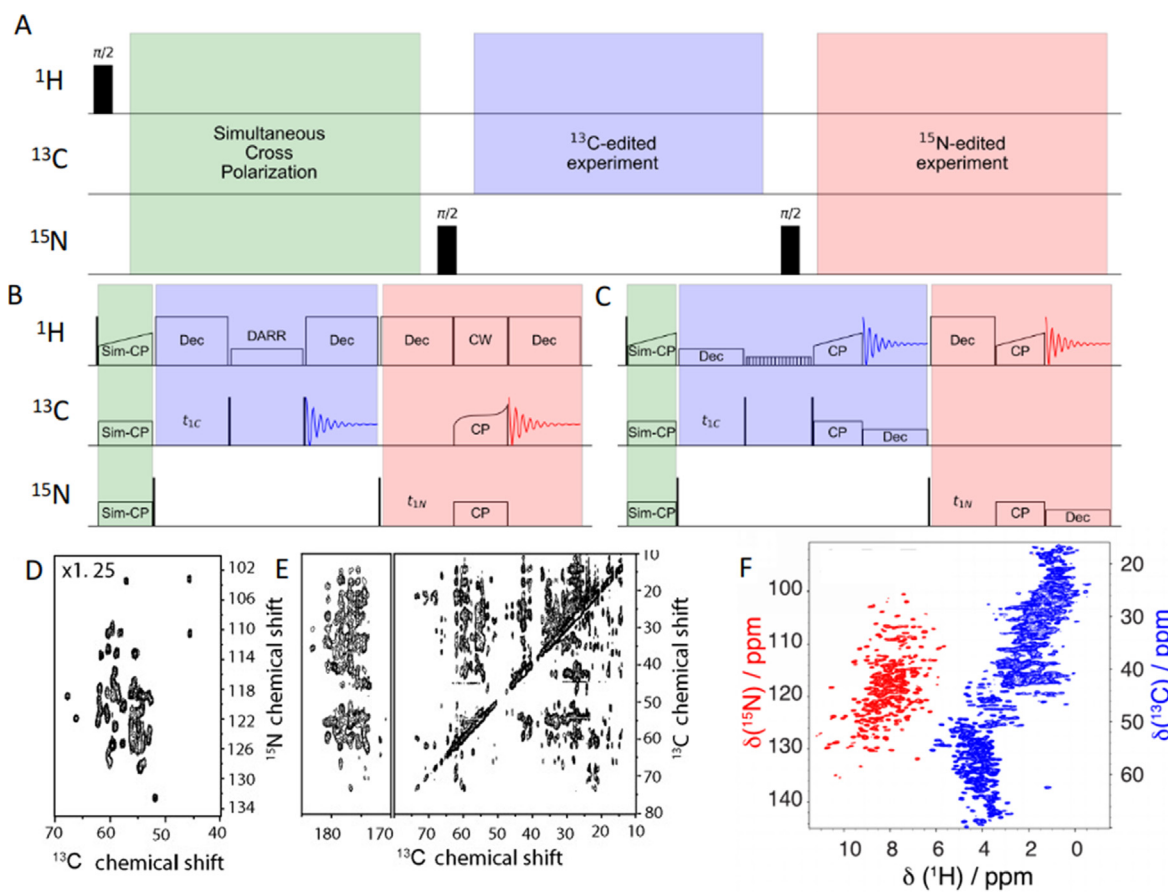
Fig. 54. A general strategy for acquiring ^{13}C and ^{15}N edited experiments. (A) A general strategy for combining pulse sequences for multiple acquisition scheme. (B) A specific implementation of the strategy in (A) for the sequential acquisition of DARR and NCa spectra under slow-moderate MAS frequencies. (C) A specific implementation of the strategy in (A) to sequentially acquire ^{13}C-^1H and ^{15}N-^1H correlation spectra. Experimental data for sequentially acquired NCa (D) and DARR (E) spectra, and sequentially acquired ^{13}C-^1H and ^{15}N-^1H correlation spectra (F). (D-E) adapted from Ref. [97] with permission. (F) adapted from Ref. [175] with permission.

are long, of the order of 10 s or more [181]. This means that $^{15}N_z$-magnetization does not decay significantly during the course of typical NMR experiments. Further, PDSD (Proton-Driven-Spin-Diffusion) [182] between neighbouring ^{15}N nuclei in proteins is inefficient due to the relatively long distances between ^{15}N nuclei in proteins and its relatively low gyromagnetic ratio. Once stored as longitudinal magnetization, this polarization thus remains unperturbed, and can be recalled with a simple 90° pulse whenever desired. The simplest way to achieve this is by applying a 90° pulse on ^{15}N after the initial Sim-CP to ^{13}C and ^{15}N. Any ^{13}C-edited experiment that does not require polarization transfer to ^{15}N (for example, 2D DARR, 2D DREAM, 2D DQSQ-correlation, 3D CCC, 3D CHH [183]) can then be done as usual. After the FID from this experiment is detected, the ^{15}N polarization can be recalled with a 90° pulse, and any desired ^{15}N-edited experiment can be performed without restriction. Fig. 54A shows a general schematic for achieving a combination of a ^{13}C-edited and a ^{15}N edited experiment. Fig. 54B shows a specific implementation for a combination 2D DARR and 2D NCA, and Fig. 54C shows the combination of a 2D ^{13}C-^1H and 2D ^{15}N-^1H correlations. These are the most commonly used 2D experiments in solid-state NMR of proteins at slow-moderate and fast MAS frequencies. Fig. 54D-F shows examples of these for a sample of ubiquitin at the MAS frequency of 12 kHz and MBP at 107 kHz (Note that the actual implementation of the pulse sequences in the original references is slightly different from the one shown in Fig. 54B-C). The increase in experiment time due to the additional detection is ~1–5%, depending on the indirect evolution and detection times, when a relatively long recycle delay

(2–3 sec) is used. Thus, an additional experiment with about 80% of the sensitivity is obtained in ~1.01–1.05 times the experiment time, representing a time saving of 35–40%. It is to be noted that when experiments are speeded up reducing the T_1 relaxation times by paramagnetic dopants [184], the relative increase in experiment time can be much higher and must be accounted for before implementing this strategy.

The evolution times and indirect spectral widths of ^{15}N and ^{13}C can be set up independently in the pulse sequence shown in Fig. 54B-C. If required, ^{15}N-decoupling and ^{13}C-decoupling during ^{13}C and ^{15}N evolution, respectively, can also be achieved using single 180° pulses in the middle of the evolution period. The only restriction is that the total number of scans acquired for the two experiments must be identical, i.e., $ns(^{13}C) \times ni(^{13}C) = ns(^{15}N) \times ni(^{15}N)$, where ns and ni are the number of scans per indirect increment and number of indirect increments for the nucleus indicated in the subscript. Given the large differences in the spectral widths required for ^{13}C (~200 ppm) and ^{15}N (~40 ppm) dimensions, it is often possible to perform several ^{15}N-edited experiments, for example, NCA, NCO, N(CA)CX, N(CO)CX, etc, while a single ^{13}C-^{13}C correlation experiment is being recorded [97,185]. Alternately, if the ^{15}N-edited experiments are insensitive due to reasons such as poor ^{15}N-^{13}C CP efficiency, a ^{13}C-edited experiment such as DARR can be repeated with different mixing times or switched altogether to other experiments such as DREAM or DQSQ-correlation.

A drawback of this approach is the doubling of the RF duty cycle required to execute the sequence. This can limit the advantages if
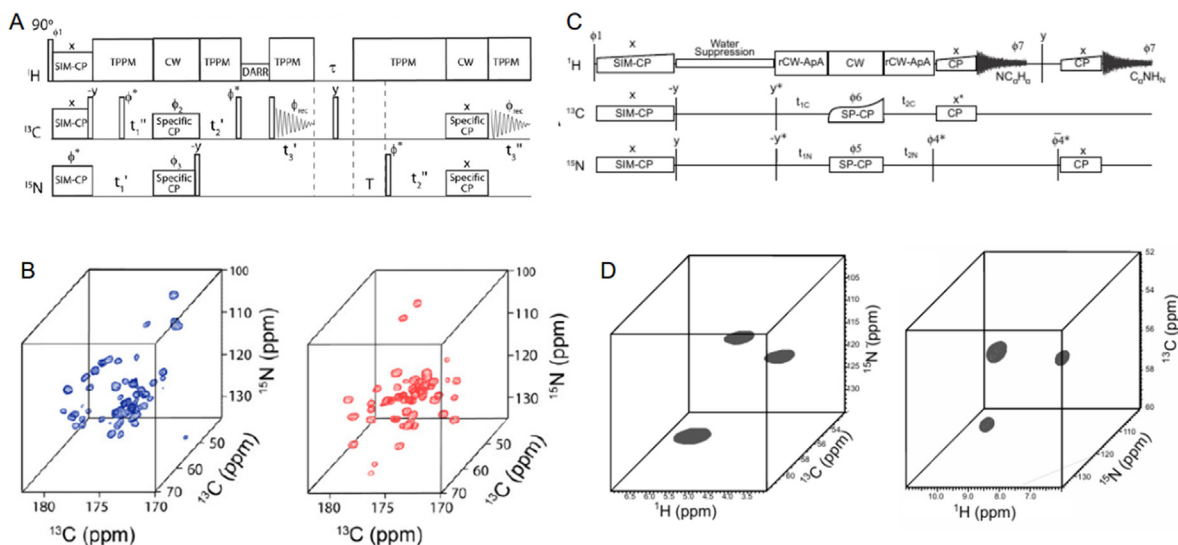
Fig. 55. Use of bi-directional polarization transfer to combine complementary 3D experiments. (A) Pulse sequence and (B) spectra for sequentially acquired 3D NCACX and 3D CANCO experiments on a sample of uniformly ^{13}C and ^{15}N labelled ubiquitin. (C) Pulse sequence and (D) spectra for sequentially acquired NCAHA and CANH spectra for a sample of ^{13}C and ^{15}N labelled MLF. (A-B) adapted from Ref. [189] with permission. (C-D) adapted from Ref. [174] with permission.
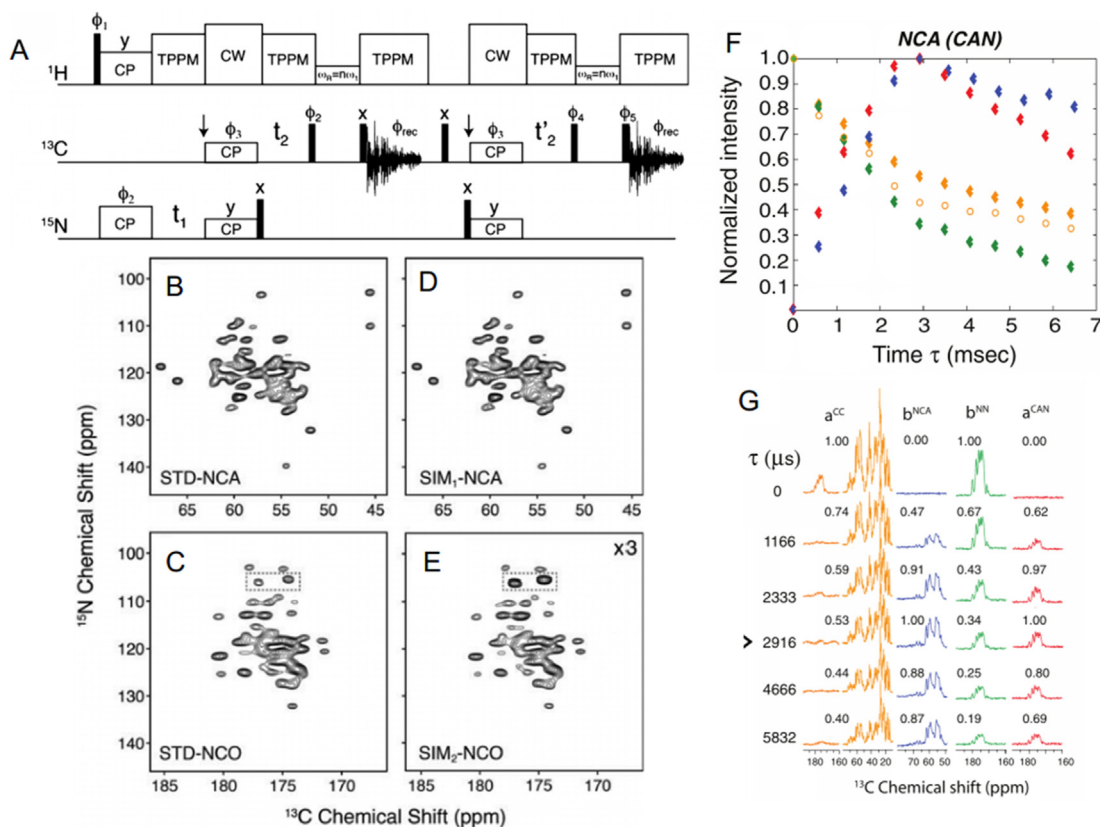
Fig. 56. Residual ^{15}N and ^{13}C polarizations after SPECIFIC-CP transfers. (A) Pulse sequence and spectra comparing standard NCA (B) and NCO (C) with sequentially acquired NCA (C) and NCO (D) spectra for microcrystalline ubiquitin. The spectrum in (E) was acquired using residual ^{15}N magnetization, which is ~30% of the starting magnetization. (F) Quantification of transferred and residual ^{13}C and ^{15}N magnetization after a bidirectional ^{13}C -^{15}N transfer (NCA and CAN). (G) 1D spectra for the comparison of sensitivity for the residual ^{13}C (yellow), residual ^{15}N (green), ^{15}N -edited ^{13}C (blue), and ^{13}C -edited ^{15}N (red) magnetization. When optimal SPECIFIC-CP contact times and conditions were used, ~50% magnetization was left behind on ^{13}C (aliphatic) and ~34% magnetization was left behind on ^{15}N. (A-E) adapted from Ref. [99] with permission and (F-H) adapted from Ref. [191] with permission.

the recycle delay is chosen to keep the RF duty cycle below some permitted maximum, rather than being determined by $T_1(^1H)$. One way out of this is to co-evolve ^{15}N and ^{13}C in the indirect dimension, as was done in the previous examples with ^{13}C-

detected [170,178] and ^{1}H-detected experiments [171,172] (Fig. 53). It is important to note that in this case, ^{15}N and ^{13}C decoupling cannot be applied during the indirect evolution. This is unlikely to result in a substantial sensitivity or resolution loss, except

for samples with very narrow resonances. However, the two direct detections still require independent decoupling blocks, and will result in an increased RF duty cycle. It is for this reason that it is often recommended that these experiments be done using so-called "Low-E" or "E-free" probes, where sample heating due to RF pulses is minimized using a coil geometry designed to minimize the electric field at the sample position from ^{1}H RF pulses [186,187]. These concerns are less applicable to data acquired at MAS frequencies > 60 kHz, as low RF amplitude decoupling schemes are sufficient under these conditions [188]. Strategies where ^{15}N and ^{13}C evolve independently can be used together with ^{1}H detection, without virtually any modifications other than the optimization of the Sim-CP conditions.

4.1.4. Bidirectional cross-polarization

None of the experiments described up to this point involve the transfer of polarization from ^{13}C to ^{15}N in the ^{13}C-edited experiments. This excludes a large class of experiments, such as 3D CaNCO or 3D CaNH, which are required in many assignment strategies. CP is inherently bidirectional, i.e., it is better described as an equilibration of polarization than a transfer. Thus, a CP step inserted in a pulse sequence when high polarization is present on both the ^{13}C and ^{15}N nuclei effectively results in an exchange of polarization, which can then be selected out using an appropriate phase cycle. Takeda and co-workers used this approach to record a combination of CAN(CA)CX and NNCA(N)N [167]. Veglia and co-workers combined it with the storage of ^{15}N$_z$-polarization to create a more generally applicable strategy: recording combinations of experiments such as 3D NCACX and 3D CANCO [189]

(Fig. 55A-B). A similar strategy can be extended to ^{1}H detection with a direct replacement of the ^{13}C detection step by a transfer from ^{13}C and ^{15}N to ^{1}H, followed by detection. Standard experiments such as CANH and NCAHA can be combined in a straightforward manner using this strategy [171,172,175] (Fig. 55C-D).

4.1.5. Residual polarization

An inescapable fact for polarization transfer based on CP is that the efficiency of transfer is much less than 100% in most biomolecular samples. A transfer efficiency of only 40–50% is observed at both slow and fast MAS frequencies for most CP transfers, although there are some sequences based on optimal control theory that can boost these efficiencies [190]. This means that under optimal conditions, close to half of the generated polarization is lost, often discarded using appropriate phase cycles. Traaseth and co-workers [99] used the strategy of storing the ^{15}N magnetization after SPECIFIC-CP to ^{13}C, as in strategies described in the previous sections, and then recalling it to perform additional experiments (Fig. 56a). This strategy was also shown to work equally well at fast MAS frequencies [98]. Similarly, residual polarization is left back on ^{15}N when magnetization is transferred from ^{15}N to ^{1}H [172]. A systematic analysis of peak intensities showed that the spectrum resulting from the residual magnetization after a ^{15}N to ^{13}C transfer is approximately 30% the intensity of an optimally acquired spectrum [98,99,191], while when ^{15}N to ^{1}H transfers are involved, the resulting spectrum can have intensities 40–50% of an optimally acquired

spectrum [172–175]. This latter result is possibly due to the use of short contact times when transferring magnetization to ^{1}H,
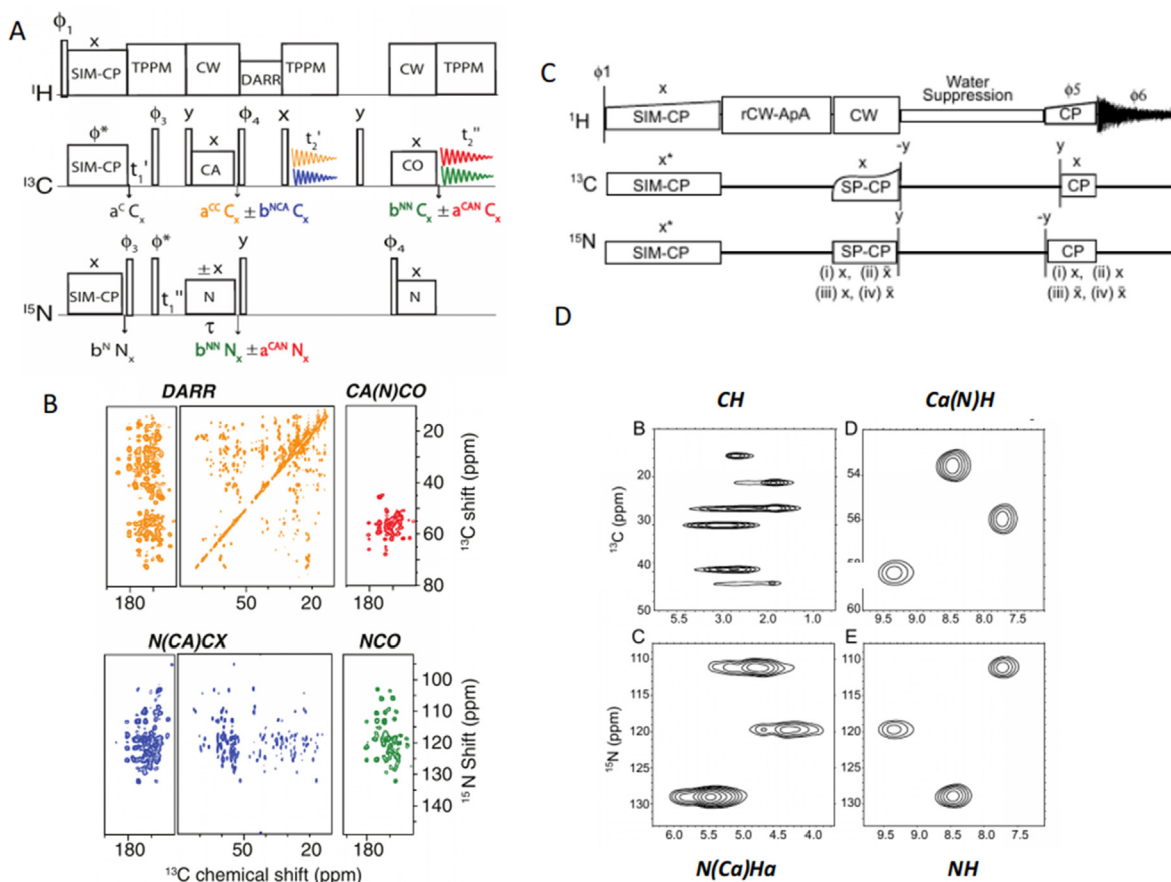
Fig. 57. Recovering multiple experiments using multiplexing. (A) Pulse sequence and (B) spectra for a combination of DARR, CA(N)CO, N(CA)CX and NCO acquired using two ^{13}C detections, each with two-fold multiplexing. (C) Pulse sequence and (D) spectra for CH, NH, CA(N)H and N(CA)HA acquired using a single direct detection and 4-fold multiplexing. (A, B) adapted from Ref. [191] with permission and (C-D) adapted from Ref. [172] with permission.

which avoids the appearance of long-range correlation peaks. Similarly, the residual polarization remaining on ^{13}C after transfer from ^{13}C to ^{15}N is ~30–50% (depending on whether the ^{13}C nucleus is coupled to ^{15}N or not) [191]. When a transfer to ^{1}H is involved, almost 50% of the magnetization is also left behind on ^{13}C [172–175].

When SPECIFIC-CP is used after Sim-CP, two sources of residual polarization are generated, one on ^{13}C and the other on ^{15}N. Thus, four independent polarization pathways occur under these conditions, two "full polarization" pathways, corresponding to magnetization that is transferred from ^{13}C to ^{15}N and vice versa, and two residual pathways, corresponding to magnetization that is not transferred. Veglia and co-workers adapted the strategy of storing ^{15}N magnetization, and acquired a combination of ^{13}C -^{13}C DARR, N (CA)CX (DARR), NCO, and CA(N)CO experiments using two separate detections [191] (Fig. 57) that form the basis of assignment strategies in solid-state NMR. Each detection is a combination of two experiments, which were separated by demultiplexing [165]. Such experiments can be easily extended to a third dimension for obtaining complete assignments in small proteins using ^{13}C detection alone [191]. When used together with ^{1}H detection, as many as 4 experiments can be recovered with a single direct detection and multiplex phase cycling, as demonstrated in Fig. 57 by the combination of CH, NH, CA(N)HN and N(CA)HA [172].

A combination of residual polarization and selective labeling schemes was demonstrated by Traaseth and co-workers in assigning highly overlapped peaks in solids [192]. They prepared samples that were labelled with ^{15}N-^{12}C on selected residue types on an otherwise ^{15}N-^{13}C -labelled background, and filtered all residues except those succeeding the ^{12}C labelled ones using a SPECIFIC-CP transfer from N to CO. The residual polarization from these was transferred to Cα, where only the residues next to the ^{12}C-labelled ones had high intensity. A combination of residue type identification from the Cα chemical shift and the primary sequence was used to assign residues. Residual polarization has also been used to acquire multiple spectra in oriented solids [193]. A combination of 2D PISEMA [194,195] and 2D PISEMA-PDSD [196], which has the potential to give assignments in small membrane proteins,

was demonstrated. This strategy can be extended to the 3rd dimension with 3D PISEMAI-HETCOR and 3D PISEMAI-HETCOR with PDSD mixing [193].

It is worth pointing out that the first CP step from ^{1}H to ^{13}C and/or ^{15}N also leaves behind residual polarization on ^{1}H. This is often dephased during subsequent decoupling sequences and is generally not recoverable. Ramamoorthy and co-workers have proposed that in situations where CW decoupling suffices (for example, in samples where the sample heterogeneity primarily determines the resolution), the residual polarization arising out of the initial 90° pulse on ^{1}H after CP transfer to a heteronucleus can be spin-locked and reused at a later stage [197]. Since CP based methods primarily give signal from the rigid parts of the sample and the single pulse results in signal primarily from the flexible part, this method has the advantage of allowing one to detect both rigid and dynamic parts in highly heterogeneous samples such as a polymer matrix. Veglia and co-workers have recently shown that ^{1}H-^{1}H, DREAM and NHHN spectra can also be recorded sequentially. In this experiment ^{1}H-^{1}H correlation arises from the residual magnetization that remains on ^{1}H after the initial CP step [168].

4.1.6. Other strategies

All strategies that are discussed above use Sim-CP as the basic building block for experiments, with one exception. Opella and co-workers have demonstrated that simultaneous dipolar-INEPT sequences can be used to transfer the magnetization [56], which results in similar time savings. The use of SPECIFIC-CP is also not a requirement. Veglia and co-workers have demonstrated the incorporation of TEDOR [198] after the initial Sim-CP step to record ^{15}N-^{13}C TEDOR and NCA spectra sequentially [199]. A specific advantage of this experiment is that the combination of 3D NCACX (which uses TEDOR) and 3D NCOCX can be acquired with full polarizations. These two experiments are commonly used together to assign proteins under slow to moderate MAS spinning frequencies, and cannot be combined using the previous approaches (unless one uses residual ^{13}C polarization left over after the first experiment, which gives only 30% of the usual sensitivity).
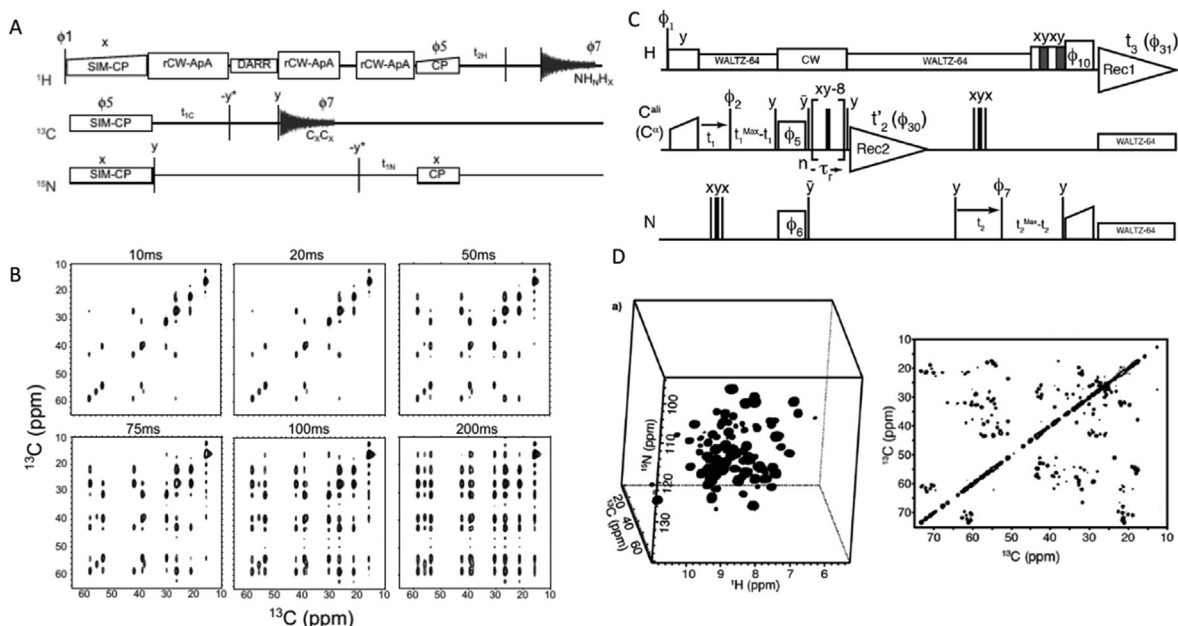
Fig. 58. Combining experiments with different dimensions. (A) Pulse sequence and (B) spectra for a combination of 6 DARR spectra with different mixing times acquired alongside a single 3D NHH spectrum. (C) Pulse sequence and spectra (D) for a single 2D ^{13}C -^{13}C correlation spectrum using RFDR acquired alongside a 3D CANH spectrum. (A-B) adapted from Ref. [172] with permission. (C-E) adapted from Ref. [203] with permission.
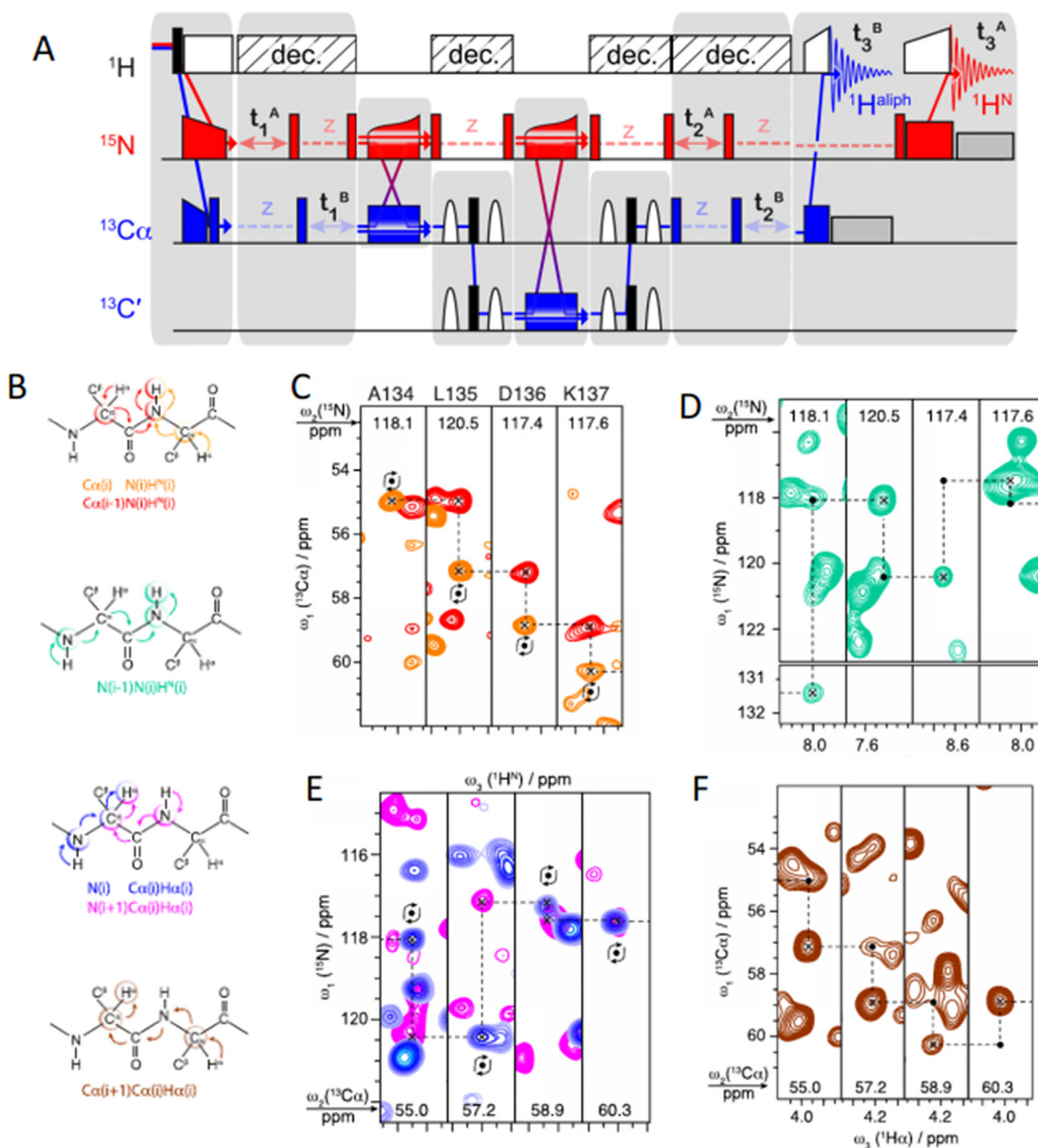
Fig. 59. (A) Pulse sequence using INEPT-based ^{13}C -^{13}C transfers for the acquisition of 8 intra- and inter-residue linking spectra in a single experimental block. (B) Eight 2D pathways corresponding to the evolution of t_1 and t_3 in (A). (C-F) Strip plots for six of the eight spectra acquired using the pulse-sequence in A on a sample of microcrystalline MBP at a MAS frequency of 107 kHz. (A-F) adapted from Ref. [174] with permission. Note that the ^{13}C-^{13}C INEPT blocks can be replaced with DREAM transfers, and the two acquisitions can be combined, as described in [174].

Another useful strategy is to combine multiple 2D experiments alongside a single 3D experiment. Often, multiple 2D (or 3D) experiments are required to study dynamics in proteins, for example ^{13}C -^1H DIPSHIFT based studies to measure dipole-dipole couplings are usually done as a series of 2D experiments [200]. These experiments can be combined with a single 3D experiment, such as NCACX or NHH. Fig. 58 shows a combination of a series of DARR experiments [201] with different mixing times acquired alongside a single 3D NHH experiment [172]. The difference in the sensitivity of ^{13}C and ^1H detection at fast MAS frequencies [202] means that performing a ^{13}C-detected experiment can be time-consuming. Under these conditions, one can repeat 2D ^{13}C-detected experiments alongside a single 3D ^1H-detected experiment and boost the sensitivity to the desired levels [203].

4.2. Assignment strategies

It is worth re-emphasizing at this stage that multi-FID detection strategies in solids do not require a redesign of experiments to fit into this experimental paradigm. Rather, the very same experiments that would have been acquired without the use of multi-FID detection are recorded in a smaller amount of time. For example, a combination of 3D NCACX and 3D CANCO was directly used to assign a small membrane protein, sarcolipin, in lipid bilayers [185]. With selectively labelled samples, the basic combination of DARR and NCA has been useful in assigning resonances in samples of Aβ [204]. One strategy that has become increasingly popular at MAS frequencies > 100 kHz is the use of residue-linking experiments [205,206]. This approach is similar to that used in the
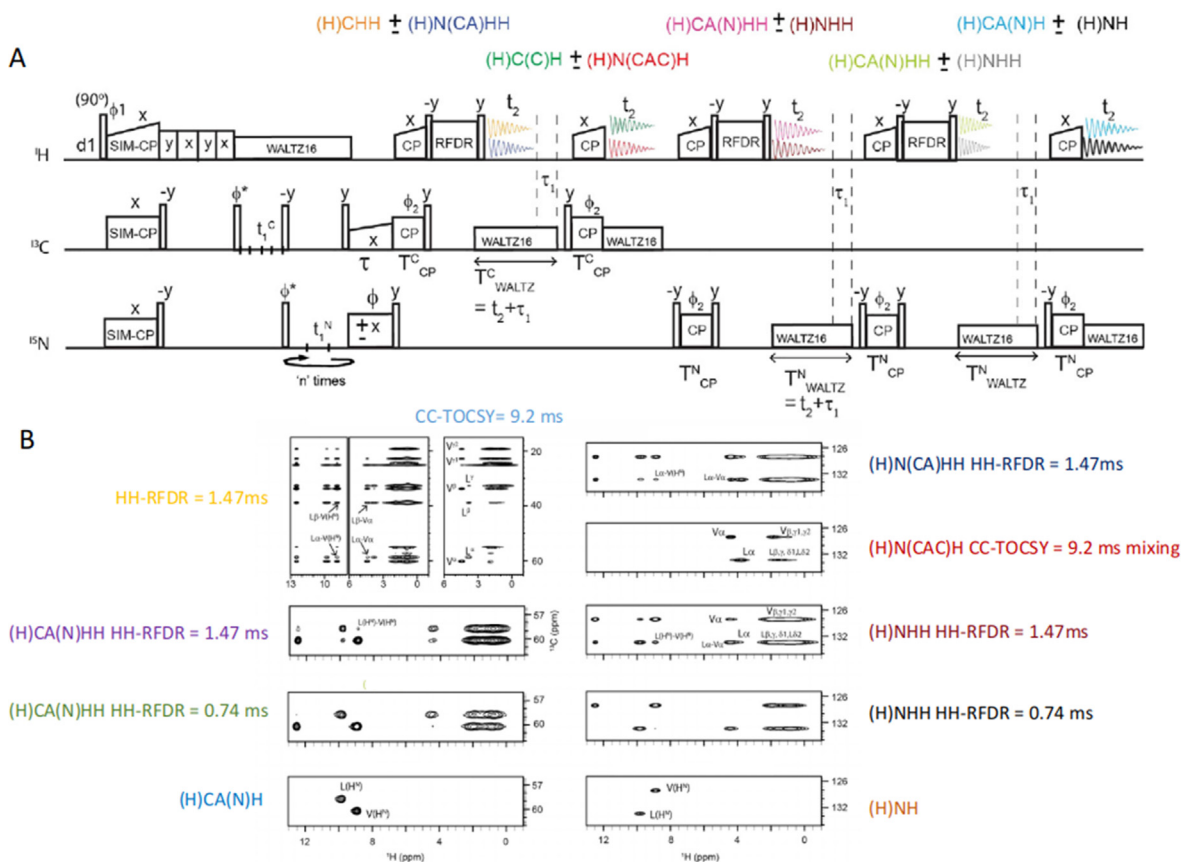
Fig. 60. Sequences with more than two direct acquisitions. (A) Pulse sequence and (B) spectra for ten 2D experiments acquired using 5 direct detections (each with 2-fold multiplexing), acquired on a sample of ^{13}C -^{15}N N-acetyl-valyl leucine, at a MAS frequency of 65 kHz. (A-B) adapted from Ref. [208] with permission; (A-B) adapted from Ref. [173] with permission.

HNN experiment in solution NMR [142] for assigning disordered proteins, and has some of the same motivations: (i) the use of two dimensions (^{15}N-^{15}N or ^{13}C-^{13}C) with high resolution to resolve resonances, (ii) poor dispersion (and hence poor resolution) in the ^{1}H dimension and (iii) the need of obtaining peaks from inter-residue correlations. The 3D N(COCA)NH experiment that has been proposed previously [205,206] also has a ^{13}C-edited analogue: 3D CA(CON)CAHA. Using Sim-CP as the initial step, these two can be combined in a straightforward manner, using either DREAM [174] or INEPT [175] sequences for ^{13}C -^{13}C transfers (Fig. 59). Since this experiment uses two SPECIFIC-CP blocks, it gives rise to a total of eight independent pathways, as discussed in the previous section. These can then be recovered either simultaneously [174] or sequentially [175], and separated using the same multiplexing/demultiplexing strategies. The experiments that are encoded include those with inter-residue connectivity (3D N(COCA)NH, 3D CA(CON)CAHA, 3D N(CO)CAHA and 3D CA(CO)NH), and with intra-residue connectivity (3D CANH, 3D NCAHA, 3D NNH and 3D CCH). A study from Pintacuda and co-workers has shown that with the use of this combination of experiments, one can obtain nearly complete assignment for the microcrystalline preparation of a relatively large protein, MBP (40 kDa) at 107 kHz MAS [175]. A combination of high sensitivity due to ^{1}H detection at these MAS frequencies, the use of very small amounts of protein, and a strategy of recording experiments that are highly complementary to each other makes this an approach that will be of immediate use at these MAS frequencies. Further validation of this strategy came with the recent demonstration of nearly complete assignments for AlkL, a membrane protein, at a MAS frequency of 110 kHz [207].

4.3. More than two direct acquisitions

A general result that emerges out of the above discussion is that residual polarization represents a large pool of polarization. As the sensitivity of NMR increases, so does signal to noise that can be obtained using this residual polarization, and as such, it is a large loss if this is just discarded in the course of an experiment. The way this residual polarization is recovered in many of the reported experiments above is by using additional CP steps. Curiously enough, an additional CP step itself gives rise to additional residual polarization. Opella and co-workers used this fact to record three separate experiments using three direct detections, each one after a new CP step [56], in a single experimental block. Veglia and co-workers demonstrated that as many as three additional SPECIFIC-CP steps can be used after the first one to generate a total of four additional detection intervals [208]. Due to the initial Sim-CP step, each of these detections is a combination of two experiments, which means that a total of eight experiments can be acquired using a single pulse sequence before the recycle delay. The sensitivity of these sequentially detected spectra falls rapidly, from 30% to 10%, and finally to 3% in the final detection step. Similar experiments at fast MAS frequencies have given a combination of as many as 10 experiments before the recycle delay (corresponding to the higher residual polarization in these cases) [168,173] (Fig. 60). In multi-FID detection strategies that have been discussed here, each additional detection increases experiment time by a definite amount. Time saving comparison should strictly be with the regular way of individually recording each experiment. For example, consider a case where 2 experiments are recorded using multi-FID detection where the sensitivity of the first experiment is 100%

and that of the second is 50% compared to those recorded individually with the same number of scans. Individual recording of the second experiment with the same sensitivity as in the multi-FID detection strategy would require only 1/4th the number of scans. Thus, the total number of scans in a conventional approach would be 1.25 times the number of scans in a multi-FID detection strategy. This represents 25% time saving if the time required for each scan is identical. However, the multi-FID detection strategy, with some exceptions, increases the time for each scan by a small fraction, typically 1–5% depending on the recycle delay used. This additional time must be subtracted from the 25% time saving mentioned above to estimate the true time saving. The "break-even" point, i.e., the amount of residual polarization needed in an additional experiment to give exactly the same SNR as a conventional approach in the same total time can be estimated to be ~7–15% for a typical setup at slow-moderate MAS (assuming a recycle delay of 2–3 s and each additional detection increasing the experimental time by 20–40 ms, i.e 0.5–2%) and ~15–25% at fast MAS frequencies (assuming a recycle delay of 0.8–1 s and each additional detection increasing the experimental time by 20–40 ms, i.e ~2–6%). For the multi-FID detection strategy to result in time-savings, either the sensitivity of the second (or subsequent) experiments should be higher than that described by the above numbers, or a single detection must be used to acquire all the spectra [174,178]. This calculation is valid when sensitivity and not the length of the phase cycle is the limiting factor in determining the number of scans, as is often the case for many of the experiments in the solid state, especially at slow-moderate MAS frequencies. Thus, the real utility of sequences with more than two direct detections will only be apparent in cases of high sensitivity, when the phase cycle becomes the limiting factor. We are rapidly approaching such a situation, with the development of dynamic nuclear polarization (DNP) [209]. With sensitivity enhancements of > 100 reported with DNP for many samples, even an experiment with residual polarization that is only 1% of the starting polarization will result in signal-to-noise ratios more than those obtained using the "full" polarization described in the above examples.

4.4. Probe duty cycles

One significant disadvantage of these strategies, especially at slow to moderate MAS frequencies, is the increase in RF duty cycles. Often, the recycle delay for biomolecular samples is limited by the duty cycle that the probe can bear, and the need to keep sample heating to a minimum, rather than the T_1 (^{1}H) times. The use of multi-FID detection strategies increases the probe duty cycle (with some exceptions), mainly due to the requirement for high-power ^{1}H decoupling sequences during each direct detection step. Hence, it is recommended that these sequences be used with low-E or E-free probes, which minimize RF-induced sample heating. This is especially important when implementing experiments with more than two direct detection steps. These considerations are less applicable at fast MAS frequencies, where low RF amplitude decoupling sequences can be used [188]. Nevertheless, it is to be noted that a large fraction of the experiments described at fast MAS frequencies can be done with either no increase in probe duty cycle, or a very small one. The rapid progress in the development of fast MAS techniques means that these strategies will become more important in the coming years.

4.5. Pulse sequences and data processing

The pulse sequences that are reported above have been implemented on instruments from all the major NMR manufacturers. Many of the pulse sequence codes have been reported in the supporting information for the individual articles [174,175,210]. Here,

we point to the GitHub repository [211], where examples of different classes of experiments have been compiled. Similarly, processing scripts for many sequences have been reported in reviews on this subject [174,175,210], as well as in the supporting information associated with many of the original articles. We point the reader to the above repository, which also has scripts to perform arbitrary recombination of multiplexed datasets using the versatile Nmrglue library [212].

4.6. The future of multi-FID detection strategies

With the rapid development of experiments adapted for both slow to moderate and for fast MAS frequencies, multi-FID detection schemes are expected to enhance the performance of most NMR protocols, for collecting data for assignments as well as for investigating dynamics. With the on-going development of DNP, one can expect these experiments to become the default mode of data acquisition to optimally utilize the large polarization that is generated. The benefits of these strategies are expected to be higher in higher-dimensional experiments (>3D), as these generally take a long time to acquire and have many more leakage pathways from which magnetization can be recovered. Similarly, combining not just experiments required for assignments, but also those required to study dynamics in proteins, is likely to be a sound strategy to speed up data acquisition. The highest benefit from these strategies is expected at fast MAS frequencies, where they can be applied without compromising probe duty cycles. An area where more work needs to be done is the development of pulse sequences at slow to moderate MAS frequencies that do not result in increased RF duty cycles. Overall, these strategies promise improved NMR throughput, especially for biomolecular samples.

5. Related technologies

5.1. Multiple microcoil probes connected to multiple receivers

Most commercial NMR probes are designed with the capability of transmitting and receiving at the frequencies of multiple (typically 2 – 5) different nuclear species, such as ^{1}H, ^{2}H, ^{13}C, ^{15}N and ^{31}P. As discussed previously, multiple receiver NMR experiments often involve multinuclear detection. However, there are also NMR probe designs that utilize multiple microcoils routed into separate receivers [53-55,213,214]. This offers the interesting possibility of recording NMR with multiple ^{1}H receivers very much as is the case for parallel MRI [50]. Up to now such probes have been far from being routinely available. In this section we briefly summarize the possibilities that this technique offers.

Parallel acquisition must either be performed using a single RF coil with multiple samples, or with a number of separate coils, each with an individual sample. The former approach can be implemented using phase encoding localization gradients (e.g., time-shared experiments [32]) or slice-selective excitation [93].

In the alternative approach, multiple coil probes have been designed with up to 8 probes in a single probehead (see Fig. 61) [53,54]. Expansion to 16 probes was deemed to be possible in the space available within a typical NMR magnet [55]. Such probes have been shown to dramatically increase NMR throughput [147,215,216], to reduce the durations of multi-dimensional NMR experiments, [217] and to enable following fast reaction kinetics [213,214,218]. The technical challenges in designing multi-coil probe include maintaining high local B_0 homogeneity for each sample in the presence of other coils, maximizing sensitivity for each individual coil, and minimizing RF cross-talk The methodology was initially demonstrated in solid-state NMR, allowing simultaneous acquisition of 1D ^{2}H, ^{17}O and ^{27}Al spectra from three different
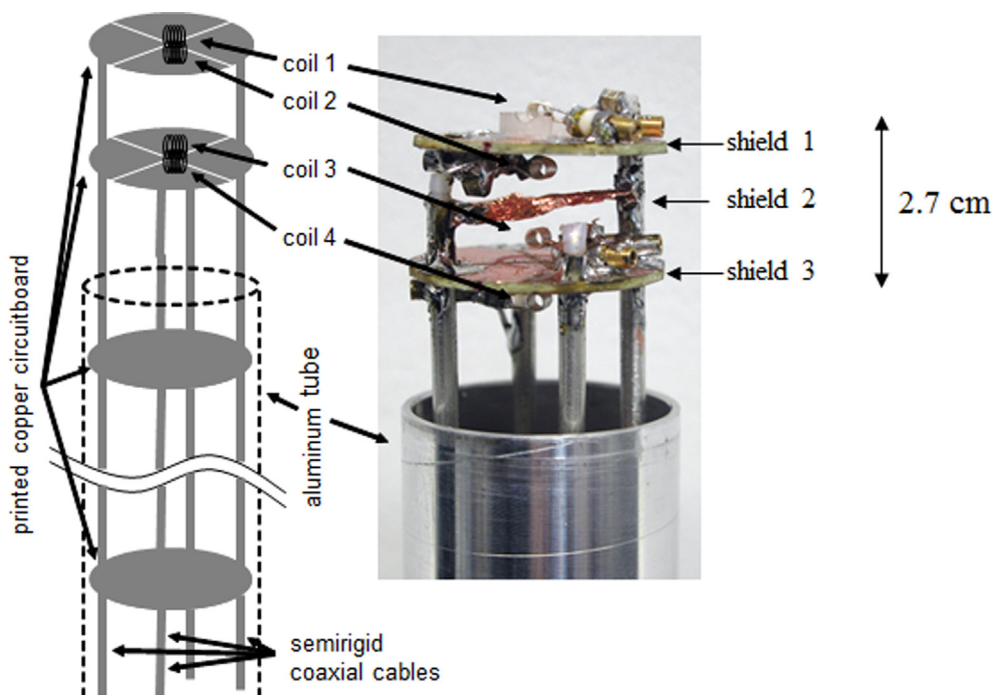
Fig. 61. Left, schematic, and right, photograph of a four-coil probehead used for microimaging oocytes. Reproduced from Ref. [237] with permission.
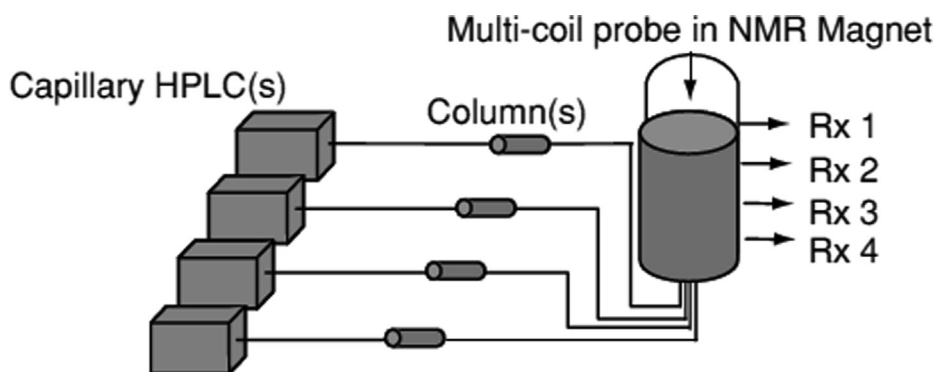
Fig. 62. Schematic representation of a parallel CapHPLC/NMR hyphenation system designed for high separation efficiency. On-flow or stop-flow NMR detection is used for simultaneous monitoring of each separation using multiple RF microcoils, each connected to a separate receiver (Rx). Adapted from Ref. [54].

samples [219]. Multiple microcoil NMR probes have been designed for both sealed samples [220] and flow probes [55,213,214]. When combined with multiple receivers and automated sample handling systems, the latter make high throughput NMR analysis of mass-limited samples feasible (see Fig. 62).

There are two kinds of multiplexed NMR probes – (i) all coils are connected in parallel and routed to a single receiver; (ii) coils with independent circuitry that are routed into separate receivers or multiplexed into a single receiver using RF switches. In the first case some encoding is required to separate the data from individual coils. Usually slice-selective pulses and spatial encoding techniques are used, as briefly discussed in the next section.

Sensitivity is dramatically improved when each sample is placed in an individual size-matched and electrically isolated RF coil connected to a separate receiver [221,222]. This implies that the coils must be small, in order to fit in the homogeneous region of the magnetic field. Alternatively, the signals can be routed into a single receiver and separated using either phase or Hadamard encoding according to principles discussed for spatial encoding

techniques [216,223,224]. Interleaved acquisition of 1D and 2D spectra from multiple coils routed sequentially to a single receiver using RF switches has also been demonstrated [220,225].

In some ways, multi-receiver multicoil homonuclear NMR techniques mimic the use of multiple surface coils in parallel MRI, [52] and in geophysics where similar technology is used in 1D and 2D NMR investigations of groundwater [226]. Multiple-coil probes have also been used in quantum computing [227]. Multi-coil multi-receiver NMR has even found applications in particle accelerator design [228].

The 2D COSY and 2D ^{15}N-^{1}H HMQC spectra from two samples have been recorded in the same total data acquisition time as for a single sample using interleaved acquisition and a probe with two coils doubly tuned to ^{1}H and ^{15}N and routed to a single receiver [220]. A probe with two microcoils – one tuned to ^{1}H and ^{2}H and the other to ^{1}H and ^{13}C – enabled the recording of 2D HETCOR and INADEQUATE experiments with active locking [229]. Two ^{1}H–^{15}N HSQC spectra were acquired simultaneously using a probehead with two ^{1}H/^{15}N double-tuned microcoils and an external
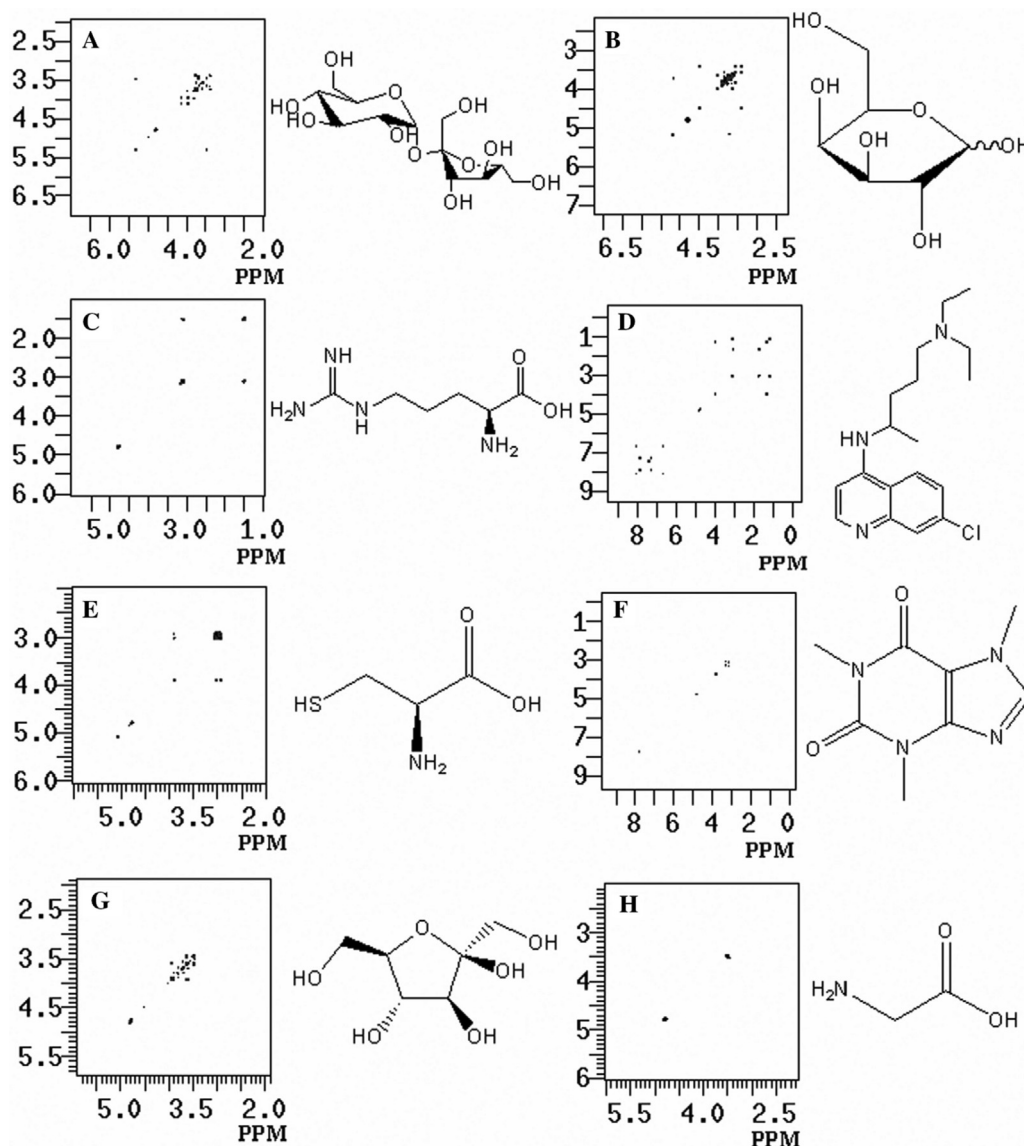
Fig. 63. 2D COSY spectra of eight different samples (10 mM solutions in D$_2$O) acquired in the time required for one conventional 2D spectrum with an 8-coil probe and a 600 MHz Varian Unity INOVA console equipped with four receivers. (A) sucrose, (B) galactose, (C) arginine, (D) chloroquine, (E) cysteine, (F) caffeine, (G) fructose, and (H) glycine. Reproduced from Ref. [147] with permission.

lock coil. The 500 MHz Varian system used was equipped with only one receiver, and the spectra from the two samples were recorded in interleaved mode.

An eight-coil probe has been designed to accommodate eight NMR samples that can be injected simultaneously, reducing the 1D sample analysis time to just a few seconds per sample [147]. An NMR system equipped with four receivers was set up to allow interleaved acquisition of two groups of four spectra, each recorded with parallel acquisition. RF pulses were applied to, and data acquired from, one coil group at a time. The same technique was employed to acquire eight homonuclear 2D H-H correlation spectra (COSY and TOCSY) from eight different samples in the time normally required for a single conventional 2D experiment of the same type (see Fig. 63).

A further advantage of using multiple microcoils in NMR is the potential for applying a different pulse sequence to each sample. Alternatively, the same pulse sequence but with different durations of t_1 evolution periods can be applied to multiple coils containing samples of the same composition, to speed up acquisition

of multi-dimensional experiments, as shown in Fig. 64. Schematically, this technique bears some similarity to Ultrafast (UF) NMR [6-9]. The scheme has been applied to 2D COSY and 2D TOCSY experiments in a probe with four coils, producing the expected a time saving by a factor of 4. Extension of this scheme to other homonuclear correlation experiments, such as DQF COSY, NOESY and ROESY, is straightforward, and implementation in heteronuclear correlation experiments should also be feasible.

A different application of parallel data acquisition using multiple microcoils has been pioneered by the group of Weissleder, in a technique that they term diagnostic magnetic resonance (DMR). DMR detection exploits targeted magnetic nanoparticles (MNPs) to alter the T_2 relaxation times of biological samples. The general principle is that in the absence of the target molecule the MNPs cluster together in solution and have a certain T_2 value. If the target molecule is present in a sample, which is introduced via a microfluidic channel, then this clustering pattern changes as do the corresponding T_2 values. DMR has been used in a wide range of applications, including proteins [230], enzymes [231],
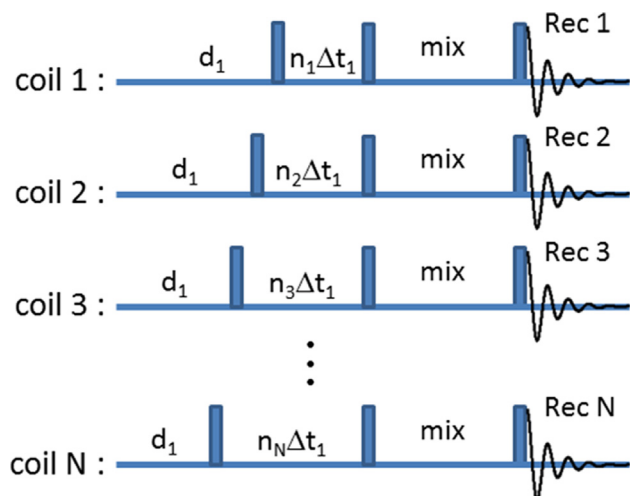
Fig. 64. Timing diagrams for the N-coil COSY experiment [217]; Δt_1 is the time increment (dwell time) in the t_1 dimension and N is the number of microcoils in the probe. Two schemes for incrementing the values of multiplier n_i (i = 1 to N) for each set of N simultaneous experiments have been suggested for regular sampling in Ref. [217], and more can be envisaged for random sampling schemes. Data were acquired on four coils simultaneously using the four receiver channels of the spectrometer.

bacteria [232] and viruses [233]. Relaxometry measurements have been made using eight microcoils positioned very close to a strong hand-held permanent magnet. Small coils have the advantage of high sensitivity and a relatively homogeneous magnetic field throughout the microsample. The design incorporated a 2 × 4 array of planar microcoils, a small permanent magnet (B = 0.5 T), custom-designed NMR electronics, and a microfluidic network [234-236]. To compensate for the magnetic field inhomogeneity, CPMG sequences were used for T_2 measurements. A feedback routine was integrated to automatically track temperature changes and adjust the measurement settings in real time.

To conclude, multiple microcoil probes tuned to one or more frequencies have proven to be a high-throughput tool for the analysis of a large number of mass-limited samples. Microcoil-based probes can increase the mass-sensitivity of NMR spectroscopy by at least 100-fold compared with conventional 5-mm commercial NMR probes. Considering the immense number of samples that have to be examined in NMR labs involved in drug screening, natural product analysis and compound library developments, multiple coil probes combined with use of multiple receivers open up new possibilities to dramatically increase sample throughput, reduce cost, and boost the efficiency of NMR analysis. The technique can be combined with other fast NMR methods, such as fast pulsing (ASAP, SOFAST, BEST), multi-fid detection (NOAH), and non-uniform sampling techniques (NUS, Hadamard, radial sampling and projection spectroscopy).

Finally, the concept of multi-coil micro-MR has also been used to image multiple oocytes (female gametocyte or germ cell involved in reproduction) simultaneously. Purea et al. [237] constructed a four solenoid probe head, shown in Fig. 61, to simultaneously obtain four three-dimensional T_1 maps of chemically fixed Xenopus laevis oocytes (see Fig. 65). Their simulations showed that for coil-shield separations on the order of a coil radius, no significant change in the homogeneity of the RF transmitter or receiver fields is expected, and therefore coils were spaced accordingly.

5.2. Multinuclear MRS and MRI

A typical clinical MRI scanner operating at either 1.5 or 3 T has between 32 and 64 receiver channels, which are typically used for proton imaging. Research systems, such as human 7 T whole body systems, may have up to 32 channels for multinuclear experiments in addition to the proton channels. As mentioned above, the independent receiver channels for proton imaging are used for parallel imaging, which enables scans to be made significantly faster than if only a single receiver channel were to be available. In contrast, multinuclear scans typically use multiple receiver channels to improve the SNR of the scans. These two topics have been extensively reviewed in the literature, and so are not discussed further here. Rather we concentrate on areas where there is a direct connection to the NMR examples shown in this article. This is intended to highlight the possibilities and research directions of interest for NMR spectroscopists, and to show common grounds between the two fields that often prove revealing and beneficial. Multinuclear MRS and MRI experiments typically are based either on interleaved experiments or parallel acquisition methods, or on a combination of the two. Sequential acquisition experiments as used in liquids and solids NMR have not yet been explored in MRI.

The most common heteronuclei studied for in vivo imaging and spectroscopy are ^{23}Na, ^{31}P, ^{19}F (of exogenous contrast agents), and ^{13}C (either using ^{13}C enriched or hyperpolarized compounds). Sodium can be used to study stroke in the brain, tumor conductivity, cartilage degeneration, myocardial infarction and kidney failure [238]. ^{31}P spectroscopy finds major applications in static and dynamic studies of energetics in the brain and muscle (resting and moving), as well as being a powerful biomarker in oncological studies. In vivo pH can be measured via the chemical shift difference between the inorganic phosphate and phosphocreatine peaks, and mitochondrial function via the levels of ATP [239]. ^{19}F is almost completely absent from the body, so there is no background signal unless contrast agents (usually injected) are used. Images have a high contrast to noise ratio (CNR [240]), but relatively low SNR due to the low concentrations that can be tolerated in vivo [241]. A similar situation exists for ^{13}C, either labelled or hyperpolarized, which is used to study dynamic metabolism in a variety of biochemical cycles in both healthy and diseased tissue [242].

Irrespective of which nucleus is studied, proton imaging must be performed in order to provide an anatomical overlay for the much coarser spatial resolution typical of heteronuclear images. Typical data acquisition times are much longer for heteronuclei than for proton imaging, due to the lower sensitivity and concentration, and so the use of efficient parallel or interleaved data acquisition schemes is highly desirable. In addition to reduced total scan times, parallel multinuclear imaging provides unique possibilities to record images that are correlated both spatially and temporally. In practice, parallel acquisition is not trivial because the magnetic field gradients (frequency and phase encoding, and slice selection) act on all nuclear species. In terms of frequency encoding gradients present during data acquisition, this scales the respective fields of view by the corresponding gyromagnetic ratios. The issue can be resolved by exciting each type of nucleus in turn, at times proportional to their gyromagnetic ratios, during the same phase-encoding gradient, so that higher-γ nuclei experience a smaller gradient area [146]. Experiments employing parallel acquisition of FIDs from several nuclear species typically require modification of commercial MRI systems [243], both in software and in hardware.

Interleaved experiments offer similar reduction in scan times, and are simpler to implement. The hardware requirements are less demanding because state-of-the-art MRI systems can switch between different transmit and receive pathways almost instantly [244]. Furthermore, any doubly tuned RF coil capable of X and ^{1}H acquisition is suitable for interleaved acquisition, whereas parallel acquisition requires RF coils capable of heteronuclear decoupling, which puts high demands on the isolation of the two channels. The two nuclear species typically have different intrinsic sensitiv-
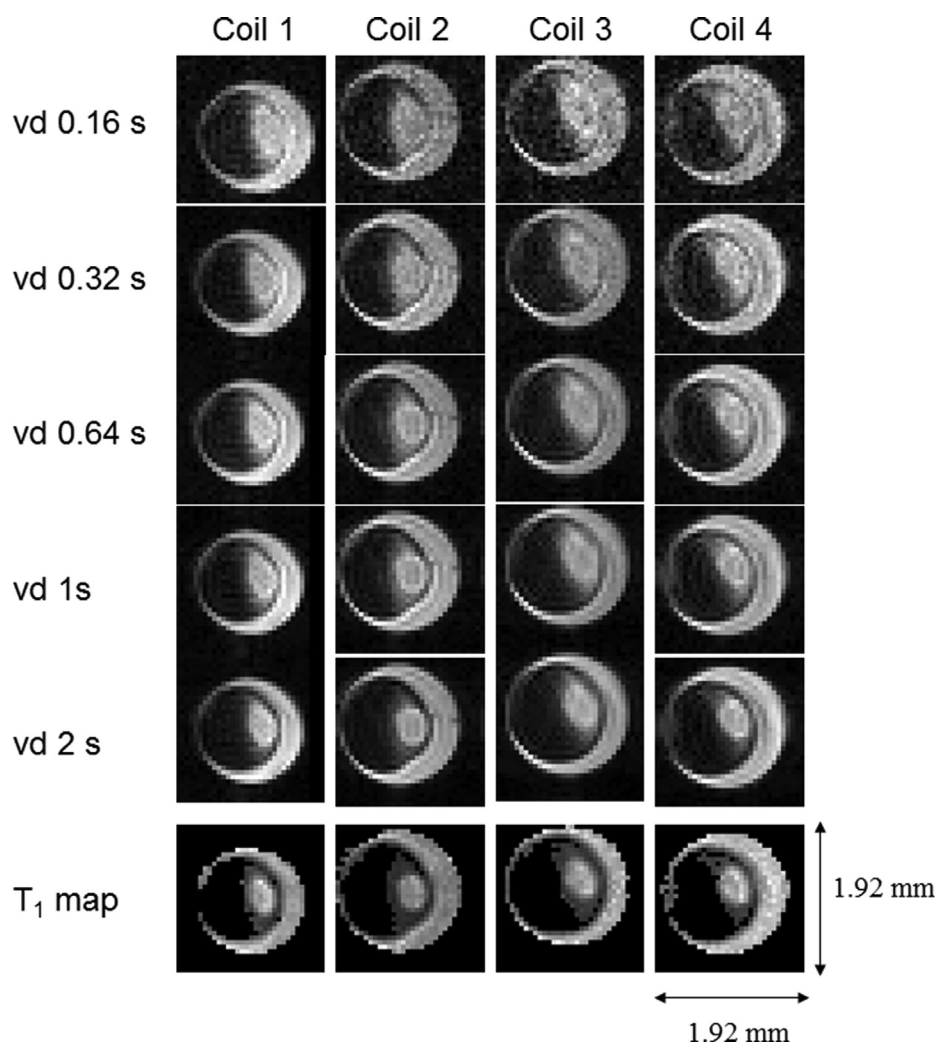
Fig. 65. Slices from 3D spin echo datasets of coils 1 to 4 (left to right) with variable delays in the inversion recovery sequence to map T1 (top to bottom). TE = 9.2 ms, variable delays 0.16 s, 0.32 s, 0.64 s, 1.00 s, 2.00 s. Two signal averages with ± phase cycling of the 180° pulse, data matrix 256 × 64 × 64; (bottom) corresponding T_1-maps. Reproduced from Ref. [237] with permission.
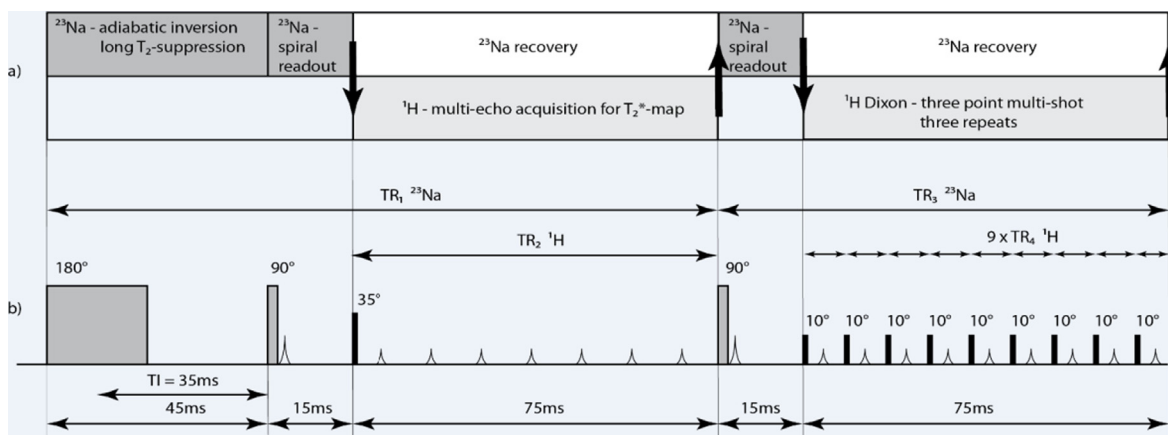
Fig. 66. ^1H / ^{23}Na sequence switching protocol. a) Sequence switching between ^{23}Na and ^1H channels during scan execution. The thick arrows indicate where the MR system switches. b) Timing diagram of the resulting ^1H / ^{23}Na blocks, which are repeated until the end of the entire scan (RF pulses and data acquisition illustrated). If one or more sequence elements is finished, corresponding dummy scans were performed with RF pulses and gradients active but signal sampling disabled, to maintain a steady state. It can be seen that switching takes place at TR and multiple TR levels. In the ^1H Dixon scan [248] the echo time is varied from shot to shot to encode chemical shifts. All four of these scans occurred within a single 225 ms period. Reproduced from Ref. [244] with permission.

ities and T_1 relaxation times. If the T_1 differences are significant, it may be possible to sample one type of nucleus more frequently than the other, which is important for achieving optimal signal-to-noise ratio (SNR) in unit time.

Both simultaneous and interleaved experiments offer significant advantages in studies of transient physiological states that are difficult or even impossible to reproduce precisely, e.g., in patients, in experiments involving hyperpolarization, or in other instances where physiological parameters are changing irreversibly. For instance, interleaved ^{1}H and ^{31}P acquisition has been used in cardiac surgery [145].

Simultaneous acquisition of ^{1}H and ^{31}P NMR spectra using a 1.9 T imaging system was reported as early as 1981 [225]. Monitoring of blood flow and oxygenation state by ^{1}H NMR, and of high-energy phosphate metabolism by ^{31}P NMR, in the skeletal muscle of a rabbit under conditions of varying exercise and systemic blood pressure was implemented using a single magnet (20 cm diameter, 1.9 T, Oxford Research Systems) and two spectrometers - one to record ^{31}P NMR signals, while the other was used to simultaneously perform the ^{1}H measurements. ^{31}P spectra were recorded continuously throughout the experiment, using a surface coil positioned over the upper hind leg of the rabbit, while ^{1}H NMR measurements were performed using a Helmholtz coil positioned within 3 cm of the ^{31}P coil.

Pulse sequences have been implemented for parallel acquisition of multi-slice proton images concurrently with phosphorus-31 spectroscopic images with the same field of view [245]. ^{1}H stimulated echo acquisition (STEAM) and ^{31}P image selected in vivo spectroscopy (ISIS) spectra were recorded simultaneously from the same volume of interest in both a phantom and a volunteer [246]. The STEAM and ISIS parts of the sequence used a common gradient scheme. In this work it was shown that simultaneous acquisition does not compromise the localization performance of the experiments. Multiple receivers have also been used for simultaneous ^{1}H and ^{31}P chemical shift imaging of human brain [146,247]. Since in vivo proton resonances typically have significantly shorter T_1 relaxation times than ^{31}P metabolites, proton-only scans were interleaved with simultaneous ^{1}H and ^{31}P acquisition.

A clinical 7 T MRI scanner has been modified to enable simultaneous or interleaved acquisition of signals from two different nuclei [243]. The system was used both for interleaved and simultaneous ^{31}P/^{1}H spectroscopy and interleaved ^{31}P/^{1}H imaging with no loss in sensitivity as compared to the standard configuration.

Fluorine-19 MRI offers broad potential for specific detection and quantification of molecularly targeted agents in diagnosis and therapy planning or monitoring, since there is no biological background ^{19}F signal. However, since these agents only accumulate in certain tissues, accompanying proton images are needed to reveal the underlying anatomy. The low concentrations that are typical for targeted molecular imaging agents require long signal averaging. Physiological motion during examination may lead to blurring, underestimation in signal quantification, and erroneous localization of the agent distribution. The feasibility of parallel acquisition of ^{1}H/^{19}F MRI data offering efficient and precise anatomical localization of ^{19}F signals enabled by motion correction based on simultaneously-acquired proton signals has been demonstrated on a modified clinical 3 T MRI system [119].

A reduction by a factor of two in experiment time has been achieved by interleaving ^{1}H and ^{23}Na scans, each with different contrasts to obtain images of the human knee at 7 T within a clinically relevant timescale [244]. Proton MRI is performed whilst the sodium nuclei relax towards thermal equilibrium, and vice versa (see Fig. 66). The significantly shorter T_1 relaxation times of ^{23}Na were exploited to acquire multiple ^{23}Na signals for each ^{1}H acquisition. A total of four different types of contrast, two for ^{23}Na and two for ^{1}H, were achieved by intelligent interleaved scanning.

Simultaneous interleaved ^{1}H / ^{23}Na in vivo images from a healthy volunteer recorded using this approach are shown in Fig. 67. A similar approach has been used to obtain simultaneous ^{1}H and ^{23}Na images on a 1.5 T NMR imaging system [249].

In the field of non-medical applications, the intrusion of seawater into cementitious materials has been studied by interleaved ^{1}H, ^{23}Na and ^{35}Cl NMR using a 1.5 T MRI scanner [250]. A stepper motor was used to transport the sample between two coils, one tuned to ^{1}H and the other doubly tuned to ^{23}Na and ^{35}Cl. Relaxation measurements of the three nuclear species provided information about the pore size and ion concentration distribution.

Liquid-state DNP based on the Overhauser effect has been used in combination with parallel multi-nuclear data acquisition in both MRS and MRI. Very large simultaneous DNP enhancements in liquids for different pairs of nuclei, such as ^{1}H and ^{23}Na, ^{1}H and ^{31}P, ^{19}F and ^{31}P, have been reported, enabling single scan multinuclear data acquisition [251].

Hyperpolarized ^{13}C imaging requires rapid and efficient imaging techniques. Typically, anatomical ^{1}H images are obtained beforehand, which takes extra time and may result in artifacts and mis-registration. Simultaneous structural ^{1}H and metabolic ^{13}C imaging has been shown to provide images that are correlated both spatially and temporally, with the additional benefit of reducing the scan times [252]. In this case the ^{1}H data were used for motion tracking, to reduce blurring and mis-registration in the parallel acquisition of multinuclear images.

Parallel acquisition of lung images from two different nuclei, ^{1}H and hyperpolarized ^{3}He in vivo, provide a high degree of mutual consistency that is impossible to achieve in separate scans and breath holds [253]. A mixture of hyperpolarized ^{3}He and ^{129}Xe gases in a 1:2 ratio was used for simultaneous triple-nuclear ^{1}H, ^{3}He and ^{129}Xe hybrid MR imaging of the lungs in a single breath hold on a re-engineered clinical 3 T whole-body system [254]. The scans provided high signal-to-noise ratio and high-resolution images with mutually complementary functional and structural spatial information.

6. Conclusions

The high information content provided by NMR spectroscopy has made this one of the primary analytical tools for molecular structure characterization of isolated compounds, complex mixtures, and materials, and its range of applications continues to expand, being driven by both technological and methodological developments. Many of these advances have led to an increase in the information content and to a reduction in the time required to collect data, and in doing so, have maximized the yield of NMR instrumentation and accelerated scientific discovery. Multidimensional NMR techniques have been in use for many decades and operate normally by using a single direct free induction decay detection period per experiment, which inherently limits their information content. The recording of multiple directly detected FIDs per experiment offers many new approaches to enhance data collection, including the ability to acquire FIDs sequentially, in parallel, or in an interleaved fashion, or possibly by using combinations of these approaches within one experiment. This review has highlighted methods that exploit a single hardware receiver channel for multi-FID detection, as found in traditional spectrometer design, and also those that employ two or more receiver channels on multi-receiver instruments that enable the true parallel detection of multiple nuclear species, and which are now commonplace on state-of-the-art spectrometers.

In addition to the increased information content of multi-FID detected experiments, multi-nuclear detection techniques provide access to additional sources of magnetization and have the potential to detect more signal than conventional methods based on single

nucleus observation. This is particularly true for experiments involving simultaneous detection of high-γ and high natural abundance nuclei such as ^{1}H, ^{19}F and ^{31}P that are of particular interest in clinical studies, pharmaceutical research, drug design and screening applications. In sensitivity-limited (low concentration) situations, the efficacy of multi-FID acquisition experiments involving ^{1}H and low-γ nuclei suffers from the significant sensitivity differences between ^{1}H and *X*-nuclei detected spectra. Such experiments are most valuable in situations where *X*-nuclei detected spectra are of prime interest while ^{1}H detected spectra are recorded to obtain complementary information, a point that is sometimes overlooked [95].

Multi-FID detection techniques, whether multinuclear or homonuclear, have led to new designs of pulse schemes and supersequences that provide all the required information in a single measurement in both solution- and solid-state NMR. In small molecules such supersequences enable fast and efficient elucidation of molecular structure [33,70,110,127,134,255]. In proteins, similar supersequences allow complete resonance assignment from a single measurement [95,107,141,144]. Likewise, in metabolomics multinuclear detection has been used for rapid resonance assignments [155,156]. Solid-state NMR has also benefited greatly from these approaches, especially in biomolecular NMR. Multiple sequential and simultaneous schemes for data collection involving multiple nuclei have come a long way in the resonance assignment of complex biomoleucles, and time savings are appreciable. There are additional advantages in solid-state NMR, where MAS frequencies of 60–120 kHz that are now commercially available make it possible to extend multi-FID detection methods with ^{1}H detection, for both sensitivity and speed. Moreover, these can be combined with DNP schemes so that the minimum number of phase-cycle steps becomes the limiting factor rather than sample quantity. Here, the large initial polarization can be efficiently manipulated for high-sensitivity data sets using multi-FID detection methods.

The advent of multiple receivers for high-resolution NMR has also enabled new types of coils to be developed to take advantage of the full capabilities. In particular, multiple RF coils, if small enough, can be accommodated within the homogeneous B_0 field region of the magnet. This allows acquisition of spectra from many different samples at the same time, significantly increasing the potential throughput in cases where high throughput of relatively concentrated or highly polarized samples is required. The principle has been developed commercially, with dual coil probes produced by Protasis. Multiple coils also allow a number of different sequences to be run simultaneously if identical samples are placed in each of the coils, again producing a much more efficient method of data collection than if the sequences had to be run one after the other. The potential combination of this type of hardware with the efficient sequences outlined in this article would result in the highest throughput capability of any NMR system.

In conclusion, multi-FID techniques allow for greater time efficiency in data collection by providing higher information content per experiment and can also offer improved sensitivity in unit time relative to conventional measurements. They also allow data sets corresponding to differing correlation methods to be recorded at the same time, thus avoiding temporal variations. These methods are often complementary to, and may be integrated with, other approaches to fast data collection, and are certain to have increasing influence on both current and future approaches to NMR data acquisition.

Declaration of Competing Interest

The authors declare that they have no known competing financial interests or personal relationships that could have appeared to influence the work reported in this paper.

Acknowledgements

References

[1] T.D.W. Claridge, High-Resolution NMR Techniques in Organic Chemistry, 3rd ed., Elsevier, Boston, 2016, https://doi.org/10.1016/B978-0-08-099986-9.00015-4.

[2] J. Cavanagh, W.J. Fairbrother, A.G. Palmer, M. Rance, N.J. Skelton, Protein NMR Spectroscopy. Principles and Practice, Academic Press (2007), https://doi.org/10.1016/B978-0-12-164491-8.50018-X.

[3] R.A. deGraaf, In vivo NMR Spectroscopy: Principles and Techniques, 2nd ed., John Wiley & Sons, Ltd, 2007, https://doi.org/10.1002/9780470512968.

[4] L. Rouger, B. Gouilleux, P. Giraudeau, Fast n-dimensional data acquisition methods, in: Encyclopedia of Spectroscopy and Spectrometry (Third Edition), 2017, 588–596, https://doi.org/10.1016/B978-0-12-409547-2.12107-9.

[5] R. Freeman, Ē. Kupče, Emerging techniques in fast multidimensional NMR, in: J.L.R. Arrondo, A. Alonso (Eds.) Advanced Techniques in Biophysics, Ch. 6, Springer-Verlag, Berlin, 2006, 131–147, https://doi.org/10.1007/3-540-30786-9_6.

[6] L. Frydman, T. Scherf, A. Lupulescu, The acquisition of multidimensional NMR spectra within a single scan, Proc. Natl. Acad. Sci. U.S.A. 99 (2002) 15858–15862, https://doi.org/10.1073/pnas.252644399.

[7] A. Tal, L. Frydman, Single-scan multidimensional magnetic resonance, Prog. NMR Spectrosc. 57 (2010) 241–292, https://doi.org/10.1016/j.pnmrs.2010.04.001.

[8] M. Gal, L. Frydman, Multidimensional NMR spectroscopy in a single scan, Magn. Reson. Chem. 53 (2015) 971–985, https://doi.org/10.1002/mrc.4271.

[9] P. Schanda, B. Brutscher, Very fast two-dimensional NMR spectroscopy for real-time investigation of dynamic events in proteins on the time scale of seconds, J. Am. Chem. Soc. 127 (2005) 8014–8015, https://doi.org/10.1021/ja051306e.

[10] P. Schanda, Ē. Kupče, B. Brutscher, SOFAST-HMQC experiments for recording two-dimensional heteronuclear correlation spectra of proteins within a few seconds, J. Biomol. NMR 33 (2005) 199–211, https://doi.org/10.1007/s10858-005-4425-x.

[11] M. Gal, P. Schanda, B. Brutscher, L. Frydman, UltraSOFAST HMQC NMR and the repetitive acquisition of 2D protein spectra at Hz rates, J. Am. Chem. Soc. 129 (2007) 1372–1377, https://doi.org/10.1021/ja066915g.

[12] P. Schanda, H. Van Melckebeke, B. Brutscher, Speeding up three-dimensional protein NMR experiments to a few minutes, J. Am. Chem. Soc. 128 (2006) 9042–9043, https://doi.org/10.1021/ja062025p.

[13] Ē. Kupče, R. Freeman, Fast multidimensional NMR by polarization sharing, Magn. Reson. Chem. 45 (2007) 2–4, https://doi.org/10.1002/mrc.1931.

[14] D. Schulze-Sünninghausen, J. Becker, M.R.M. Koos, Burkhard Luy, Improvements, extensions, and practical aspects of rapid ASAP-HSQC and ALSOFAST-HSQC pulse sequences for studying small molecules at natural abundance, J. Magn. Reson. 281 (2017) 151–161, https://doi.org/10.1016/j.jmr.2017.05.012.

[15] J.C.J. Barna, E.D. Laue, M.R. Mayger, J. Skilling, S.J.P. Worrall, Exponential sampling, an alternative method for sampling in two-dimensional NMR experiments, J. Magn. Reson. 73 (1987) 69–77, https://doi.org/10.1016/0022-2364(87)90225-3.

[16] M. Mobli, J.C. Hoch, Nonuniform sampling and non-Fourier signal processing methods in multidimensional NMR, Prog. NMR Spectrosc. 83 (2014) 21–41, https://doi.org/10.1016/j.pnmrs.2014.09.002.

[17] K. Kazimierczuk, J. Stanek, A. Zawadzka-Kazimierczuk, W. Koźmiński, Random sampling in multidimensional NMR spectroscopy, Prog. NMR Spectrosc. 57 (2010) 420–434, https://doi.org/10.1016/j.pnmrs.2010.07.002.

[18] Ē. Kupče, R. Freeman, Two-dimensional hadamard spectroscopy, J. Magn. Reson. 162 (2003) 300–310, https://doi.org/10.1016/S1090-7807(02)00196-9.

[19] Ē. Kupče, T. Nishida, R. Freeman, Hadamard NMR spectroscopy, Prog. NMR Spectrosc. 42 (2003) 95–122, https://doi.org/10.1016/S0079-6565(03)00022-0.

[20] Ē. Kupče, R. Freeman, Fast multidimensional NMR: radial sampling of evolution space, J. Magn. Reson. 173 (2005) 317–321, https://doi.org/10.1016/j.jmr.2004.12.004.

[21] B.E. Coggins, R.A. Venters, P. Zhou, Radial sampling for fast NMR: concepts and practices over three decades, Prog. NMR Spectrosc. 57 (2010) 381–419, https://doi.org/10.1016/j.pnmrs.2010.07.001.

[22] Ē. Kupče, R. Freeman, SPEED: single-point evaluation of the evolution dimension, Magn. Reson. Chem. 45 (2007) 711–713, https://doi.org/10.1002/mrc.2052.

[23] A.L. Hansen, R. Brüschweiler, Absolute minimal sampling in high-dimensional NMR spectroscopy, Angew. Chem. Int. Ed. 55 (2016) 14169–14172, https://doi.org/10.1002/anie.201608048.

[24] Ē. Kupče, R. Freeman, B.K. John, Parallel acquisition of two-dimensional NMR spectra of several nuclear species, J. Am. Chem. Soc. 128 (2006) 9606–9607, https://doi.org/10.1021/ja0634876.

[25] Ē. Kupče, R. Freeman, NMR Spectroscopy Using Several Parallel Receivers, in: A. J. Williams, G. E. Martin and D. Rovnyak (Eds.) Modern NMR Approaches To The Structure Elucidation of Natural Products, vol. 1, Ch. 7, 117-145, Royal Soc. Chem. (2016), https://doi.org/10.1039/9781849735186-00119.

[26] Ē. Kupče, R. Freeman, Hyperdimensional NMR spectroscopy, J. Am. Chem. Soc. 128 (2006) 6020–6021, https://doi.org/10.1021/ja0609598.

[27] Ē. Kupče, R. Freeman, Hyperdimensional NMR spectroscopy, Prog. NMR Spectrosc. 52 (2008) 22–30, https://doi.org/10.1016/j.pnmrs.2007.07.003.

[28] V.A. Jaravine, A.V. Zhuravleva, P. Permi, I. Ibraghimov, V.Yu. Orekhov, Hyperdimensional NMR spectroscopy with nonlinear sampling, J. Am. Chem. Soc. 130 (2008) 3927–3936, https://doi.org/10.1021/ja077282o.

[29] Yu. Pustovalova, M. Mayzel, V. Yu, Orekhov XLSY: Extra-Large NMR spectroscopy, Angew. Chem. Int. Ed. 57 (2018) 14043–14045, https://doi.org/10.1002/anie.201806144.

[30] C.A.G. Haasnoot, F.J.M. van de Ven, C.W. Hilbers COCONOSY. Combination of 2D correlated and 2D nuclear Overhauser enhancement spectroscopy in a single experiment, J. Magn. Reson., 56 (1984) 343-349, https://doi.org/10.1016/0022-2364(84)90114-8.

[31] A.Z. Gurevich, I.L. Barsukov, A.S. Arseniev, V.F. Bystrov, Combined COSY-NOESY experiment, J. Magn. Reson. 56 (1984) 471–478, https://doi.org/10.1016/0022-2364(84)90311-1.

[32] T. Parella, P. Nolis, Time-shared NMR experiments, Concepts Magn. Reson. 36A (2010) 1–23, https://doi.org/10.1002/cmr.a.20150.

[33] Ē. Kupče, T.D.W. Claridge, New NOAH modules for structure elucidation at natural isotopic abundance, J. Magn. Reson. 307 (2019), https://doi.org/10.1016/j.jmr.2019.106568 106568.

[34] J. Battiste, R.A. Newmark, Applications of ^{19}F Multidimensional NMR, Prog. NMR Spectrosc. 48 (2006) 1–23, https://doi.org/10.1016/chin.200634298.

[35] J.-X. Yu, R.R. Hallac, S. Chiguru, R.P. Mason, New frontiers and developing applications in ^{19}F NMR, Prog. NMR Spectrosc. 70 (2013) 25–49, https://doi.org/10.1016/j.pnmrs.2012.10.001.

[36] C. Dalvit, Theoretical analysis of the competition ligand-based NMR experiments and selected applications to fragment screening and binding constant measurements, Concepts in Magn. Reson. 32A (2008) 341–372, https://doi.org/10.1002/cmr.a.20121.

[37] J.L. Kitevski-LeBlanc, R.S. Prosser, Current applications of ^{19}F NMR to studies of protein structure and dynamics, Prog. NMR Spectrosc. 62 (2012) 1–33, https://doi.org/10.1016/j.pnmrs.2011.06.003.

[38] H. Kovacs, Ē. Kupče, Parallel NMR spectroscopy with simultaneous detection of ^{1}H and ^{19}F nuclei, Magn. Reson. Chem. 54 (2016) 544–560, https://doi.org/10.1002/mrc.4428.

[39] E.D. Becker, J.A. Ferretti, T.C. Farrer, Driven equilibrium Fourier transform spectroscopy. A new method for nuclear magnetic resonance signal enhancement, J. Am. Chem. SOC. 91 (1969) 7784.

[40] A. Allerhand, D.W. Cochran, Carbon-13 Fourier-transform nuclear magnetic resonance. I. Comparison of a simple spin-echo procedure with other methods, J. Am. Chem. Soc. 92 (1970) 4482–4484.

[41] A. Pines, M.G. Gibby, J.S. Waugh, Proton-enhanced NMR of dilute spins in solids, The J. Chem. Phys. 59 (1973) 569–590, https://doi.org/10.1063/1.1680061.

[42] K.R. Thulborn, N.F. Soffe, G.K. Radda, Simultaneous in vivo measurement of oxygen utilization and high-energy phosphate metabolism in rabbit skeletal muscle by multinuclear ^{1}H and ^{31}P NMR, J Magn. Reson. 45 (1981) 362–366, https://doi.org/10.1016/0022-2364(81)90136-0.

[43] P.B. Roemer, W.A. Edelstein, C.E. Hayes, S.P. Souza, O.M. Mueller, The NMR phased array, Magn. Reson. Med. 16 (1990) 192–225, https://doi.org/10.1002/mrm.1910160203.

[44] S.M. Wright, R.L. Magin, J.R. Kelton, Arrays of mutually coupled receiver coils: Theory and application, Magn. Reson. Med. 17 (1991) 252–268, https://doi.org/10.1002/mrm.1910170128.

[45] J.W. Carlson, An algorithm for NMR imaging reconstruction based on multiple RF receiver coils, J. Magn. Reson. 74 (1987) 376–380, https://doi.org/10.1016/0022-2364(87)90348-9.

[46] M. Hutchinson, U. Raff, Fast MRI data acquisition using multiple detectors, Magn. Reson. Med. 6 (1988) 87–91, https://doi.org/10.1002/mrm.1910060110.

[47] D.K. Sodickson, W.J. Manning, Simultaneous acquisition of spatial harmonics (SMASH): Fast imaging with radiofrequency coil arrays, Magn. Reson. Med 38 (1997) 591–603, https://doi.org/10.1002/mrm.1910380441.

[48] K.P. Pruessmann, M. Weiger, M.B. Scheidegger, P. Boesiger, SENSE: Sensitivity encoding for fast MRI, Magn. Reson. Med. 42 (1999) 952–962, https://doi.org/10.1002/(SICI)1522-2594(199911)42:5%3c952::AID-MRM16%3e3.0.CO;2-S.

[49] M.A. Griswold, P.M. Jakob, R.M. Heidemann, M. Nittka, V. Jellus, J. Wang, B. Kiefer, A. Haase, Magn. Reson. Med. 47 (2002) 1202–1210, https://doi.org/10.1002/mrm.10171.

[50] J. Hamilton, D. Franson, N. Seiberlich, Recent advances in parallel imaging for MRI, Prog. NMR Spectrosc. 101 (2017) 71–95, https://doi.org/10.1016/j.pnmrs.2017.04.002.

[51] Y. Qian, T. Zhao, G.C. Wiggins, L.L. Wald, H. Zheng, J. Weimer, F.E. Boada, Sodium imaging of human brain at 7 T with 15-channel array coil, Magn. Reson. Med. 68 (2012) 1808–1814, https://doi.org/10.1002/mrm.24192.

[52] Ē. Kupče, NMR with multiple receivers, in: R.K. Harris, R.L. Wasylishen (Eds.) eMagRes, 4 (2015) 721–732, https://doi.org/10.1002/9780470034590.emrstm1404.

[53] A.G. Webb, Microcoil nuclear magnetic resonance spectroscopy, J. Pharm. Biomed. Anal. 38 (2005) 892–903, https://doi.org/10.1016/j.jpba.2005.01.048.

[54] A.G. Webb, J.V. Sweedler, D. Raftery, Parallel NMR detection, in: K. Albert (Ed.) On-Line LC-NMR and Related Techniques, John Wiley & Sons, Ltd, 2002, pp. 259–279, https://doi.org/10.1002/0470854820.ch8b.

[55] O. Gökay, K. Albert, From single to multiple microcoil flow probe NMR and related capillary techniques: a review, Anal. Bioanal. Chem. 402 (2012) 647–669, https://doi.org/10.1007/s00216-011-5419-z.

[56] B.B. Das, S.J. Opella, Multiple acquisition/multiple observation separated local field/chemical shift correlation solid-state magic angle spinning NMR spectroscopy, J. Magn. Reson. 245 (2014) 98–104, https://doi.org/10.1016/j.jmr.2014.06.011.

[57] J.-N. Dumez, Spatial encoding and spatial selection methods in high-resolution NMR spectroscopy, Prog. NMR Spectrosc. 109 (2018) 101–134, https://doi.org/10.1016/j.pnmrs.2018.08.001.

[58] Ē. Kupče, R. Freeman, Multisite correlation spectroscopy with soft pulses. A new phase-encoding scheme, J. Magn. Reson. 105A (1993) 310–315, https://doi.org/10.1006/jmra.1993.1287.

[59] B.T. Farmer II, Simultaneous [^{13}C,^{15}N]-HMQC, a pseudo-triple-resonance experiment, J. Magn. Reson. 93 (1991) 635–641, https://doi.org/10.1016/0022-2364(91)90093-9.

[60] B.T. Farmer, L. Mueller, Simultaneous acquisition of [13C, 15N]- and [15N, 15N]-separated 4D gradient-enhanced NOESY spectra in proteins, J. Biomol. NMR. 4 (1994) 673–687, https://doi.org/10.1007/BF00404277.

[61] S.M. Pascal, D.R. Muhandiram, T. Yamazaki, J.D. Forman-Kay, L.E. Kay, Simultaneous acquisition of ^{15}N- and ^{13}C-edited NOE spectra of proteins dissolved in H$_2$O, J. Magn. Reson. 103B (1994) 197–201, https://doi.org/10.1006/jmrb.1994.1031.

[62] F. Lohr, A. Laguerre, C. Bock, S. Reckel, P.J. Connolly, N. Abdul-Manan, F. Tumulka, R. Abele, J.M. Moore, V. Dotsch, Time-shared experiments for efficient assignment of triple-selectively labeled proteins, J. Magn. Reson. 248 (2014) 81–95, https://doi.org/10.1016/j.jmr.2014.09.014.

[63] D. Yang, K. Nagayama, A sensitivity-enhanced method for measuring heteronuclear long-range coupling constants from the displacement of signals in two 1D subspectra, J. Magn. Reson. 118 (1996) 117–121, https://doi.org/10.1006/jmra.1996.0017.

[64] T. Kern, P. Schanda, B. Brutscher, Sensitivity-enhanced IPAP-SOFAST-HMQC for fast-pulsing 2D NMR with reduced radiofrequency load, J. Magn. Reson. 190 (2008) 333–338, https://doi.org/10.1016/j.jmr.2007.11.015.

[65] C. Richter, H. Kovacs, J. Buck, A. Wacker, B. Fürtig, W. Bermel, H. Schwalbe, ^{13}C-direct detected NMR experiments for the sequential J-based resonance assignment of RNA oligonucleotides, J. Biomol. NMR 47 (2010) 259–269, https://doi.org/10.1007/s10858-010-9429-5.

[66] C. Fontana, H. Kovacs, G. Widmalm, NMR structure analysis of uniformly ^{13}C-labeled carbohydrates, J. Biomol. NMR. 59 (2014) 95–110, https://doi.org/10.1007/s10858-014-9830-6.

[67] J. Cavanagh, M. Rance, Sensitivity improvement in isotropic mixing (TOCSY) experiments, J. Magn. Reson. 88 (1990) 72–85, https://doi.org/10.1016/0022-2364(90)90109-M.

[68] L.E. Kay, P. Keifer, T. Saarinen, Pure absorption gradient enhanced heteronuclear single quantum correlation spectroscopy with improved sensitivity, J. Am. Chem. Soc. 114 (1992) 10663–10665, https://doi.org/10.1021/ja00052a088.

[69] Ē. Kupče, T.D.W. Claridge, NOAH: NMR supersequences for small molecule analysis and structure elucidation, Angew. Chem. Int. Ed. 56 (2017) 11779–11783, https://doi.org/10.1002/anie.201705506.

[70] Ē. Kupče, T.D.W. Claridge, Molecular structure from a single NMR Supersequence, Chem. Commun. 54 (2018) 7139–7142, https://doi.org/10.1039/C8CC03296C.

[71] Ē. Kupče, R. Freeman, Binomial filters, J. Magn. Reson. 99 (1992) 644–651, https://doi.org/10.1016/0022-2364(92)90222-S.

[72] A. Meissner, O.W. Sorensen, Economizing spectrometer time and broadband excitation in small-molecule heteronuclear NMR correlation spectroscopy. Broadband HMBC, Magn. Reson. Chem. 38 (2000) 981–984, https://doi.org/10.1002/1097-458X(200011)38:11<981::AID-MRC778>3.0.CO;2-L.

[73] R. Burger, C. Schorn, P. Bigler, HMSC: simultaneously detected heteronuclear shift correlation through multiple and single bonds, J. Magn. Reson. 148 (2001) 88–94, https://doi.org/10.1006/jmre.2000.2223.

[74] W. Schoefberger, J. Schlagnitweit, N. Müller, Recent developments in heteronuclear multiple-bond correlation experiments, Ann. Rep. NMR Spectros. 72 (2011) 1–60, https://doi.org/10.1016/B978-0-12-385857-3.00001-3.

[75] V.M.R. Kakita, K. Rachineni, M. Bopardikar, R.V. Hosur, NMR supersequences with real-time homonuclear broadband decoupling: sequential acquisition of protein and small molecule spectra in a single experiment, J. Magn. Reson. 297 (2018) 108–112, https://doi.org/10.1016/j.jmr.2018.10.013.

[76] K. Zangger, H. Sterk, Homonuclear broadband-decoupled NMR spectra, J. Magn. Reson. 124 (1997) 486–489, https://doi.org/10.1006/jmre.1996.1063.

[77] J.A. Aguilar, S. Faulkner, M. Nilsson, G.A. Morris, Pure shift ^{1}H NMR: a resolution of the resolution problem?, Angew. Chem. Int. Ed 49 (2010) 3901–3903, https://doi.org/10.1002/anie.201001107.

[78] Ē. Kupče, H. Matsuo, G. Wagner, Homonuclear decoupling in proteins, in: N.R. Krishna, L.J. Berliner Heise (Eds.), Modern Techniques in Protein NMR.

Biological Magnetic Resonance, vol 16. Springer, Boston, MA, 1998, pp. 149-193, https://doi.org/10.1007/0-306-47083-7_5.

[79] M. Fukuchi, K. Takegoshi, Combination of ^{13}C–^{13}C COSY and DARR (COCODARR) in solid-state NMR, Solid State NMR. 34 (2008) 151–153, https://doi.org/10.1016/j.ssnmr.2008.05.001.

[80] G. Wagner, K. Wüthrich, Sequential resonance assignments in protein ^1H nuclear magnetic resonance spectra: Basic pancreatic trypsin inhibitor, J. Mol. Biol. 155 (1982) 347–366, https://doi.org/10.1016/0022-2836(82)90009-2.

[81] J. Cavanagh, M. Rance, A combined two-dimensional relayed NOESY/TOCSY experiment, J. Magn. Reson. 87 (1990) 408–414, https://doi.org/10.1016/0022-2364(90)90019-6.

[82] K. Motiram-Corral, M. Pérez-Trujillo, P. Nolis, T. Parella, Implementing one-shot multiple-FID acquisition into homonuclear and heteronuclear NMR experiments, Chem. Commun. 54 (2018) 13507–13510, https://doi.org/10.1039/C8CC08065H.

[83] P. Nolis, T. Parella, Practical aspects of the simultaneous collection of COSY and TOCSY spectra, Magn. Reson. Chem. 57 (2019) 85–94, https://doi.org/10.1002/mrc.4835.

[84] P. Nolis, K. Motiram-Corral, M. Perez-Trujillo, T. Parella, Interleaved dual NMR acquisition of equivalent transfer pathways in TOCSY and HSQC experiments, ChemPhysChem 20 (2019) 356–360, https://doi.org/10.1002/cphc.201801034.

[85] P. Nolis, M. Prez-Trujillo, T. Parella, Multiple FID acquisition of complementary HMBC data, Angew. Chem. Int. Ed. Engl. 46 (2007) 7495–7497, https://doi.org/10.1002/anie.200702258.

[86] T.D.W. Claridge, M. Mayzel, Ē. Kupče, Triplet NOAH supersequences optimised for small molecule structure characterisation, Magn. Reson. Chem. 57 (2019) 946–952, https://doi.org/10.1002/mrc.4887.

[87] L. Paudel, R.W. Adams, P. Király, J.A. Aguilar, M. Foroozandeh, M.J. Cliff, M. Nilsson, P. Sándor, J.P. Waltho, G.A. Morris, Simultaneously enhancing spectral resolution and sensitivity in heteronuclear correlation NMR spectroscopy, Angew. Chem. Int. Ed. 52 (2013) 11616–11619, https://doi.org/10.1002/anie.201305709.

[88] P. Giraudeau, Y. Shrot, L. Frydman, Multiple ultrafast, broadband 2D NMR spectra of hyperpolarized natural products, J. Am. Chem. Soc. 131 (2009) 13902–13903, https://doi.org/10.1021/ja905096f.

[89] J.H. Ardenkjær-Larsen, B. Fridlund, A. Gram, G. Hansson, L. Hansson, M.H. Lerche, R. Servin, M. Thaning, K. Golman, Proc. Natl. Acad. Sci. U.S.A. 100 (2003) 10158–10163.

[90] S. Jannin, J.-N. Dumez, P. Giraudeau, D. Kurzbach, Application and methodology of dissolution dynamic nuclear polarization in physical, chemical and biological contexts, J. Magn. Reson. 305 (2019) 41–50, https://doi.org/10.1016/j.jmr.2019.06.001.

[91] K.V. Kovtunov, E.V. Pokochueva, O.G. Salnikov, S.F. Cousin, D. Kurzbach, B. Vuichoud, S. Jannin, E.Y. Chekmenev, B.M. Goodson, Dr. D.A. Barskiy, I.V. Koptyug, Hyperpolarized NMR spectroscopy: d -DNP, PHIP, and SABRE Techniques, Chem. - Asian J. 13 (2018) 1857–1871, https://doi.org/10.1002/asia.201800551.

[92] N. Murali, W.M. Miller, B.K. John, D.A. Avizonis, S.H. Smallcombe, Spectral unraveling by space-selective Hadamard spectroscopy, J. Magn. Reson. 179 (2006) 182–189, https://doi.org/10.1016/j.jmr.2005.11.017.

[93] M. Vega-Vazquez, J.C. Cobas, M. Martin-Pastor, Fast multidimensional localized parallel NMR spectroscopy for the analysis of samples, Magn. Reson. Chem. 48 (2010) 749–752, https://doi.org/10.1002/mrc.2659.

[94] T.R. Brown, B.M. Kincaid, K. Ugurbil, NMR chemical shift imaging in three dimensions, Proc. Acad. Natl. Sci. USA 79 (1982) 3523–3526, https://doi.org/10.1073/pnas.79.11.3523.

[95] P. Bellstedt, Y. Ihle, C. Wiedemann, A. Kirschstein, C. Herbst, M. Görlach, R. Ramachandran, Sequential acquisition of multi-dimensional heteronuclear chemical shift correlation spectra with ^1H detection, Sci. Rep. 4 (2015) 4490, https://doi.org/10.1038/srep04490.

[96] C. Wiedemann, P. Bellstedt, A. Kirschstein, S. Häfner, C. Herbst, M. Görlach, R. Ramachandran, Sequential protein NMR assignments in the liquid state via sequential data acquisition, J. Magn. Reson. 239 (2014) 23–28, https://doi.org/10.1016/j.jmr.2013.12.002.

[97] T. Gopinath, G. Veglia, Dual acquisition magic angle spinning solid-state NMR-spectroscopy: Simultaneous acquisition of multidimensional spectra of biomacromolecules, Angew. Chem. Int. Ed. 51 (2012) 2731–2735, https://doi.org/10.1002/anie.201108132.

[98] P. Bellstedt, C. Herbst, S. Hafner, J. Leppert, M. Gorlach, R. Ramachandran, Solid state NMR of proteins at high MAS frequencies: symmetry-based mixing and simultaneous acquisition of chemical shift correlation spectra, J. Biomol. NMR. 54 (2012) 325–335, https://doi.org/10.1007/s10858-012-9680-z.

[99] J.R. Banigan, N.J. Traaseth, Utilizing afterglow magnetization from cross-polarization magic-angle-spinning solid-state NMR spectroscopy to obtain simultaneous heteronuclear multidimensional spectra, J. Phys. Chem. 116B (2012) 7138–7144, https://doi.org/10.1021/jp303269m.

[100] Ē. Kupče, R. Freeman, Parallel receivers and sparse sampling in multidimensional NMR, J. Magn. Reson. 213 (2011) 1–13, https://doi.org/10.1016/j.jmr.2011.08.027.

[101] Ē. Kupče, NMR with Multiple Receivers, in: H. Heise, S. Matthews (Eds.) Modern NMR Methodology. Top. Curr. Chem. 335, pp. 71-96, Springer, Berlin, Heidelberg (2011), https://doi.org/10.1007/128_2011_226.

[102] J.N. Robinson, A. Coy, R. Dykstra, C.D. Eccles, M.W. Hunter, P.T. Callaghan, Two-dimensional NMR spectroscopy in Earth's magnetic field, J. Magn. Reson. 182 (2006) 343–347, https://doi.org/10.1016/j.jmr.2006.06.027.

[103] Y. Zhu, Y. Gao, S. Rodocker, I. Savukov, C. Hilty, Multinuclear detection of nuclear spin optical rotation at low field, J. Phys. Chem. Lett. 9 (2018) 3323–3327, https://doi.org/10.1021/acs.jpclett.8b01053.

[104] R.M. Fratila, M.V. Gomez, S. Sýkora, A.H. Velders, Multinuclear nanoliter one-dimensional and two-dimensional NMR spectroscopy with a single non-resonant microcoil, Nat. Commun. 5 (2014) 3025, https://doi.org/10.1038/ncomms4025.

[105] P. Gierth, A. Codina, F. Schumann, H. Kovacs, Ē. Kupče, Fast experiments for structure elucidation of small molecules: hadamard NMR with multiple receivers, Magn. Reson. Chem. 53 (2015) 940–944, https://doi.org/10.1002/mrc.4292.

[106] Ē. Kupče, S. Cheatham, R. Freeman, Two-dimensional spectroscopy with parallel acquisition of ^1H–X and ^{19}F–X correlations, Magn. Reson. Chem. 45 (2007) 378–380, https://doi.org/10.1002/mrc.1988.

[107] Ē. Kupče, L.E. Kay, Parallel acquisition of multi-dimensional spectra in protein NMR, J. Biomol. NMR. 54 (2012) 1–7, https://doi.org/10.1007/s10858-012-9646-1.

[108] K.J. Donovan, Ē. Kupče, L. Frydman, Multiple parallel 2D NMR acquisitions in a single scan, Angew. Chem. Int. Ed. 52 (2013) 4152–4155, https://doi.org/10.1002/anie.201210070.

[109] D. Jeannerat, High resolution in heteronuclear ^1H–^{13}C NMR experiments by optimizing spectral aliasing with one-dimensional carbon data, Magn. Reson. Chem. 41 (2003) 3–17, https://doi.org/10.1002/mrc.1118.

[110] Ē. Kupče, R. Freeman, Molecular structure from a single NMR experiment, J. Am. Chem. Soc. 130 (2008) 10788–10792, https://doi.org/10.1021/ja8036492.

[111] Ē. Kupče, unpublished data.

[112] K.F. Morris, C.S. Johnson Jr., Diffusion-ordered two-dimensional nuclear magnetic resonance spectroscopy, J. Am. Chem. Soc. 114 (1992) 3139–3141, https://doi.org/10.1021/ja00034a071.

[113] Y.-B. Wan, X.-H. Li, Two-dimensional nuclear magnetic resonance spectroscopy with parallel acquisition of ^1H–^1H and ^{19}F–^{19}F correlations, Chin. J. Anal. Chem. 43 (2015) 1203–1209, https://doi.org/10.1016/S1872-2040(15)60849-0.

[114] Ē. Kupče, R. Freeman, Molecular structure from a single NMR sequence (fast-PANACEA), J. Magn. Reson. 206 (2010) 147–153, https://doi.org/10.1016/j.jmr.2010.06.018.

[115] Ē. Kupče, R. Freeman, High-resolution NMR correlation experiments in a single measurement (HR-PANACEA), Magn. Reson. Chem. 48 (2010) 333–336, https://doi.org/10.1002/mrc.2595.

[116] A. Bax, R. Freeman, S.P. Kempsell, Natural abundance carbon-13-carbon-13 coupling observed via double-quantum coherence, J. Am. Chem. Soc. 102 (1980) 4849–4851, https://doi.org/10.1021/ja00534a056.

[117] A. Bax, R. Freeman, S.P. Kempsell, Investigation of ^{13}C–^{13}C long-range couplings in natural-abundance samples, J. Magn. Reson. 41 (1980) 349–353, https://doi.org/10.1016/0022-2364(80)90083-9.

[118] A. Bax, R. Freeman, T.A. Frenkiel, M.H. Levitt, Assignment of carbon-13 NMR spectra via double-quantum coherence, J. Magn. Reson. 43 (1981) 478–483, https://doi.org/10.1016/0022-2364(81)90060-3.

[119] J. Keupp, J. Rahmer, I Grässlin, P.C. Mazurkewitz, T. Schaeffter, G.M. Lanza, S. A. Wickline, S.D. Caruthers, Simultaneous dual-nuclei imaging for motion corrected detection and quantification of ^{19}F imaging agents, Magn. Reson. Med. 66 (2011) 1116–1122, https://doi.org/10.1002/mrm.22877.

[120] Ē. Kupče, B. Wrackmeyer, Multiple receiver experiments for NMR spectroscopy of organosilicon compounds, Appl. Organometal. Chem. 24 (2010) 837–841, https://doi.org/10.1002/aoc.1692.

[121] M.E. Elyashberg, A.J. Williams, G.E. Martin, Computer-assisted structure verification and elucidation tools in NMR-based structure elucidation, Prog. NMR Spectrosc. 53 (2008) 1–104, https://doi.org/10.1016/j.pnmrs.2007.04.003.

[122] J.-M. Nuzillard, Automated Interpretation of NMR Spectra for Small Organic Molecules in Solution, in: R.K. Harris, R.L. Wasylishen (Eds.) eMagRes, 3 (2014) 287–294, https://doi.org/10.1002/9780470034590.emrstm1384.

[123] A.V. Buevich, M.E. Elyashberg, Synergistic combination of CASE algorithms and DFT chemical shift predictions: a powerful approach for structure elucidation, verification, and revision, J. Nat. Prod. 79 (2016) 3105–3116, https://doi.org/10.1021/acs.jnatprod.6b00799.

[124] M. Elyashberg, A. Williams, K. Blinov, Contemporary Computer-Assisted Approaches to Molecular Structure Elucidation, Royal Society of Chemistry, Cambridge, UK, 2011, https://doi.org/10.1039/9781849734578.

[125] P. Kessler, M. Godejohann, Identification of tentative marker in Corvina and Primitivo wines with CMC-se, Magn. Reson. Chem. 56 (2018) 480–492, https://doi.org/10.1002/mrc.4712.

[126] Ē. Kupče, O.W. Sørensen, 2BOB – extracting an H2BC and an HSQC-type spectrum from the same data set, and H2OBC – a fast experiment delineating the protonated ^{13}C backbone, Magn. Reson. Chem. 55 (2017) 515–518, https://doi.org/10.1002/mrc.4584.

[127] T.M. Nagy, T. Gyöngyösi, K.E. Kövér, O.W. Sørensen, BANGO SEA XLOC/HMBC–H2OBC: complete heteronuclear correlation within minutes from one NMR pulse sequence, Chem. Commun. 55 (2019) 12208, https://doi.org/10.1039/C9CC06253J.

[128] J. Briand, O.W. Sørensen, Simultaneous and independent rotations with arbitrary flip angles and phases for I, IS$^\alpha$, and IS$^\beta$ spin systems, J. Magn. Reson. 135 (1998) 44–49, https://doi.org/10.1006/jmre.1998.1556.

[129] T.M. Nagy, K.E. Kövér, O.W. Sørensen, Double and adiabatic BANGO for concatenating two NMR experiments relying on the same pool of magnetization, J. Magn. Reson. 316 (2020), https://doi.org/10.1016/j.jmr.2020.106767 106767.

[130] Ē. Kupče, Ray freeman, compensation for spin-spin coupling effects during adiabatic pulses, J. Magn. Reson. 127 (1997) 36–48, https://doi.org/10.1006/jmre.1997.1193.

[131] C. Zwahlen, P. Legault, S.J.F. Vincent, J. Greenblatt, R. Konrat, L.E. Kay, Methods for measurement of intermolecular NOEs by multinuclear NMR spectroscopy: application to a bacteriophage λ N-Peptide/*boxB* RNA complex, J. Am. Chem. Soc. 119 (1997) 6711–6721, https://doi.org/10.1021/ja970224q.

[132] B. Reif, M. Kock, R. Kerssebaum, H. Kang, W. Fenical, C. Griesinger, ADEQUATE- a new set of experiments to determine the constitution of small molecules at natural abundance, J. Magn. Reson. 118A (1996) 282–285, https://doi.org/10.1006/jmra.1996.0038.

[133] M. Kock, R. Kerssebaum, W. Bermel, A broadband ADEQUATE pulse sequence using chirp pulses, Magn. Reson. Chem. 41 (2003) 65–69, https://doi.org/10.1002/mrc.1097.

[134] V.M.R. Kakita, R.V. Hosur, All-in-one NMR spectroscopy of small organic molecules: complete chemical shift assignment from a single NMR experiment, RSC Adv. 10 (2020) 21174–21179, https://doi.org/10.1039/D0RA03417G.

[135] W. Bermel, I. Bertini, I.C. Felli, M. Piccioli, R. Pierattelli, ^{13}C-detected protonless NMR spectroscopy of proteins in solution, Prog. NMR Spectrosc. 48 (2006) 25–45, https://doi.org/10.1016/j.pnmrs.2005.09.002.

[136] L.E. Kay, M. Ikura, R. Tschudin, A. Bax, Three-dimensional triple-resonance NMR spectroscopy of isotopically enriched proteins, J. Magn. Reson. 89 (1990) 496–514, https://doi.org/10.0022-2364(90)90333-5.

[137] S. Grzesiek, A. Bax, Amino acid type determination in the sequential assignment procedure of uniformly ^{13}C/^{15}N-enriched proteins, J. Biomol. NMR 3 (1993) 185–204, https://doi.org/10.1007/BF00178261.

[138] Ē. Kupče, L.E. Kay, R. Freeman, Detecting the afterglow of ^{13}C NMR in proteins using multiple receivers, J. Am. Chem. Soc. 132 (2010) 18008–18011, https://doi.org/10.1021/ja1080025.

[139] Ē. Kupče, R. Freeman, Projection–reconstruction technique for speeding up multidimensional NMR spectroscopy, J. Am. Chem. Soc. 126 (2004) 6429–6440, https://doi.org/10.1021/ja049432q.

[140] R. Freeman, Ē. Kupče, Distant echoes of the accordion: Reduced dimensionality, GFT-NMR, and projection-reconstruction of multidimensional spectra, Concepts Magn. Reson. 23A (2008) 63–75, https://doi.org/10.1002/cmr.a.20021.

[141] S. Chakraborty, S. Paul, R.V. Hosur, Simultaneous acquisition of ^{13}Cα-^{15}N and ^{1}H-^{15}N-^{15}N sequential correlations in proteins: application of dual receivers in 3D HNN, J. Biomol. NMR 52 (2012) 5–10, https://doi.org/10.1007/s10858-011-9596-z.

[142] S.C. Panchal, N.S. Bhavesh, R.V. Hosur, Improved 3D triple resonance experiments, HNN and HN(C)N, for HN and ^{15}N sequential correlations in (^{13}C, ^{15}N) labeled proteins: Application to unfolded proteins, J. Biomol. NMR 20 (2001) 135–147, https://doi.org/10.1023/A:1011239023422.

[143] J.G. Reddy, R.V. Hosur, Parallel acquisition of 3D-HA(CA)NH and 3D-HACACO spectra, J. Biomol. NMR 56 (2013) 77–84, https://doi.org/10.1007/s10858-013-9735-9.

[144] J.G. Reddy, R.V. Hosur, Complete backbone and DENQ side chain NMR assignments in proteins from a single experiment: implications to structure–function studies, J. Struct. Funct. Genomics 15 (2014) 25–32, https://doi.org/10.1007/s10969-014-9175-0.

[145] R. Deslauriers, S. Lareau, R.S. Labow, W.J. Keon, G.-H. Tian, A.L. Panos, C.A.M. Barrozo, I.S. Ali, O. Al-Nowaiser, T.A. Salerno, NMR spectroscopy in cardiac surgery, Bull. Magn. Reson. 14 (1992) 15–23.

[146] O. Gonen, J. Murphy-Boesch, J. Srinivasan, J.N. Hu, H. Jiang, R. Stoyanova, T.R. Brown, Simultaneous and interleaved multinuclear chemical-shift imaging, a method for concurrent, localized spectroscopy, J. Magn. Reson. 104B (1994) 26–33, https://doi.org/10.1006/jmrb.1994.1050.

[147] H. Wang, L. Ciobanu, A.S. Edison, A.G. Webb, An eight-coil high-frequency probehead design for high-throughput nuclear magnetic resonance spectroscopy, J. Magn. Reson. 170 (2004) 206–212, https://doi.org/10.1016/j.jmr.2004.07.001.

[148] C. Martineau, F. Decker, F. Engelke, F. Taulelle, Parallelizing acquisitions of solid-state NMR spectra with multi-channel probe and multi-receivers: Applications to nanoporous solids, Solid State NMR 55–56 (2013) 48–53, https://doi.org/10.1016/j.ssnmr.2013.08.001.

[149] A. Viegas, T. Viennet, T.-Y. Yu, Schumann, W. Bermel, G. Wagner, M. Etzkorn, UTOPIA NMR: activating unexploited magnetization using interleaved low-gamma detection, J. Biomol. NMR 64 (2016) 9–15, https://doi.org/10.1007/s10858-015-0008-7.

[150] M. Schiavina, M.G. Murrali, L. Pontoriero, V. Sainati, R. Kümmerle, W. Bermel, R. Pierattelli, I.C. Felli, Taking simultaneous snapshots of intrinsically disordered proteins in action, Biophys. J. 117 (2019) 46–55, https://doi.org/10.1016/j.bpj.2019.05.017.

[151] Z. Solyom, M. Schwarten, L. Geist, R. Konrat, D. Willbold, B. Brutscher, BEST-TROSY experiments for time-efficient sequential resonance assignment of large disordered proteins, J. Biomol. NMR 55 (2013) 311–321, https://doi.org/10.1007/s10858-013-9715-0.

[152] M. Gal, K.A. Edmonds, A.G. Milbradt, K. Takeuchi, G. Wagner, Speeding up direct 15N detection: hCaN 2D NMR experiment, J. Biomol. NMR 51 (2011) 497–504, https://doi.org/10.1007/s10858-011-9580-7.

[153] J.L. Markley, R. Brüschweiler, A.S. Edison, H.R. Eghbalnia, R. Powers, D. Raftery, D.S. Wishart, The future of NMR-based metabolomics, Curr. Opin. Biotechnol. 43 (2017) 34–40, https://doi.org/10.1016/j.copbio.2016.08.001.

[154] Ē. Kupče, R. Freeman, Resolving ambiguities in two-dimensional NMR spectra: the 'TILT' experiment, J. Magn. Reson. 172 (2005) 329–332, https://doi.org/10.1016/j.jmr.2004.11.007.

[155] S.M. Pudakalakatti, A. Dubey, G. Jaipuria, U. Shubhashree, S.K. Adiga, D. Moskau, H.S. Atreya, A fast NMR method for resonance assignments: application to metabolomics, J. Biomol. NMR 58 (2014) 165–173, https://doi.org/10.1007/s10858-014-9814-6.

[156] S.M. Pudakalakatti, A. Dubey, H.S. Atreya, Simultaneous acquisition of three NMR spectra in a single experiment for rapid resonance assignments in metabolomics, J. Chem. Sci. 127 (2015) 1091–1097, https://doi.org/10.1007/s12039-015-0868-0.

[157] M. Tang, D.A. Berthold, C.M. Rienstra, Solid-state NMR of a large membrane protein by paramagnetic relaxation enhancement, J. Phys. Chem. Lett. 2 (2011) 1836–1841, https://doi.org/10.1021/jz200768r.

[158] M. Bjerring, B. Paaske, H. Oschkinat, Ü. Akbey, N.C. Nielsen, Rapid solid-state NMR of deuterated proteins by interleaved cross-polarization from ^{1}H and ^{2}H nuclei, J. Magn. Reson. 214 (2012) 324–328, https://doi.org/10.1016/j.jmr.2011.10.020.

[159] R. Zhang, Y. Chen, N. Rodriguez-Hornedo, A. Ramamoorthy, Enhancing NMR sensitivity of natural-abundance low-γ nuclei by ultrafast magic-angle-spinning solid-state NMR spectroscopy, ChemPhysChem 17 (2016) 2962–2966, https://doi.org/10.1002/cphc.201600637.

[160] J.J. Lopez, C. Kaiser, S. Asami, C. Glaubitz, Higher sensitivity through selective ^{13}C excitation in solid-state NMR spectroscopy, J. Am. Chem. Soc. 131 (2009) 15970–15971, https://doi.org/10.1021/ja904963n.

[161] F.H. Larsen, H.J. Jakobsen, P.D. Ellis, N.C. Nielsen, QCPMG-MAS NMR of half-integer quadrupolar nuclei, J. Magn. Reson. 131 (1998) 144–147, https://doi.org/10.1006/jmre.1997.1341.

[162] I. Hung, A.J. Rossini, R.W. Schurko, Application of the Carr-Purcell-Meiboom-Gill pulse sequence for the acquisition of solid-state nmr spectra of spin-1/2 nuclei, J. Phys. Chem. 108A (2004) 7112–7120, https://doi.org/10.1021/jp0401123.

[163] D. Jardon-Alvarez, M.O. Bovee, J.H. Baltisberger, P.J. Grandinetti, Natural abundance ^{17}O and ^{33}S nuclear magnetic resonance spectroscopy in solids achieved through extended coherence lifetimes, Phys. Rev. 100B (2019), https://doi.org/10.1103/PhysRevB.100.140103 140103.

[164] L. Thomas, J. Kahr, P. Schmidt, U. Krug, H.A. Scheidt, D. Huster, The dynamics of the G protein-coupled neuropeptide Y2 receptor in monounsaturated membranes investigated by solid-state NMR spectroscopy, J. Biomol. NMR 61 (2015) 347–359, https://doi.org/10.1007/s10858-014-9892-5.

[165] N. Ivchenko, C.E. Hughes, M.H. Levitt, Multiplex phase cycling, J. Magn. Reson. 160 (2003) 52–58, https://doi.org/10.1016/S1090-7807(02)00108-8.

[166] C. Herbst, K. Riedel, Y. Ihle, J. Leppert, O. Ohlenschläger, M. Görlach, R. Ramachandran, MAS solid state NMR of RNAs with multiple receivers, J. Biomol. NMR 41 (2008) 121–125, https://doi.org/10.1007/s10858-008-9247-1.

[167] K. Takeda, Y. Kusakabe, Y. Noda, M. Fukuchi, K. Takegoshi, Homo- and heteronuclear two dimensional covariance solid-state NMR spectroscopy with a dual-receiver system, Phys. Chem. Chem. Phys. 14 (2012) 9715–9721, https://doi.org/10.1039/c2cp41191a.

[168] T. Gopinath, D.K. Weber, G. Veglia, Multi-receiver solid-state NMR using polarization optimized experiments (POE) at ultrafast magic angle spinning, J. Biomol. NMR 74 (2020) 267–285, https://doi.org/10.1007/s10858-020-00316-y.

[169] I. Hung, Z. Gan, Spin-locking and cross-polarization under magic-angle spinning of uniformly labeled solids, J. Magn. Reson. 256 (2015) 23–29, https://doi.org/10.1016/j.jmr.2015.04.005.

[170] R. Linser, B. Bardiaux, V. Higman, U. Fink, B. Reif, Structure calculation from unambiguous long-range amide and methyl ^{1}H–^{1}H distance restraints for a microcrystalline protein with MAS solid-state NMR spectroscopy, J. Am. Chem. Soc. 133 (2011) 5905–5912, https://doi.org/10.1021/ja110222h.

[171] B.B. Das, S.J. Opella, Simultaneous cross polarization to ^{13}C and ^{15}N with ^{1}H detection at 60kHz MAS solid-state NMR, J. Magn. Reson. 262 (2016) 20–26, https://doi.org/10.1016/j.jmr.2015.12.004.

[172] K. Sharma, P.K. Madhu, K.R. Mote, A suite of pulse sequences based on multiple sequential acquisitions at one and two radiofrequency channels for solid-state magic-angle spinning NMR studies of proteins, J. Biomol. NMR 65 (2016) 127–141, https://doi.org/10.1007/s10858-016-0043-z.

[173] T. Gopinath, G. Veglia, Proton-detected polarization optimized experiments (POE) using ultrafast magic angle spinning solid-state NMR: Multi-acquisition of membrane protein spectra, J. Magn. Reson. 310 (2020), https://doi.org/10.1016/j.jmr.2019.106664 106664.

[174] K. Sharma, P.K. Madhu, V. Agarwal, K.R. Mote, Simultaneous recording of intra- and inter-residue linking experiments for backbone assignments in proteins at MAS frequencies higher than 60 kHz, J. Biomol. NMR 74 (2020) 229–237, https://doi.org/10.1007/s10858-019-00292-y.

[175] J. Stanek, T. Schubeis, P. Paluch, P. Guntert, L.B. Andreas, G. Pintacuda, Automated backbone nmr resonance assignment of large proteins using redundant linking from a single simultaneous acquisition, J. Am. Chem. Soc. 142 (2020) 5793–5799, https://doi.org/10.1021/jacs.0c00251.

[176] G. De Paëpe, J.R. Lewandowski, A. Loquet, A. Böckmann, R.G. Griffin, Proton assisted recoupling and protein structure determination, J. Chem. Phys. 129 (2008), https://doi.org/10.1063/1.3036928 245101.

[177] J.R. Lewandowski, G. De Paëpe, R.G. Griffin, Proton assisted insensitive nuclei cross polarization, J. Amer. Chem. Soc. 129 (2007) 728–729, https://doi.org/10.1021/ja0650394.

[178] A.B. Nielsen, K. Székely, J. Gath, M. Ernst, N.C. Nielsen, B.H. Meier, Simultaneous acquisition of PAR and PAIN spectra, J. Biomol. NMR 52 (2012) 283–288, https://doi.org/10.1007/s10858-012-9616-7.

[179] J.M. Lamley, J.R. Lewandowski, Simultaneous acquisition of homonuclear and heteronuclear long-distance contacts with time-shared third spin assisted recoupling, J. Magn. Reson. 218 (2012) 30–34, https://doi.org/10.1016/j.jmr.2012.03.013.

[180] V. Agarwal, M. Sardo, I. Scholz, A. Bockmann, M. Ernst, B.H. Meier, PAIN with and without PAR: Variants for third-spin assisted heteronuclear polarization transfer, J. Biomol. NMR 56 (2013) 365–377, https://doi.org/10.1007/s10858-013-9756-4.

[181] V. Chevelkov, A. Diehl, B. Reif, Measurement of ^{15}N–T_1 relaxation rates in a perdeuterated protein by magic angle spinning solid-state nuclear magnetic resonance spectroscopy, J. Chem. Phys. 128 (2008) 52316, https://doi.org/10.1063/1.2819311.

[182] D. Suter, R.R. Ernst, Spin diffusion in resolved solid-state NMR spectra, Phys. Rev. B 32 (1985) 5608–5627, https://doi.org/10.1103/PhysRevB.32.5608.

[183] V.A. Higman, Solid-state MAS NMR resonance assignment methods for proteins, Prog. Nucl. Magn. Reson. Spectrosc. 106 (2018) 37–65, https://doi.org/10.1016/j.pnmrs.2018.04.002.

[184] N.P. Wickramasinghe, S. Parthasarathy, C.R. Jones, C. Bhardwaj, F. Long, M. Kotecha, S. Mehboob, L.W.-M. Fung, J. Past, A. Samoson, Y. Ishii, Nanomole-scale protein solid-state NMR by breaking intrinsic ^1H T_1 boundaries, Nat. Methods 6 (2009) 215–218, https://doi.org/10.1038/nmeth.1300.

[185] K.R. Mote, T. Gopinath, G. Veglia, Determination of structural topology of a membrane protein in lipid bilayers using polarization optimized experiments (POE) for static and MAS solid state NMR spectroscopy, J. Biomol. NMR 57 (2013) 91–102, https://doi.org/10.1007/s10858-013-9766-2.

[186] P. L. Gor'kov, E.Y. Chekmenev, C. Li, M. Cotten J.J. Buffy, N.J. Traaseth, G. Veglia, W.W. Brey, Using low-E resonators to reduce RF heating in biological samples for static solid-state NMR up to 900 MHz, J. Magn. Reson 185(1) (2007) 77–93, https://doi.org/10.1016/j.jmr.2006.11.008.

[187] J.A. Stringer, C.E. Bronnimann, C.G. Mullen, D.H. Zhou, S.A. Stellfox, Y. Li, E.H. Williams, C.M. Rienstra, Reduction of RF-induced sample heating with a scroll coil resonator structure for solid-state NMR probes, J. Magn. Reson 173 (1) (2005) 40–48, https://doi.org/10.1016/j.jmr.2004.11.015.

[188] A. Equbal, P.K. Madhu, B.H. Meier, N.C. Nielsen, M. Ernst, V. Agarwal, Parameter independent low-power heteronuclear decoupling for fast magic-angle spinning solid-state NMR, J. Chem. Phys. 146 (2017), https://doi.org/10.1063/1.4976997 084202.

[189] T. Gopinath, G. Veglia, 3D DUMAS: Simultaneous acquisition of three-dimensional magic angle spinning solid-state NMR experiments of proteins, J. Magn. Reson. 220 (2012) 79–84, https://doi.org/10.1016/j.jmr.2012.04.006.

[190] Z. Tošner, R. Sarkar, J. Becker-Baldus, C. Glaubitz, S. Wegner, F. Engelke, S.J. Glaser, B. Reif, Overcoming volume selectivity of dipolar recoupling in biological solid-state NMR spectroscopy, Angew. Chem. Int. Ed. 57 (2018) 14514–14518, https://doi.org/10.1002/anie.201805002.

[191] T. Gopinath, G. Veglia, Orphan spin operators enable the acquisition of multiple 2D and 3D magic angle spinning solid-state NMR spectra, J. Chem. Phys. 138 (2013), https://doi.org/10.1063/1.4803126 184201.

[192] J.R. Banigan, A. Gayen, N.J. Traaseth, Combination of ^{15}N reverse labeling and afterglow spectroscopy for assigning membrane protein spectra by magic-angle-spinning solid-state NMR: Application to the multidrug resistance protein EmrE, J. Biomol. NMR 55 (2013) 391–399, https://doi.org/10.1007/s10858-013-9724-z.

[193] T. Gopinath, K.R. Mote, G. Veglia, Simultaneous acquisition of 2D and 3D solid-state NMR experiments for sequential assignment of oriented membrane protein samples, J. Biomol. NMR 62 (2015) 53–61, https://doi.org/10.1007/s10858-015-9916-9.

[194] C.H. Wu, A. Ramamoorthy, S.J. Opella, High-resolution heteronuclear dipolar solid-state NMR spectroscopy, J. Magn. Reson. 109 (1994) 270–272, https://doi.org/10.1006/jmra.1994.1169.

[195] T. Gopinath, G. Veglia, Sensitivity enhancement in static solid-state nmr experiments via single and multiple-quantum dipolar coherences, J. Am. Chem. Soc. 131 (2009) 5754–5756, https://doi.org/10.1021/ja900096d.

[196] K.R. Mote, T. Gopinath, N.J. Traaseth, J. Kitchen, P.L. Gor'kov, W.W. Brey, G. Veglia, Multidimensional oriented solid-stateNMR experiments enable the sequential assignment of uniformly 15N labeled integral membrane proteins in magnetically aligned lipid bilayers, J. Biomol. NMR, 51 (2011) 339–346, https://doi.org/10.1007/s10858-011-9571-8.

[197] R. Zhang, Y. Nishiyama, A. Ramamoorthy, Exploiting heterogeneous time scale of dynamics to enhance 2D HETCOR solid-state NMR sensitivity, J. Magn. Reson. 309 (2019), https://doi.org/10.1016/j.jmr.2019.106615 106615.

[198] C.P. Jaroniec, C. Filip, R.G. Griffin, 3D TEDOR NMR experiments for the simultaneous measurement of multiple carbon–nitrogen distances in uniformly $^{13}C,^{15}N$-labeled solids, J. Am. Chem. Soc. 124 (2002) 10728–10742, https://doi.org/10.1021/ja026385y.

[199] T. Gopinath, S. Wang, J. Lee, H. Aihara, G. Veglia, Hybridization of TEDOR and NCX MAS solid-state NMR experiments for simultaneous acquisition of heteronuclear correlation spectra and distance measurements, J. Biomol. NMR 73 (2019) 141–153, https://doi.org/10.1007/s10858-019-00237-5.

[200] H. Ivanir-Dabora, E. Nimerovsky, P.K. Madhu, A. Goldbourt, Site-resolved backbone and side-chain intermediate dynamics in a carbohydrate-binding module protein studied by magic-angle spinning NMR spectroscopy, Chem. – A Eur. J. 21 (2015) 10778–10785, https://doi.org/10.1002/chem.201500856.

[201] K. Takegoshi, S. Nakamura, T. Terao, ^{13}C–^1H dipolar-assisted rotational resonance in magic-angle spinning NMR, Chem. Phys. Lett. 344 (2001) 631–637, https://doi.org/10.1016/S0009-2614(01)00791-6.

[202] H.R.W. Dannatt, G.F. Taylor, K. Varga, V.A. Higman, M.-P. Pfeil, L. Asilmovska, P.J. Judge, A. Watts, ^{13}C- and ^1H-detection under fast MAS for the study of poorly available proteins: application to sub-milligram quantities of a 7 trans-membrane protein, J. Biomol. NMR 62 (2015) 17–23, https://doi.org/10.1007/s10858-015-9911-1.

[203] A. Gallo, W. Franks, J. Lewandowski, A suite of solid-state NMR experiments to utilize orphaned magnetization for assignment of proteins using parallel high and low gamma detection, J. Magn. Reson. 305 (2019) 219–231, https://doi.org/10.1016/j.jmr.2019.07.006.

[204] H.A. Scheidt, J. Adler, U. Zeitschel, C. Höfling, A. Korn, M. Krueger, S. Rossner, D. Huster, Pyroglutamate-modified amyloid β (11–40) fibrils are more toxic than wildtype fibrils but structurally very similar, Chem. - A Eur. J. 23 (2017) 15834–15838, https://doi.org/10.1002/chem.201703909.

[205] L.B. Andreas, J. Stanek, T.L. Marchand, A. Bertarello, D.C.-D. Paepe, D. Lalli, M. Krejčíková, C. Doyen, C. Öster, B. Knott, S. Wegner, F. Engelke, I.C. Felli, R. Pierattelli, N.E. Dixon, L. Emsley, T. Herrmann, G. Pintacuda, Protein residue linking in a single spectrum for magic-angle spinning NMR assignment, J. Biomol. NMR, 62 (2015) 253–261, https://doi.org/10.1007/s10858-015-9956-1.

[206] S. Xiang, K. Grohe, P. Rovó, S.K. Vasa, K. Giller, S. Becker, R. Linser, Sequential backbone assignment based on dipolar amide-to-amide correlation experiments, J. Biomol. NMR 62 (2015) 303–311, https://doi.org/10.1007/s10858-015-9945-4.

[207] T. Schubeis, T.S. Schwarzer, T.L. Marchand, J. Stanek, K.T. Movellan, K. Castiglione, G. Pintacuda, L.B. Andreas, Resonance assignment of the outer membrane protein AlkL in lipid bilayers by proton-detected solid-state NMR, Biomol. NMR Assign. (2020), https://doi.org/10.1007/s12104-020-09964-5.

[208] T. Gopinath, G. Veglia, Multiple acquisitions via sequential transfer of orphan spin polarization (MAeSTOSO): How far can we push residual spin polarization in solid-state NMR?, J. Magn. Reson. 267 (2016) 1–8, https://doi.org/10.1016/j.jmr.2016.03.001.

[209] A.S.L. Thankamony, J.J. Wittmann, M. Kaushik, B. Corzilius, Dynamic nuclear polarization for sensitivity enhancement in modern solid-state NMR, Prog. NMR Spectrosc. 102–103 (2017) 120–195, https://doi.org/10.1016/j.pnmrs.2017.06.002.

[210] T. Gopinath, G. Veglia, Experimental aspects of polarization optimized experiments (POE) for magic angle spinning solid-state NMR of microcrystalline and membrane-bound proteins, in: R. Ghose (Ed.) Protein NMR. Methods in Molecular Biology, vol. 1688, Humana Press, New York, 2018, https://doi.org/10.1007/978-1-4939-7386-6_2.

[211] GitHub repository, https://github.com/kaustubhmote/pulseseq.

[212] J.J. Helmus, C.P. Jaroniec, Nmrglue: An open source Python package for the analysis of multidimensional NMR data, J. Biomol. NMR 55 (2013) 355–367, https://doi.org/10.1007/s10858-013-9718-x.

[213] Y. Kim, M. Liu, C. Hilty, Parallelized ligand screening using dissolution dynamic nuclear polarization, Anal. Chem. 88 (2016) 11178–11183, https://doi.org/10.1021/acs.analchem.6b03382.

[214] Y. Kim, M. Liu, C. Hilty, Determination of binding affinities using hyperpolarized NMR with simultaneous 4-channel detection, J. Magn. Reson. 295 (2018) 80–86, https://doi.org/10.1016/j.jmr.2018.08.002.

[215] M.A. Macnaughtan, T. Hou, J. Xu, D. Raftery, High-throughput nuclear magnetic resonance analysis using a multiple coil flow probe, Anal. Chem. 75 (2003) 5116–5123, https://doi.org/10.1021/ac025903k.

[216] E. MacNamara, T. Hou, G. Fisher, S. Williams, D. Raftery, Multiplex sample NMR: an approach to high-throughput NMR using a parallel coil probe, Anal. Chim. Acta 397 (1999) 9–16, https://doi.org/10.1016/S0003-2670(99)00387-6.

[217] H. Wang, L. Ciobanu, A. Webb, Reduced data acquisition time in multi-dimensional NMR spectroscopy using multiple-coil probes, J. Magn. Reson. 173 (2005) 134–139, https://doi.org/10.1016/j.jmr.2004.11.024.

[218] L. Ciobanu, D.A. Jayawickrama, X. Zhang, A.G. Webb, J.V. Sweedler, Measuring reaction kinetics by using multiple microcoil NMR spectroscopy, Angew. Chem. Int. Ed. Engl. 42 (2003) 4669–4672, https://doi.org/10.1002/anie.200351901.

[219] E. Oldfield, A multiple-probe strategy for ultra high field nuclear magnetic resonance spectroscopy, J. Mag. Res. 107A (1994) 255–257, https://doi.org/10.1006/jmra.1994.1079.

[220] X. Zhang, J.V. Sweedler, A.G. Webb, A probe design for the acquisition of homonuclear, heteronuclear, and inverse detected NMR spectra from multiple samples, J. Magn. Reson. 153 (2001) 254–258, https://doi.org/10.1006/jmre.2001.2441.

[221] G. Fisher, C. Petucci, E. MacNamara, D. Raftery, NMR probe for the simultaneous acquisition of multiple samples, J. Magn. Reson. 138 (1999) 160–163, https://doi.org/10.1006/jmre.1999.1725.

[222] A.M. Wolters, D.A. Jayawickrama, A.G. Webb, J.V. Sweedler, NMR detection with multiple solenoidal microcoils for continuous-flow capillary electrophoresis, Anal. Chem. 74 (2002) 5550–5555, https://doi.org/10.1021/ac025903k.

[223] T. Hou, E. MacNamara, D. Raftery, NMR analysis of multiple samples using parallel coils: improved performance using reference deconvolution and multidimensional methods, Anal. Chim. Acta 400 (1999) 297–305, https://doi.org/10.1016/S0003-2670(99)00706-0.

[224] T. Hou, J. Smith, E. MacNamara, M. MacNaughton, D. Raftery, Analysis of multiple samples using multiplex sample NMR, selective excitation and chemical shift imaging approaches, Anal. Chem. 73 (2001) 2541–2546, https://doi.org/10.1021/ac0100751.

[225] Y. Li, A. Wolters, P. Malaway, J.V. Sweedler, A.G. Webb, Multiple Solenoidal microcoil probes for high-sensitivity, high-throughput nuclear magnetic resonance spectroscopy, Anal. Chem. 71 (1999) 4815–4820, https://doi.org/10.1021/ac990855y.

[226] D.O. Walsh, Multi-channel surface NMR instrumentation and software for 1D/2D groundwater investigations, J. Appl. Geophys. 66 (2008) 140–150, https://doi.org/10.1016/j.jappgeo.2008.03.006.

[227] Lisa C. Siskind, Bruce E. Hammer, Nelson L. Christensen, Jeffrey Yepez, Multiple RF coil nuclear magnetic resonance quantum computing, Quantum Inf. Process. 4 (2005) 433–455, https://doi.org/10.1007/s11128-005-0007-9.

[228] W.G. Clark, T.W. Hijmans, W.H. Wong, Multiple coil pulsed NMR method for measuring the multipole moments of particle accelerator bending magnets, J. Appl. Phys. 63 (1988) 4185–4186, https://doi.org/10.1063/1.340244.

[229] R. Kc, I.D. Henry, G.H.J. Park, D. Raftery, Design and construction of a versatile dual volume heteronuclear double resonance microcoil NMR probe, J. Magn. Reson. 197 (2009) 186–192, https://doi.org/10.1016/j.jmr.2004.11.024.

[230] G.Y. Kim, l. Josephson, R. Langer, M.J. Cima, Magnetic relaxation switch detection of human chorionic gonadotrophin, Bioconjug. Chem. 18 (2007) 2024–2028. https://doi.org/10.1021/bc070110w.

[231] A. Tsourkas, O. Hofstetter, H. Hofstetter, R. Weissleder, L. Josephson, Magnetic relaxation switch immunosensors detect enantiomeric impurities, Angew. Chem. Int. Ed. Engl. 43 (2004) 2395–2399, https://doi.org/10.1002/anie.200352998.

[232] H. Lee, T.J. Yoon, R. Weissleder, Ultrasensitive detection of bacteria using core-shell nanoparticles and an NMR-filter system, Angew. Chem. Int. Ed. Engl. 48 (2009) 5657–5660, https://doi.org/10.1002/anie.200901791.

[233] J.M. Perez, F.J. Simeone, Y. Saeki, L. Josephson, R. Weissleder, Viral-induced self-assembly of magnetic nanoparticles allows the detection of viral particles in biological media, J. Am. Chem. Soc. 125 (2003) 10192–10193, https://doi.org/10.1021/ja036409g.

[234] H. Lee, E Sun, D. Ham, R. Weissleder, Chip-NMR biosensor for detection and molecular analysis of cells, Nat. Med. 14 (2008) 869–874, https://doi.org/10.1038/nm.1711.

[235] H. Lee, T.J. Yoon, J.L. Figueiredo, F.K. Swirski, R. Weissleder, Rapid detection and profiling of cancer cells in fine-needle aspirates, Proc. Natl. Acad. Sci. U S A. 106 (2009) 12459–12464, https://doi.org/10.1073/pnas.0902365106.

[236] H. Shao, C. Min, D. Issadore, M. Liong, T.J. Yoon, R. Weissleder, H. Lee, Magnetic nanoparticles and microNMR for diagnostic applications, Theranostics 2 (2012) 55–65, https://doi.org/10.7150/thno.3465.

[237] A. Purea, T. Neuberger, A.G. Webb, Simultaneous NMR microimaging of multiple single-cell samples, Concepts in Magn. Reson. 22B (2004) 7–14, https://doi.org/10.1002/cmr.b.20015.

[238] G. Madelin, R.R. Regatte, Biomedical applications of sodium MRI in Vivo, J. Magn. Reson. Imaging 38 (2013) 511–529, https://doi.org/10.1002/jmri.24168.

[239] Y. Liu, Yu. Gu, X. Yu, Assessing tissue metabolism by phosphorous-31 magnetic resonance spectroscopy and imaging: a methodology review, Quant. Imaging Med. Surg. 7 (2017) 707–726, 10.21037%2Fqims.2017.11.03.

[240] M. Welvaert, Y. Rosseel, On the definition of signal-to-noise ratio and contrast-to-noise ratio for fMRI data, PLoS ONE 8 (2013), https://doi.org/10.1371/journal.pone.0077089 e77089.

[241] E.T. Ahrens, J. Zhong, In vivo MRI cell tracking using perfluorocarbon probes and fluorine-19 detection, NMR Biomed. 26 (2013) 860–871, https://doi.org/10.1002/nbm.2948.

[242] Z.J. Wang, M.A. Ohliger, P.E.Z. Larson, J.W. Gordon, R.A. Bok, J. Slater, J.E. Villanueva-Meyer, C.P. Hess, J. Kurhanewicz, D.B. Vigneron, Hyperpolarized ^{13}C MRI: state of the art and future directions, Radiology 291 (2019) 273–284, https://doi.org/10.1148/radiol.2019182391.

[243] M. Meyerspeer, A.W. Magill, A. Kuehne, R. Gruetter, E. Moser, A.I. Schmid, Simultaneous and interleaved acquisition of NMR signals from different nuclei with a clinical MRI scanner, Magn. Reson. Med. 76 (2016) 1636–1641, https://doi.org/10.1002/mrm.26056.

[244] P.W. de Bruin, P. Koken, M.J. Versluis, S.A. Aussenhofer, I. Meulenbelt, P. Börnert, A.G. Webb, Time-efficient interleaved human ^{23}Na and ^{1}H data acquisition at 7 T, NMR Biomed. 28 (2015) 1228–1235, https://doi.org/10.1002/nbm.3368.

[245] G.J. Moore, M.I. Hrovat, R.G. González, Simultaneous multinuclear magnetic resonance imaging and spectroscopy, Magn. Reson. Med. 19 (1991) 105–112, https://doi.org/10.1002/mrm.1910190110.

[246] R. van Sluis, N.M. Yongbi, G.S. Payne, M.O. Leach, Simultaneous localized ^{1}H STEAM/^{31}P ISIS spectroscopy in Vivo, Magn. Reson. Med. 35 (1996) 465–470, https://doi.org/10.1002/mrm.1910350404.

[247] O. Gonen, J. Hu, J. Murphy-Boesch, R. Stoyanova, T.R. Brown, Dual interleaved ^{1}H and proton-decoupled ^{31}P in vivo chemical shift imaging of human brain, Magn. Reson. Med. 32 (1994) 104–109, https://doi.org/10.1002/mrm.1910320114.

[248] J. Ma, Dixon techniques for water and fat imaging, J. Magn. Reson. Imaging 28 (2008) 543–548, https://doi.org/10.1002/jmri.21492.

[249] S.W. Lee, S.K. Hilal, Z.H. Cho, A multinuclear magnetic resonance imaging technique - simultaneous proton and sodium imaging, Magn. Reson. Imag. 4 (1986) 343–350, https://doi.org/10.1016/0730-725X(86)91044-1.

[250] L. Pel, P.A.J. Donkers, K. Kopinga, J.J.P.A.W. Noijen, ^{1}H, ^{23}Na and ^{35}Cl imaging in cementitious materials with NMR, Appl. Magn. Reson. 47 (2016) 265–276, https://doi.org/10.1007/s00723-015-0752-6.

[251] Y. He, Z. Zhang, J. Feng, C. Huang, F. Chen, M. Liu, C. Liu, Simultaneous acquisition of multi-nuclei enhanced NMR/MRI by solution state dynamic nuclear polarization, Sci. China Chem. 59 (2016) 830–835, https://doi.org/10.1007/s11426-015-0512-0.

[252] M. Meyerspeer, A.W. Magill, A. Kuehne, R. Gruetter, E. Moser, A.I. Schmid, Simultaneous imaging of ^{13}C metabolism and ^{1}H structure: technical considerations and potential applications, NMR Biomed. 28 (2015) 576–582, https://doi.org/10.1002/nbm.3279.

[253] J.M. Wild, S. Ajraoui, M.H. Deppe, S.R. Parnell, H. Marshall, J. Parra-Robles, R. H. Ireland, Synchronous acquisition of hyperpolarised ^{3}He and ^{1}H MR images of the lungs – maximising mutual anatomical and functional information, NMR Biomed. 24 (2011) 130–134, https://doi.org/10.1002/nbm.1565.

[254] J.M. Wild, H. Marshall, X. Xu, G. Norquay, S.R. Parnell, M. Clemence, P.D. Griffiths, J. Parra-Robles, Simultaneous imaging of lung structure and function with triple-nuclear hybrid MR imaging, Radiology 267 (2013) 251–255, https://doi.org/10.1148/radiol.12121153.

[255] Bruker online User Library, https://www.bruker.com/en/services/bruker-user-library.html.

Glossary

2BOB: 2-Bond, One-Bond correlation experiment
ADEQUATE: Adequate sensitivity DoublE-QUAnTum spEctroscopy
ASAP: Acceleration by Sharing Adjacent Polarisation
ATP: Adenosine TriPhosphate
BANGO: Beta testing for Adjacent Nuclei with a Gyration Operator
BEST: Band-selective Excitation Short-Transient
BPTI: Bovine Pancreatic Trypsin Inhibitor
CA-WURST: Constant Adiabaticity WURST
CASE: Computer-Assisted Structure Elucidation
CLIP-COSY: Clean, In-Phase COSY
COCOHOSY: Combined COsy and HOesy SpectroscopY
COCONOSY: Combined COsy and NOesy SpectroscopY
COSY: COrrelation SpectroscopY
CP: Cross-Polarization
CPMG: Carr-Purcell-Meiboom-Gill
CSA: Chemical-Shift Anisotropy
CTP: Coherence Transfer Pathway
CW: Continuous Wave
DARR: Dipolar Assisted Rotational Resonance
Demultiplexing: data separation at the processing stage that may involve additional data manipulation (decoding).
DIPSHIFT: DIPolar chemical SHIFT correlation
DIPSI: Decoupling In the Presence of Scalar Interactions
DMR: Diagnostic Magnetic Resonance
DNP: Dynamic Nuclear Polarization
DOSY: Diffusion-Ordered SpectroscopY
DQF-COSY: Double Quantum Filtered COSY
DQSQ: Double Quantum Single Quantum
DREAM: Dipolar Recoupling Enhanced by Amplitude Modulation
DUMAS: Dual-Acquisition Magic-Angle Spinning
FABP: Fatty Acid Binding Protein
FID: Free Induction Decay
H2BC: Heteronuclear Two-Bond Correlation experiment
H2OBC: Heteronuclear Two and One-Bond Correlation experiment
HETCOR: HETeronuclear CORrelation
HMBC: Heteronuclear Multiple Bond Correlation
HMQC: Heteronuclear Multiple Quantum Correlation
HOESY: Heteronuclear Overhauser Effect Spectroscopy
HSQC: Heteronuclear Single Quantum Correlation
INEPT: Insensitive Nuclei Enhanced by Polarization Transfer
INADEQUATE: Incredible Natural Abundance Double Quantum Transfer Experiment
IPAP: In-Phase Anti-Phase
ISIS: Image-Selected In vivo Spectroscopy
MACSY: Multiple ACquisition SpectroscopY
MAS: Magic Angle Spinning

MATS: Multiple-Acquisition Time-Shared

MBP: Maltose Binding Protein

MLF: Methionyl-Leucyl-Phenylalanine (tripeptide)

MNP: Magnetic NanoParticle

MRI: Magnetic Resonance Imaging

MRS: Magnetic Resonance Spectroscopy

NMR: Nuclear Magnetic Resonance

NOAH: Nmr by Ordered Acquisition using ^{1}H-detection

NOESY: Nuclear Overhauser Effect SpectroscopY

NUS: Non-Uniform Sampling

PAIN: Proton Assisted Insensitive Nuclei

PALSY: PArallel Localized SpectroscopY

PANACEA: Parallel Acquisition NMR, an All-in-one Combination of Experimental Applications

PANSY: Parallel Acquisition NMR SpectroscopY

PAR: Proton-Assisted Recoupling

PEP: Preservation of Equivalent Pathways

PISEMA: Polarization Inversion Spin-Exchange at Magic Angle

PISEMAI: PISEMA with evolution of I-spin dipolar coherence in the indirect dimension

PROSMASH: PROtein-HSQC and SMAll molecule-HSQC Signals with Homonuclear decoupling

PDSD: Proton Driven Spin Diffusion

PSYCHE: Pure Shift Yielded by CHirp Excitation

PUFSY: Parallel Ultra-Fast SpectroscopY

RELOAD-CP: Relaxation Enhancement by a LOwer spin temperature of ADjacent spins

RF: Radio Frequency

RFDR: Radio Frequency Driven Recoupling

RNA: RiboNucleic Acid

ROESY: Rotating-frame Overhauser Effect SpectroscopY

SEA-XLOC: Separate Echo and Antiecho X-nucleus for LOng-range Couplings

Sim-CP: Simultaneous Cross-Polarization

SNR: Signal to Noise Ratio

SOFAST: band-Selective Optimised Flip Angle Short Transient

SPC5: Supercycled Post-C5

SPECIFIC-CP: SPECtrally Induced Filtering In Combination with Cross Polarization

SQ: Single Quantum

STEAM: STimulated Echo Acquisition Mode

SUSHY: Spectral Unraveling by Space-selective Hadamard spectroscopY

TEDOR: Transferred Echo Double Resonance

TILT: Time Increments Linked Together

TOCSY: TOtal Correlation SpectroscopY

TQF-COSY: Triple Quantum Filtered COSY

TROSY: Transverse Relaxation Optimized SpectroscopY

TS: Time-Shared

UF: UltraFast

UTOPIA: Unified Time-OPtimized Interleaved Acquisition

WURST: Wideband Uniform Rate Smooth Truncation